Neutron Imaging at the neutron radiography and tomography facility ANTARES

Burkhard Schillinger,
Johannes Brunner, Elbio Calzada, Florian Grünauer,
Hongyun Li, Klaus Lorenz, Martin Mühlbauer, Michael Schulz

FRM-II and Physics E21, Technische Universität München, D-85748 Garching, Germany

Introduction: Why we use neutron radiography

Using all kinds of different radiation

Small angle scattering in neutron radiography and tomography

Phase contrast imaging with neutrons

Stroboscopic imaging with neutrons

Why we do neutron radiography: The mass attenuation coefficient of elements

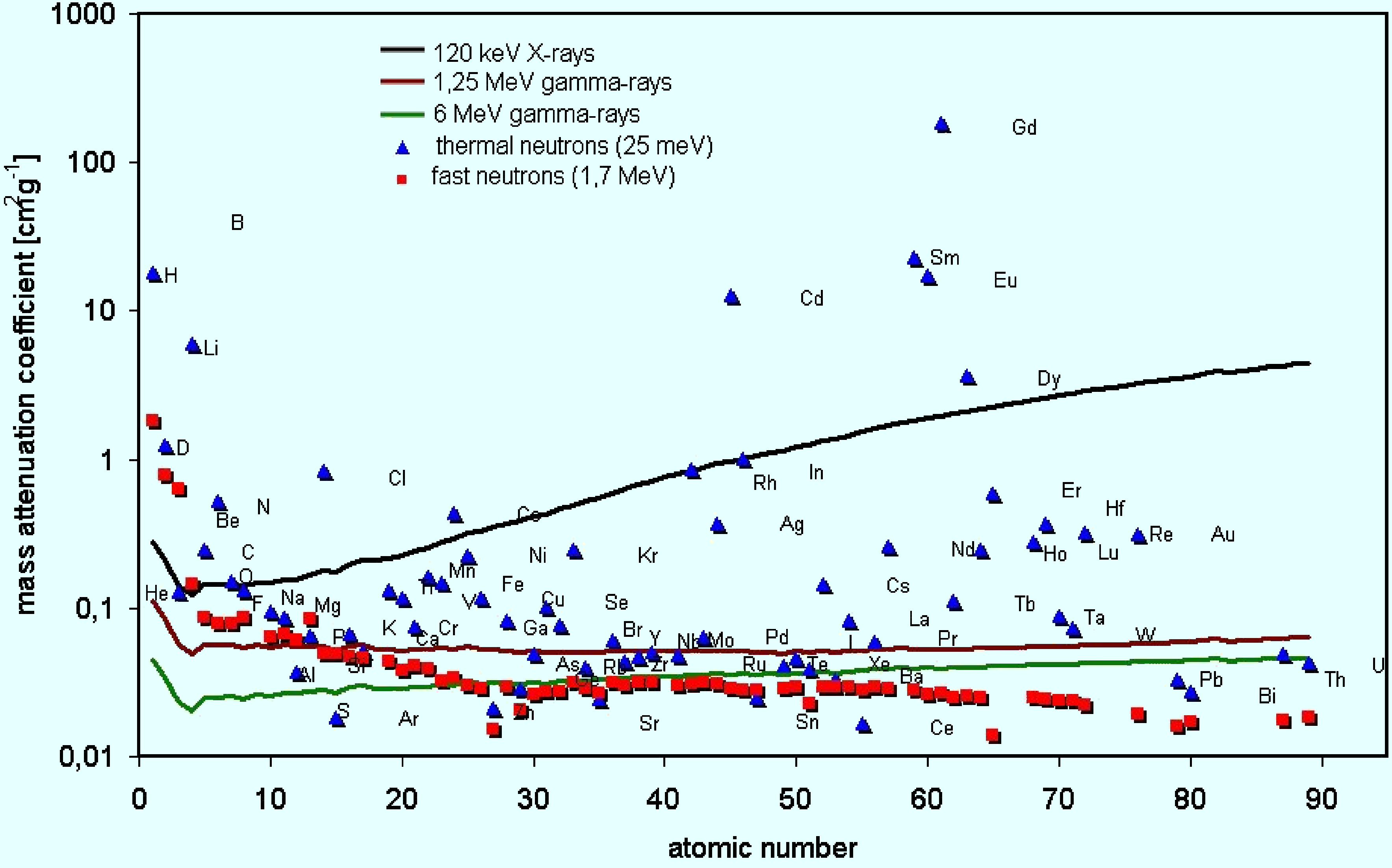

Actual attenuation for technical materials

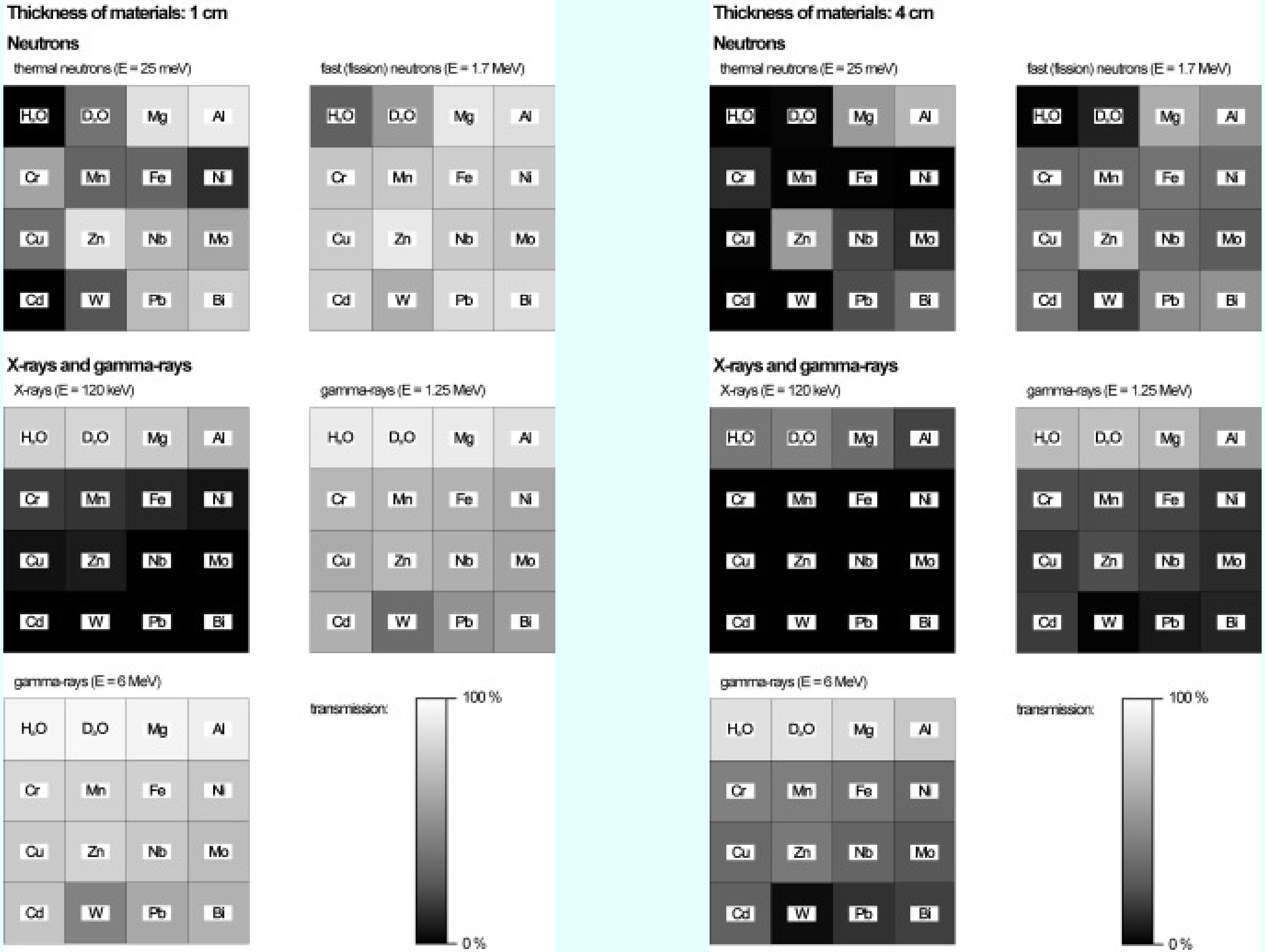

Introduction:
Setup for neutron tomography rotation table, scintillator screen and CCD camera

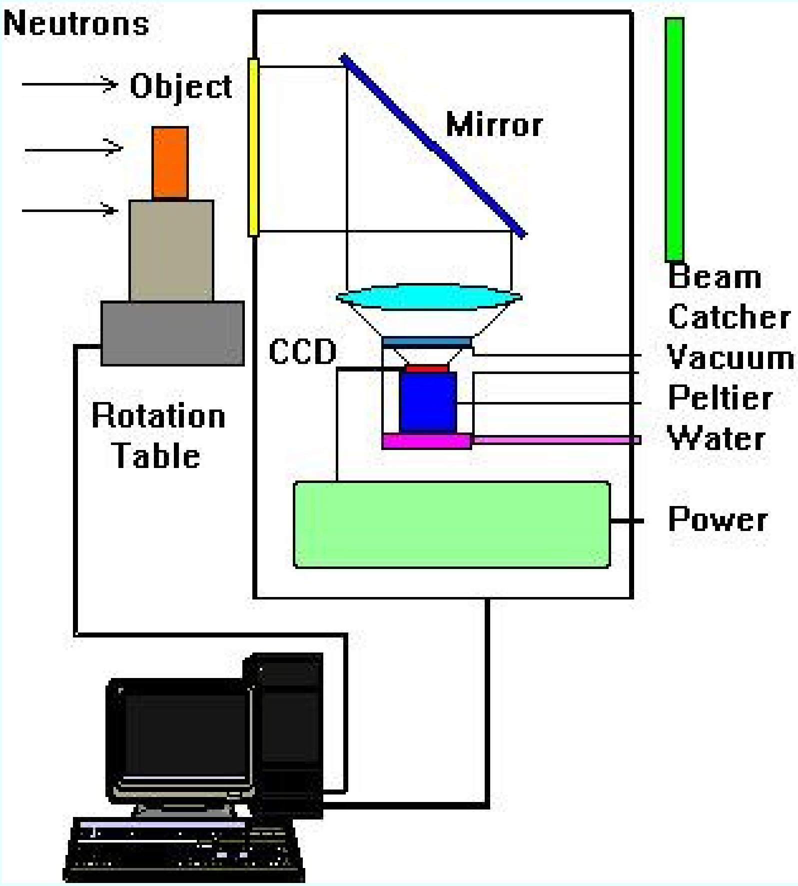

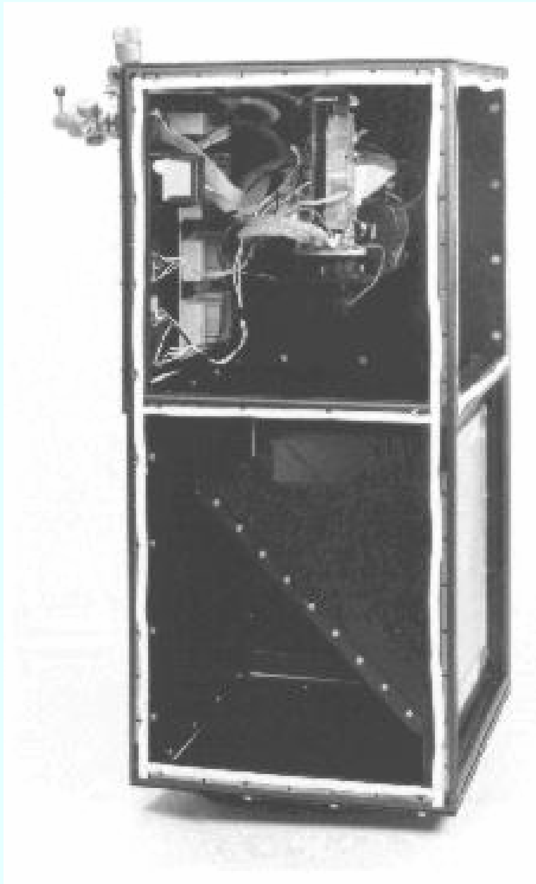

Antares

Advanced **N**eutron **T**omography **A**nd **R**adiography **E**xperimental **S**ystem

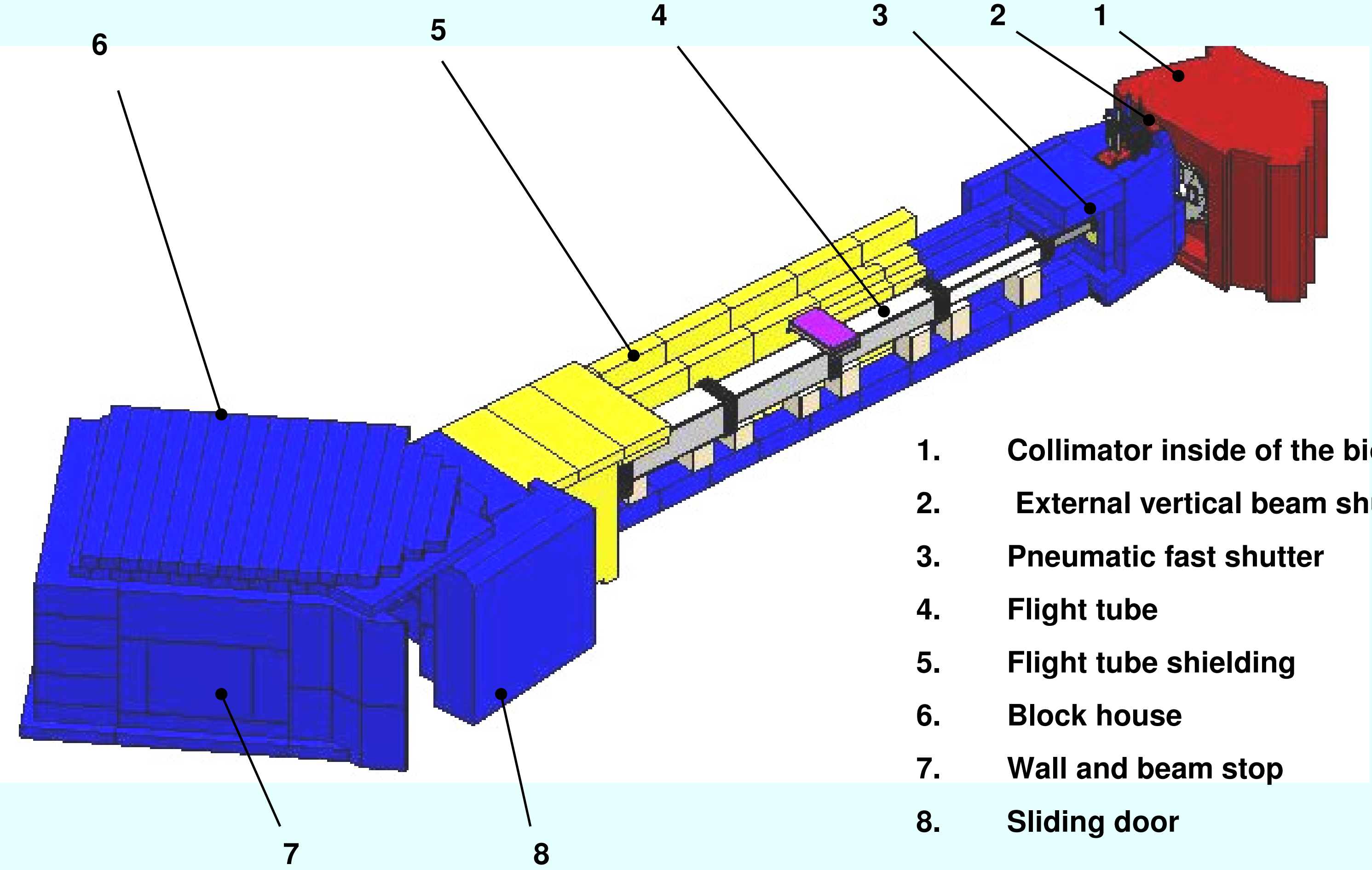

1. Collimator inside of the biological shielding
2. External vertical beam shutter
3. Pneumatic fast shutter
4. Flight tube
5. Flight tube shielding
6. Block house
7. Wall and beam stop
8. Sliding door

Introduction:

The sample manipulator can carry up to 500 kg samples up to 1 m diameter.

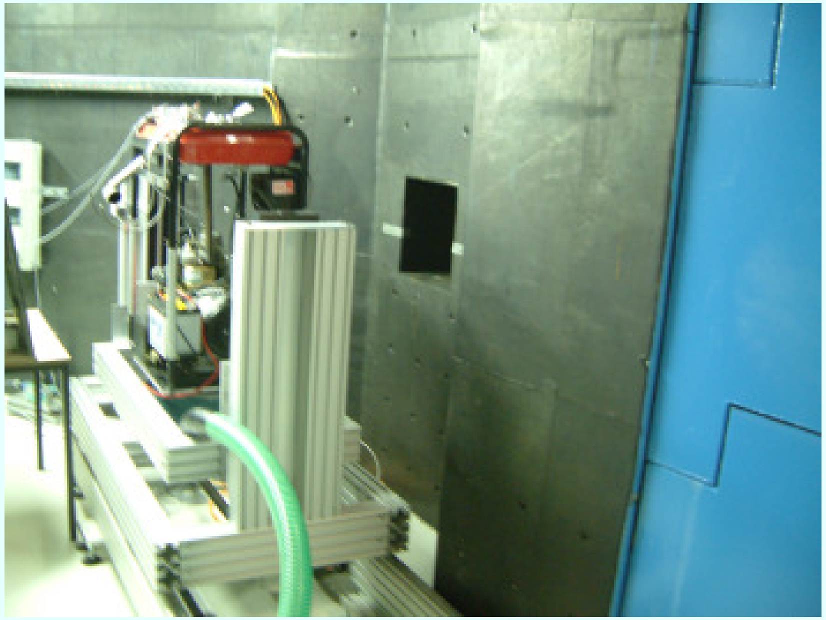

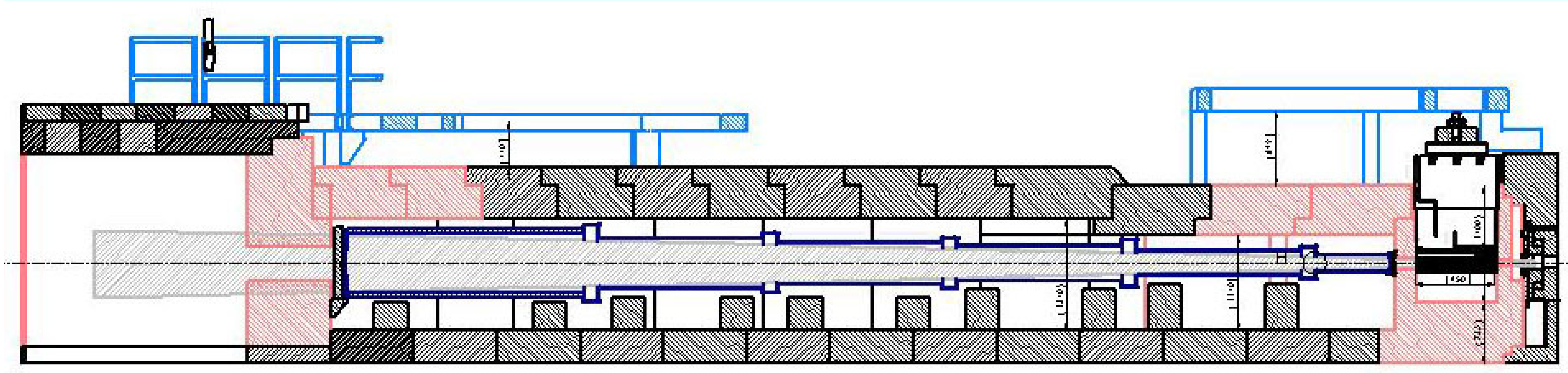

Cross section of the ANTARES facility at FRM-II.
From the reactor(on the right), the beam passes the shutter and collimator and the flight tube towards the block house.

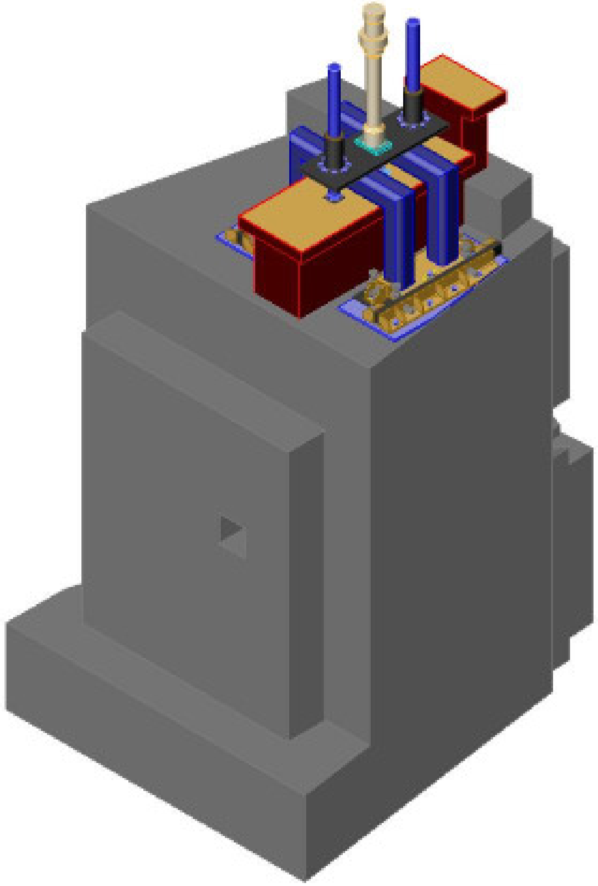

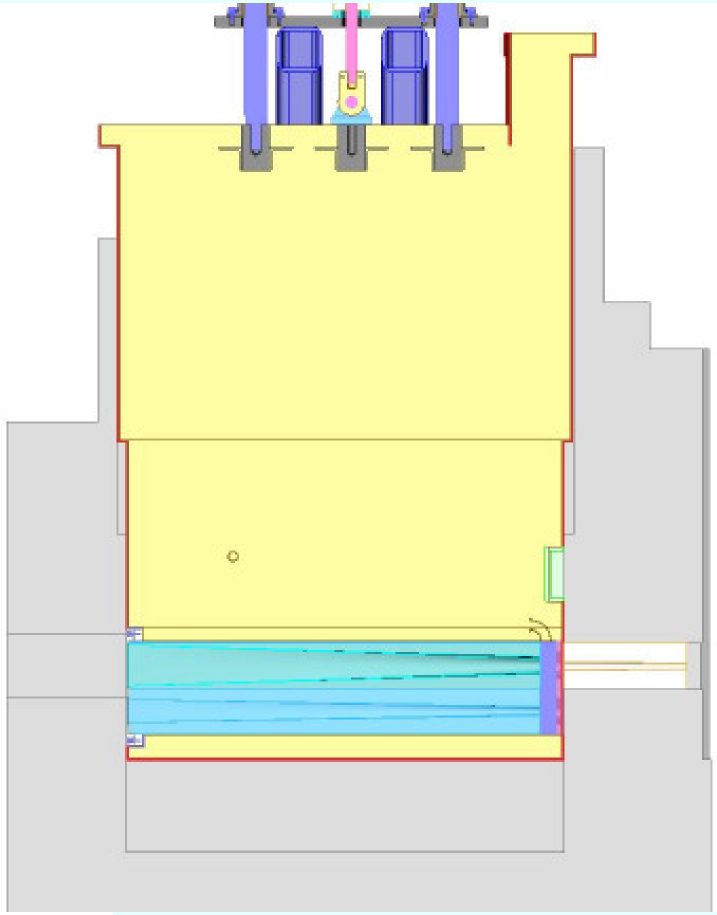

External hydraulic shutter of the ANTARES facility.
The slider contains two different collimators that can be positioned and locked in place by a position-controlled hydraulic system and hydraulic clamps.

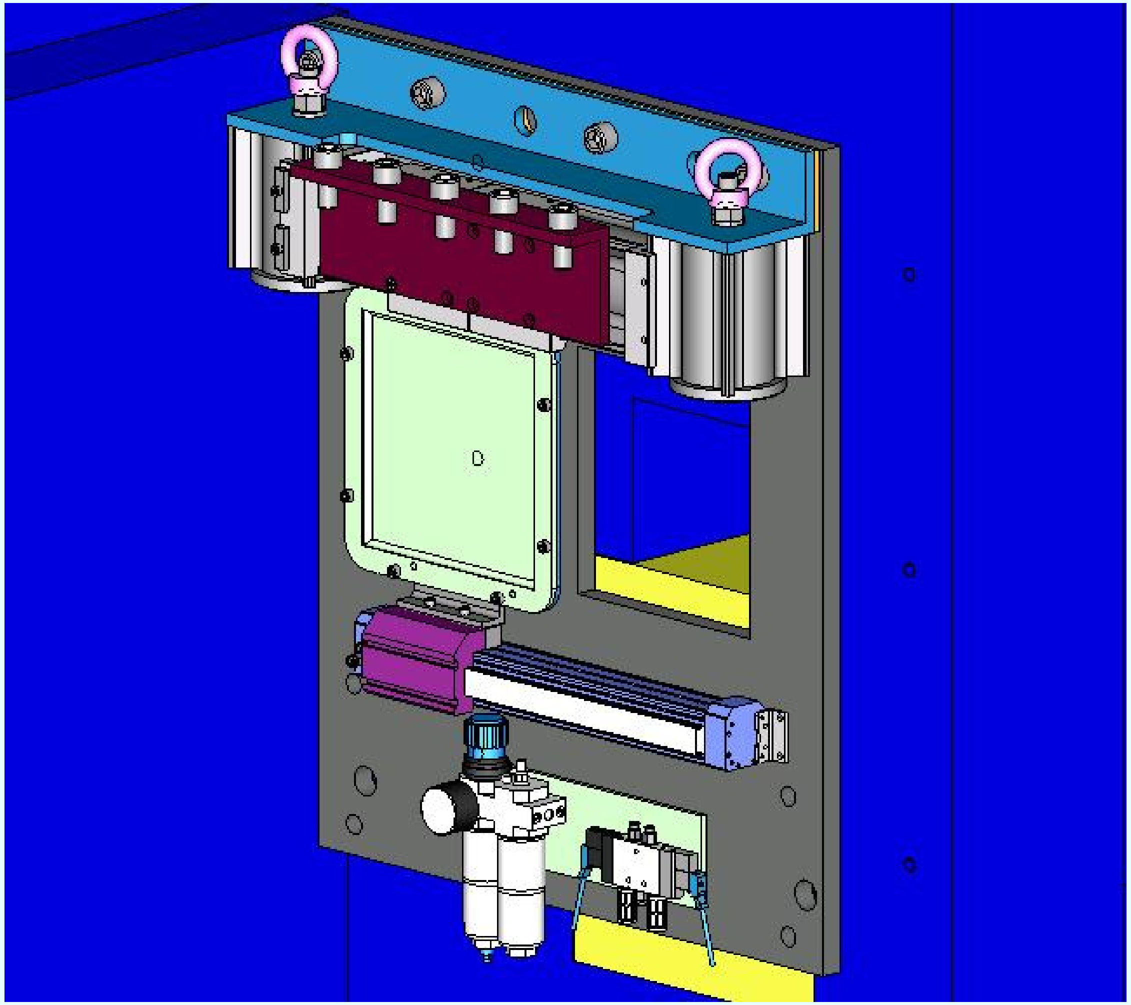

A pneumatic fast shutter at the beginning of the flight tube is used to shut off the thermal beam between exposures in order to minimize activation of the sample.
The Shutter consists of a casing with B_4C powder.

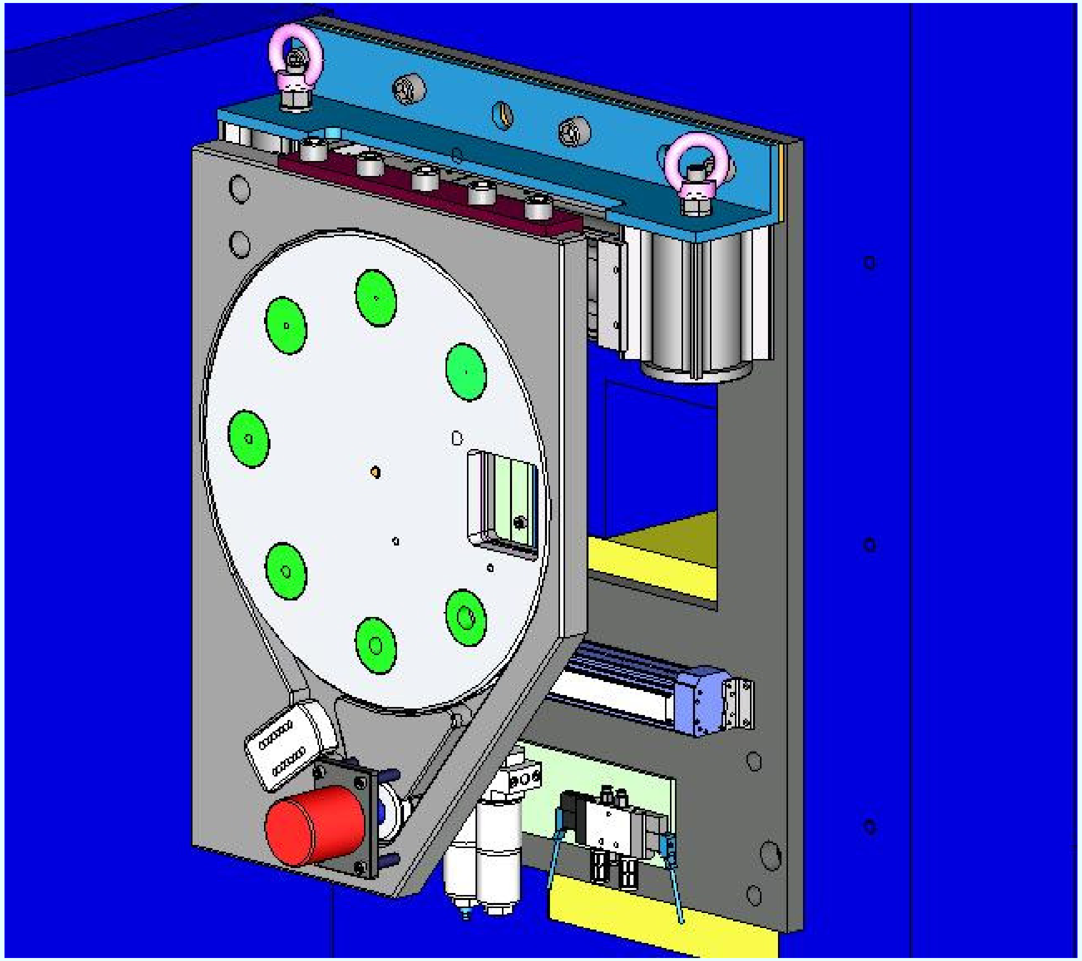

A selector wheel with different masks for will allow to switch the facility to phase contrast imaging within seconds.
It also contains a 2mm Cadmium plate to absorb the thermal and cold part of the spectrum and to pass on only epithermal and fast neutrons.

A standard neutron radiography: A diesel injector pump

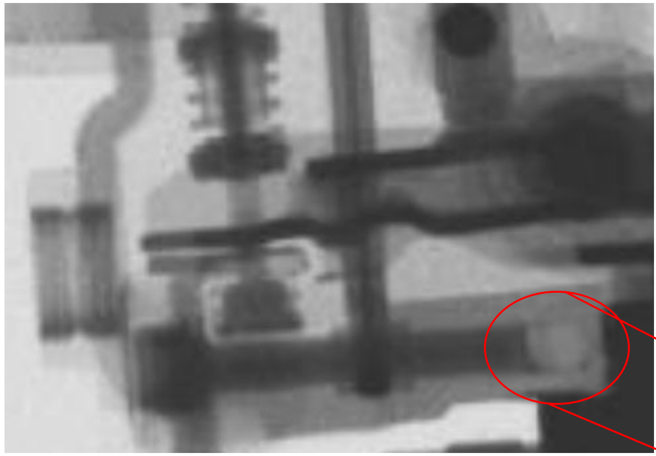

Oil remains

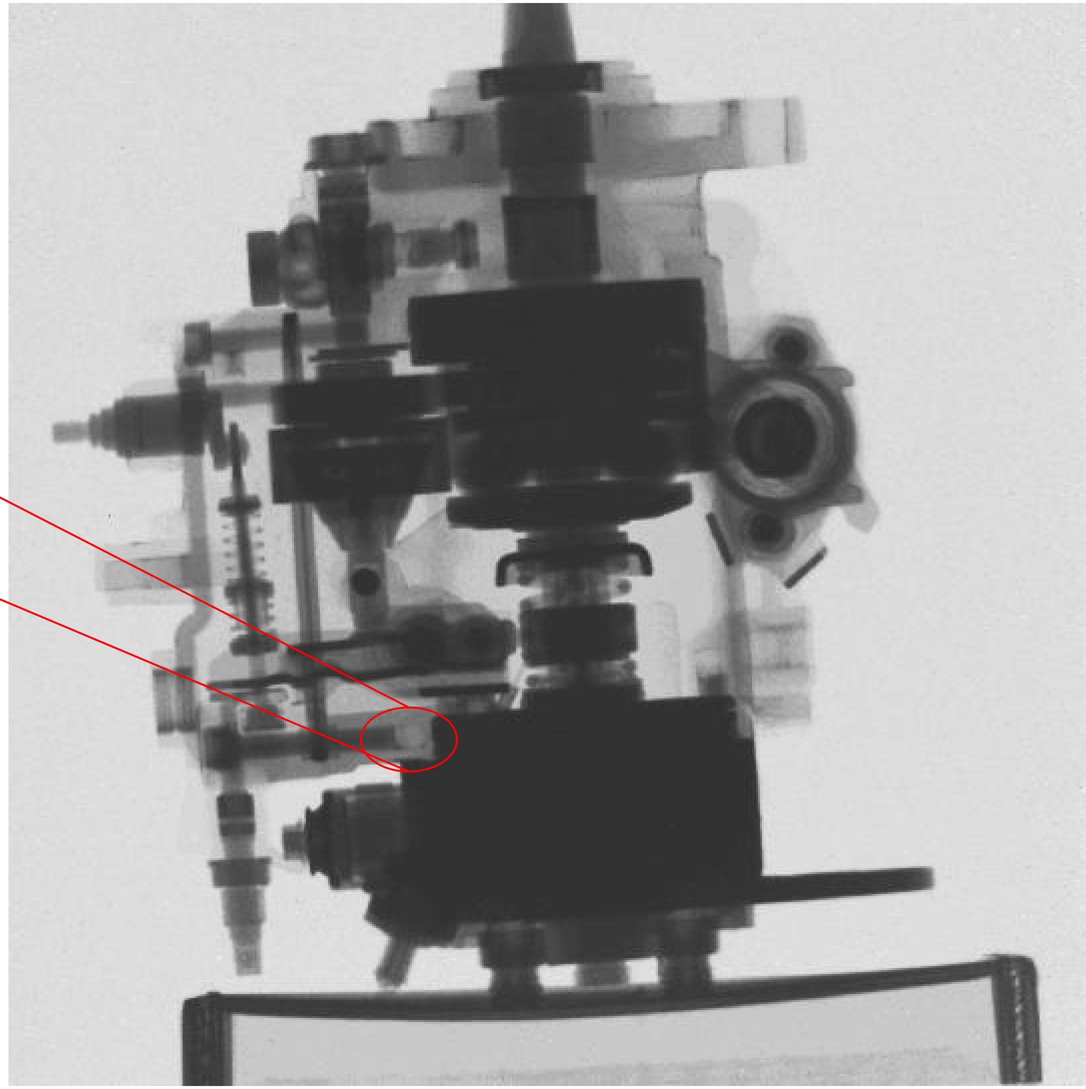

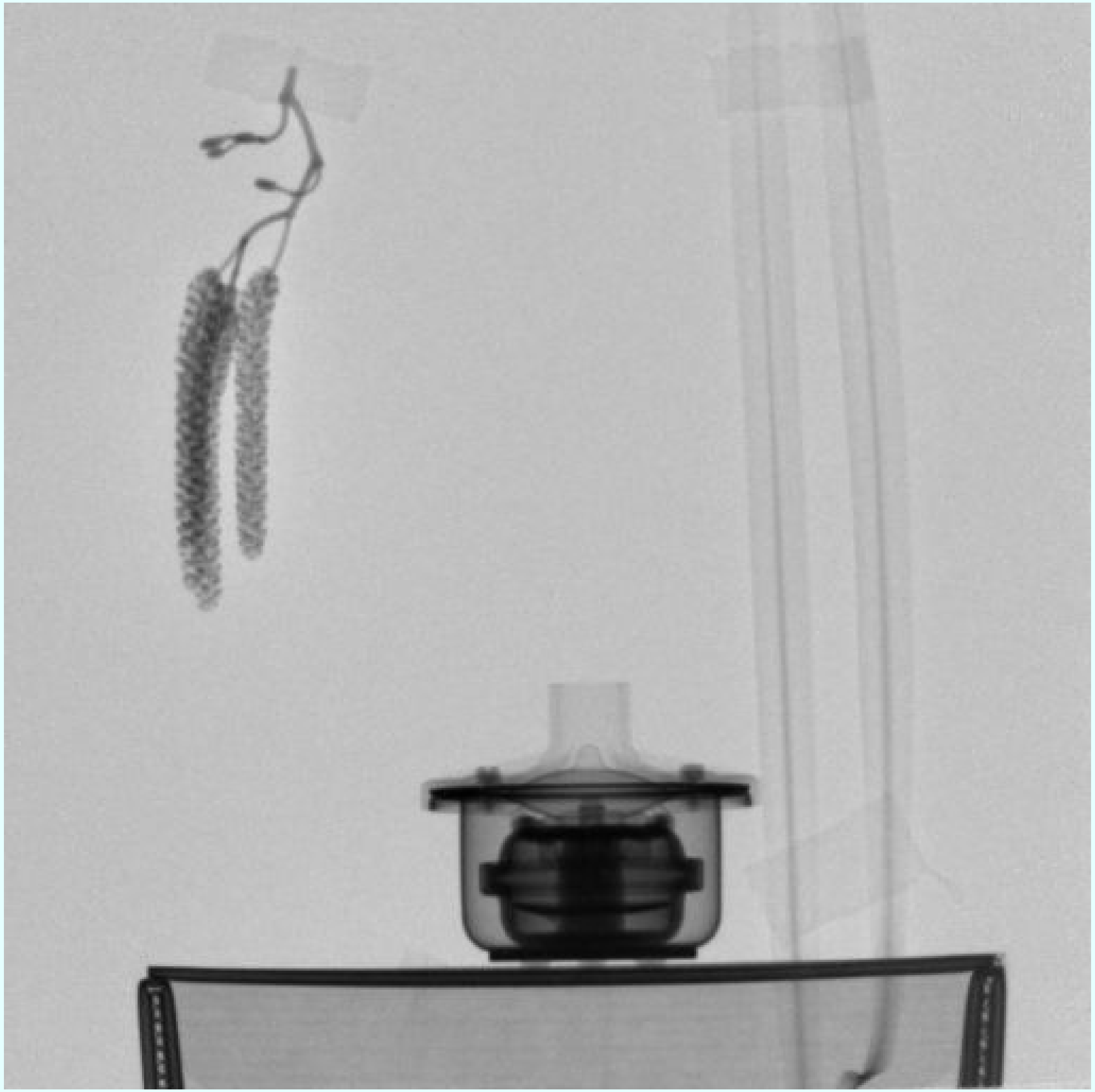

Huge contrast range: Loudspeaker with steel casing on cardboard box, plant seeds and grass, tape

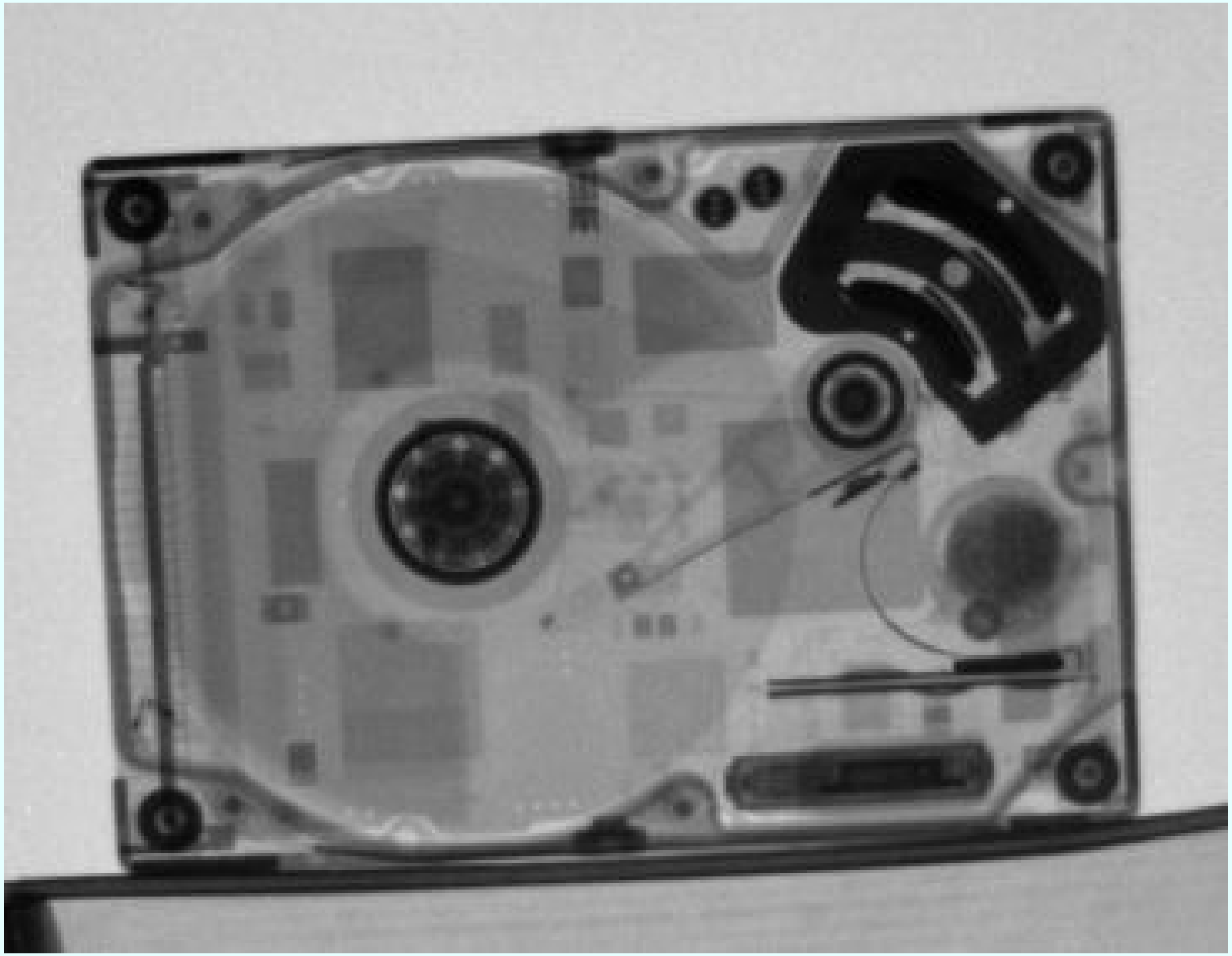

Computer hard disk (cutout of big image)

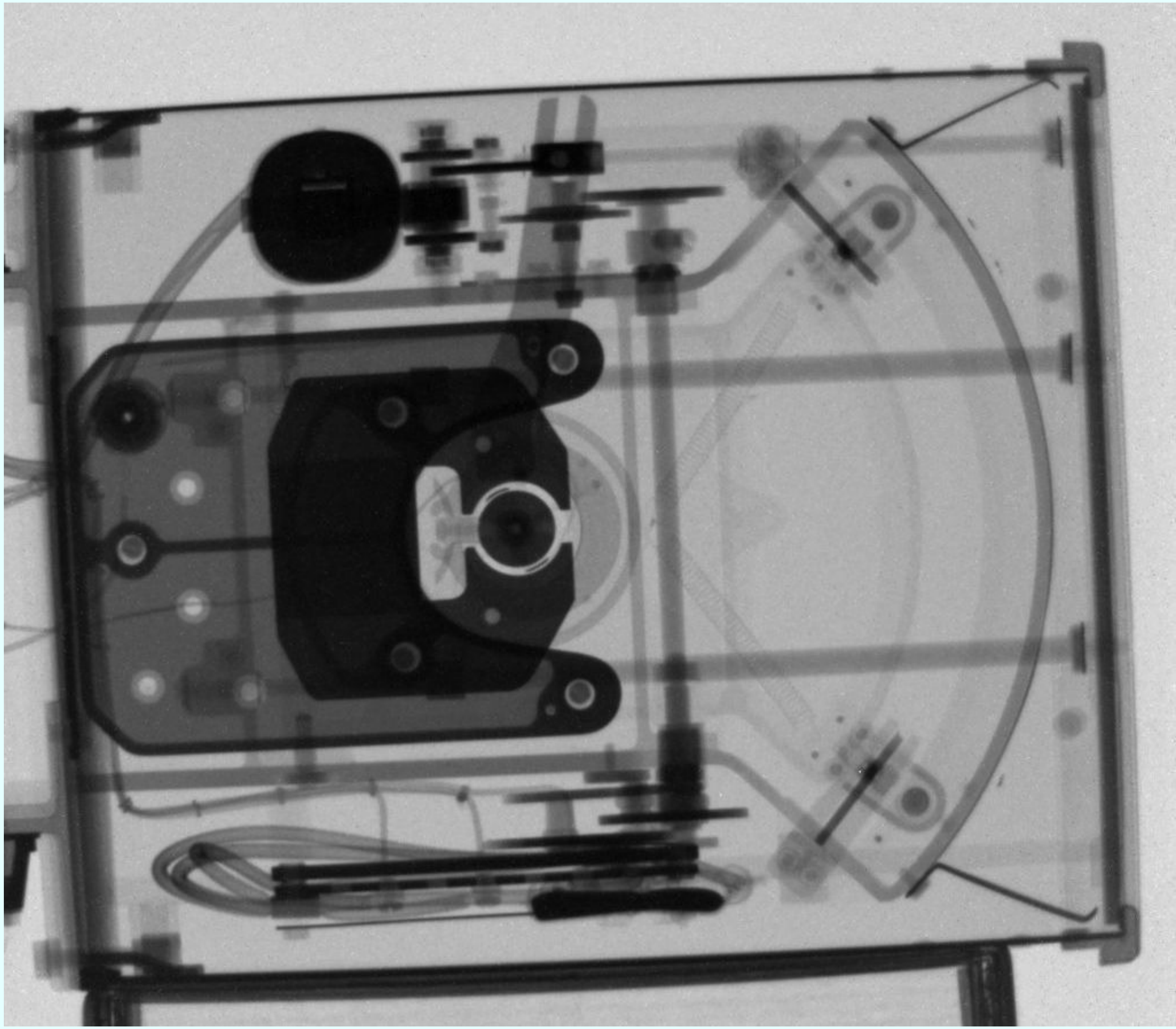

A remote sensing thermometer..
Well visible: cable ties, insulation, plastic cogwheels.

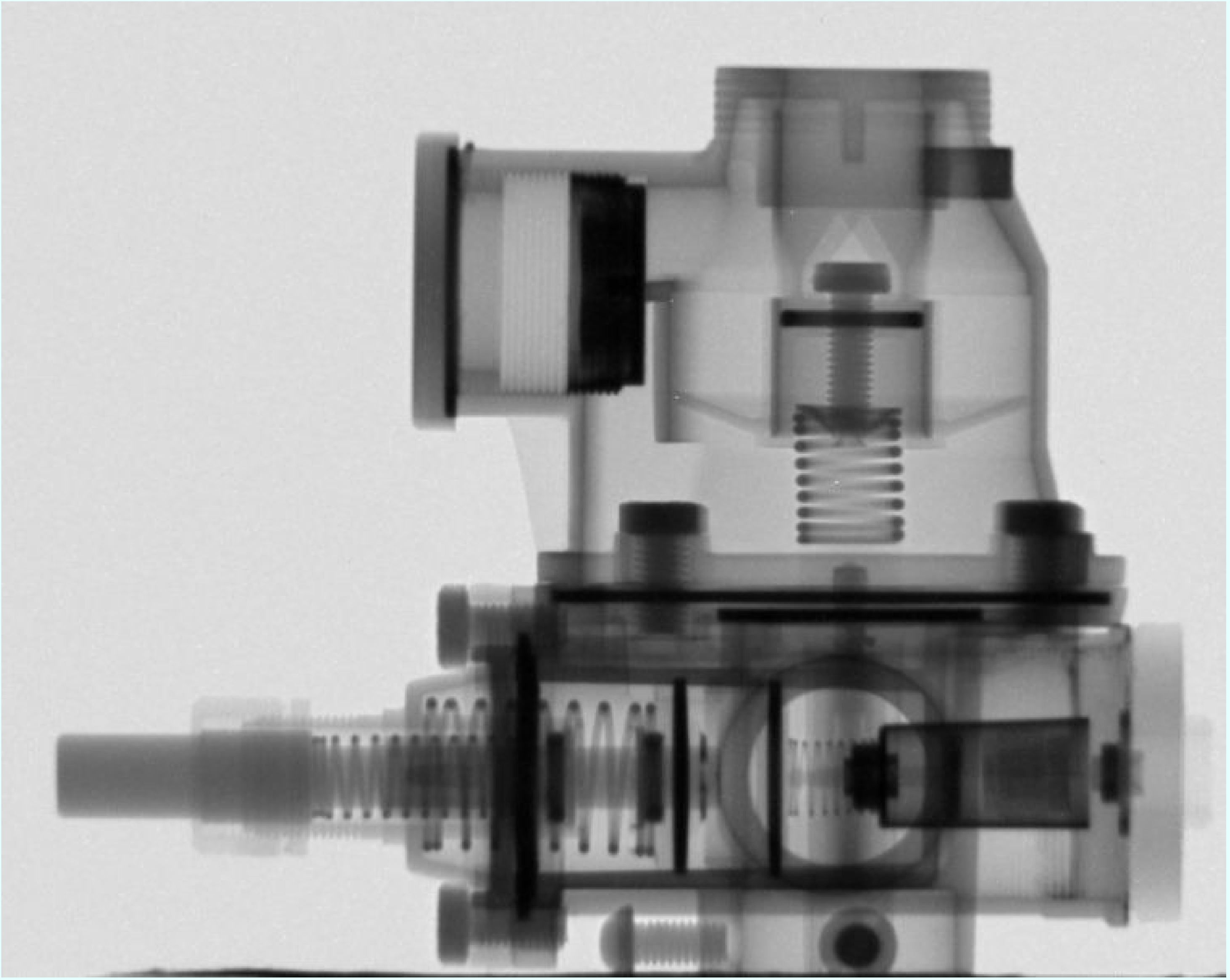

Huge contrast range: A gas pressure reducer with sealants and o-rings

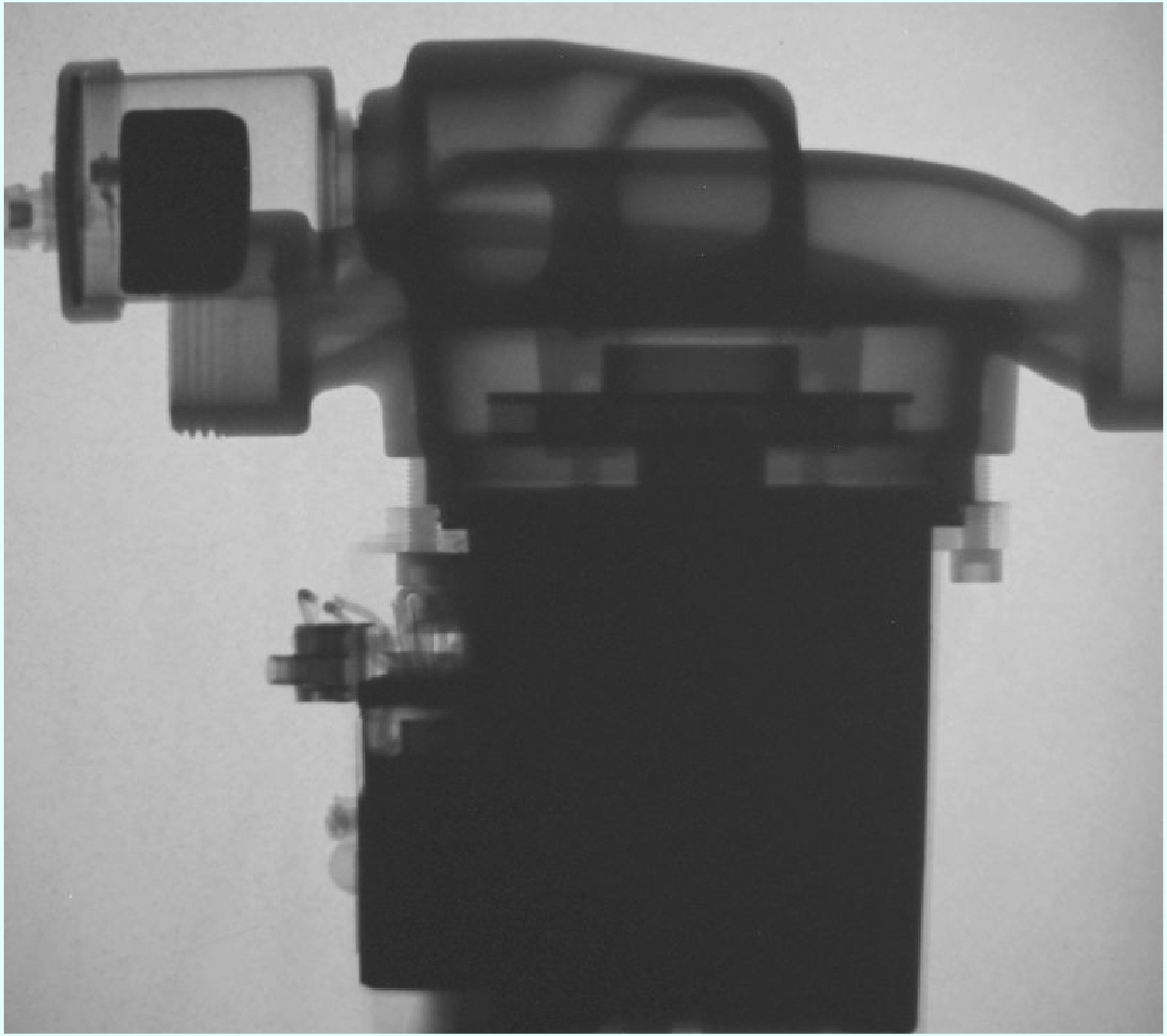

But on this oil-filled pump, thermal neutrons must fail….

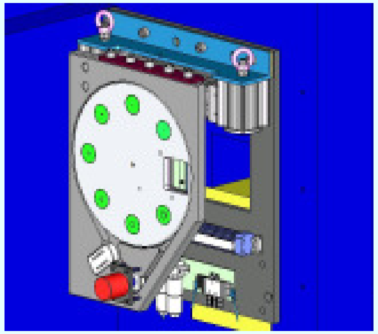

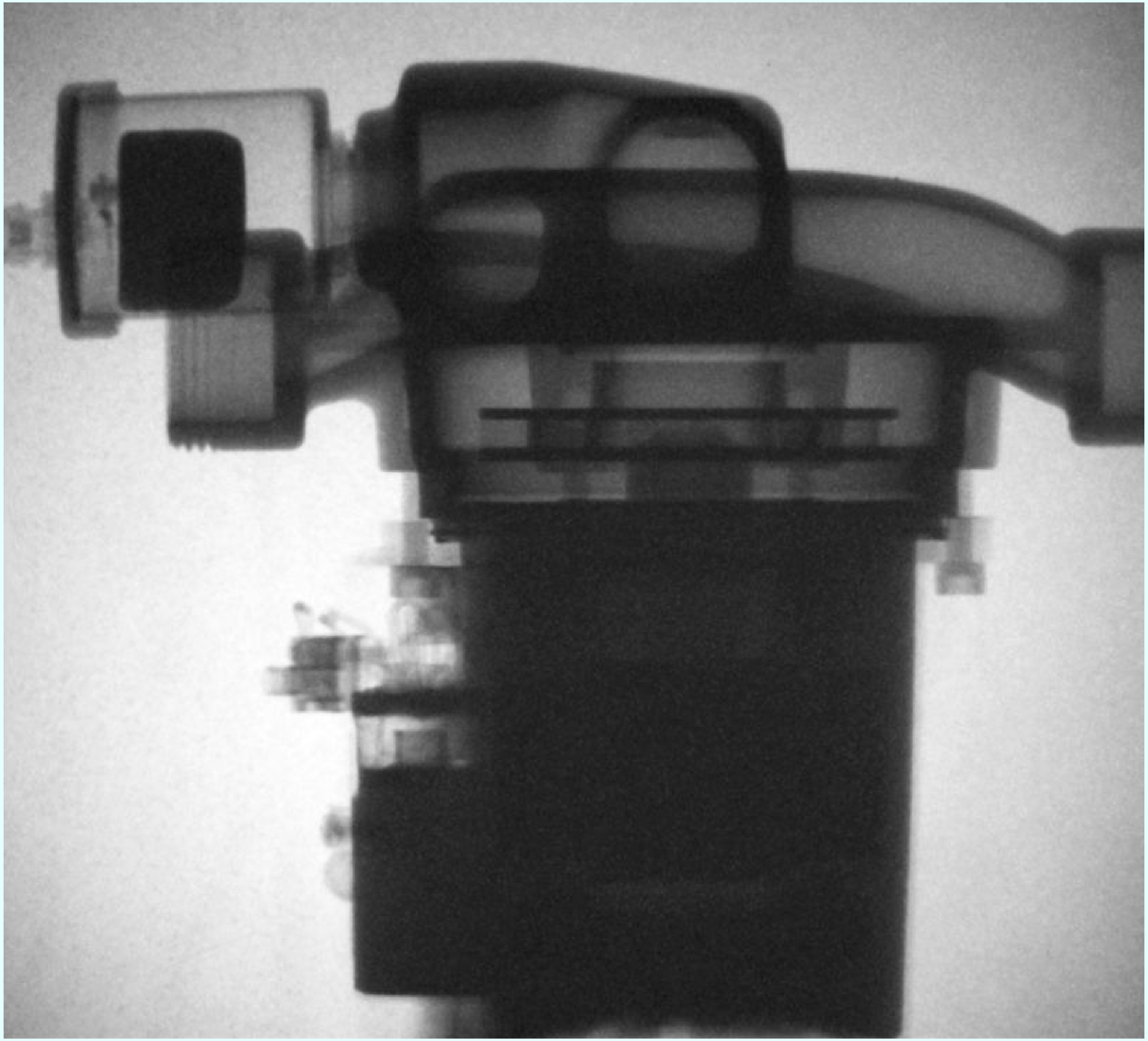

The epithermal picture, using the filter wheel with the Cd filter, shows better penetration….

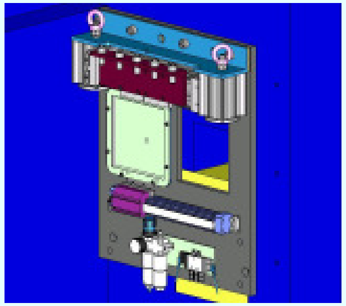

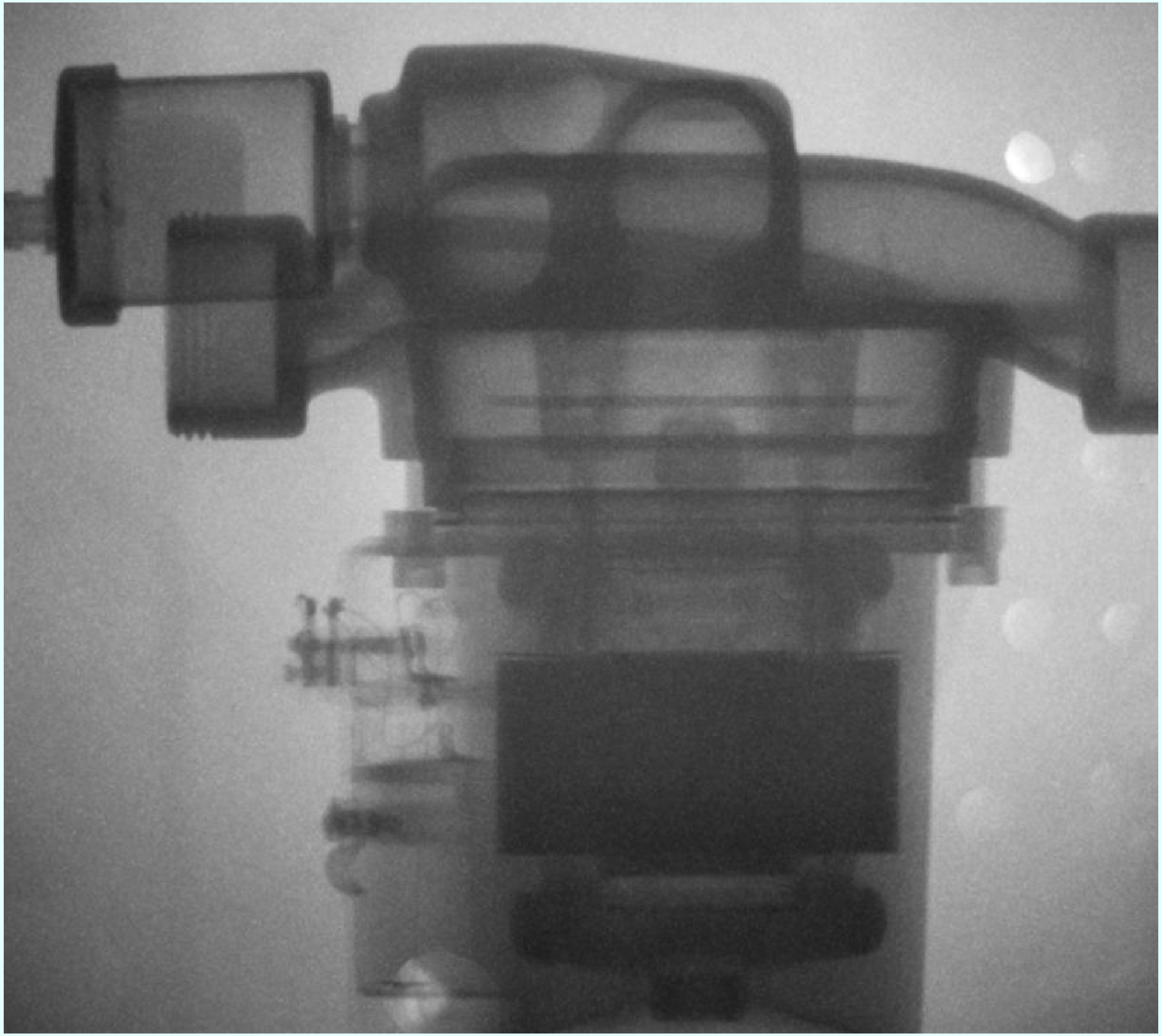

If we use the reactor as a gamma source, with the the fast neutron shutter closed and a gamma scintillation screen, we can still find a lot of information! (We cleaned off the finger prints afterwards.)

Extension: Planning accessories and more possibilities

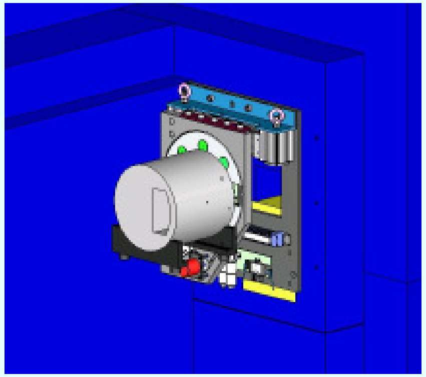

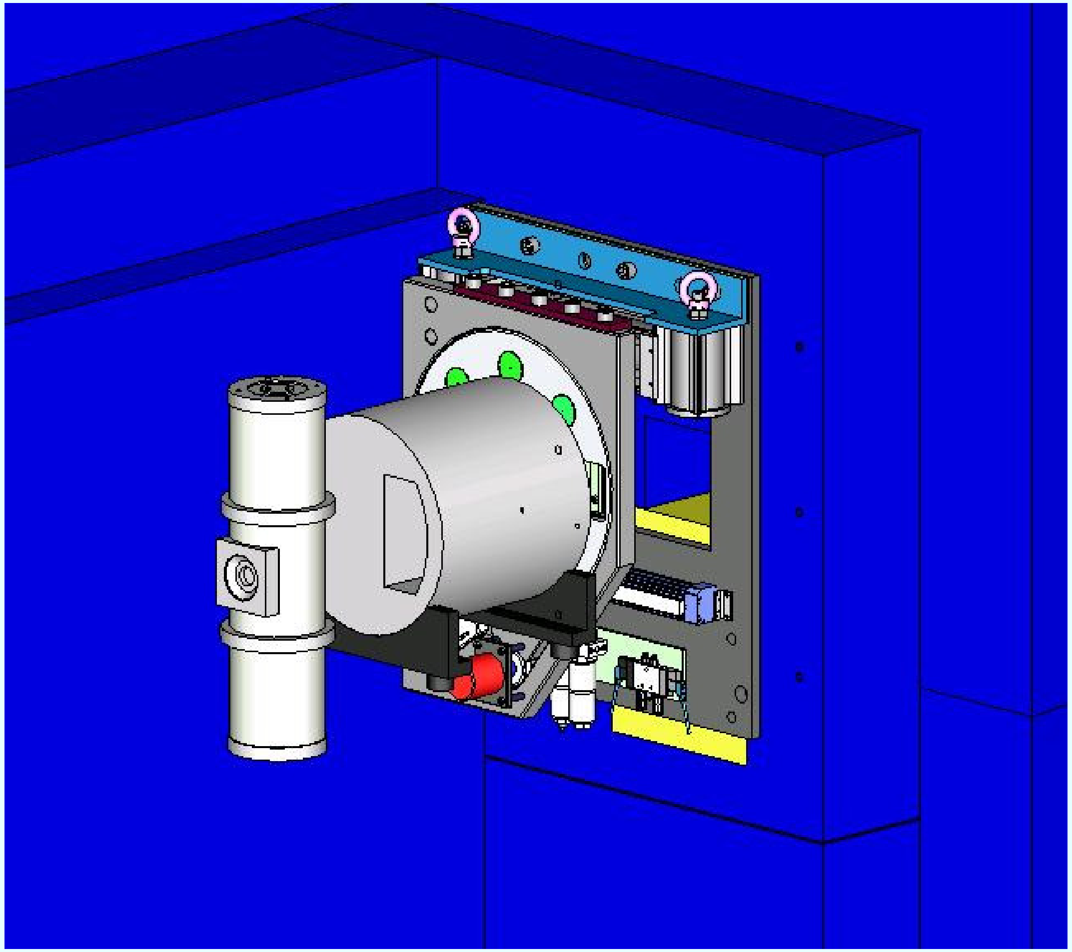

A removable 320 kV X-ray tube has been mounted before the flight tube.
This allows for alternate X-ray tomography in the identical beam geometry!

4. Extension: Planning accessories and more possibilities

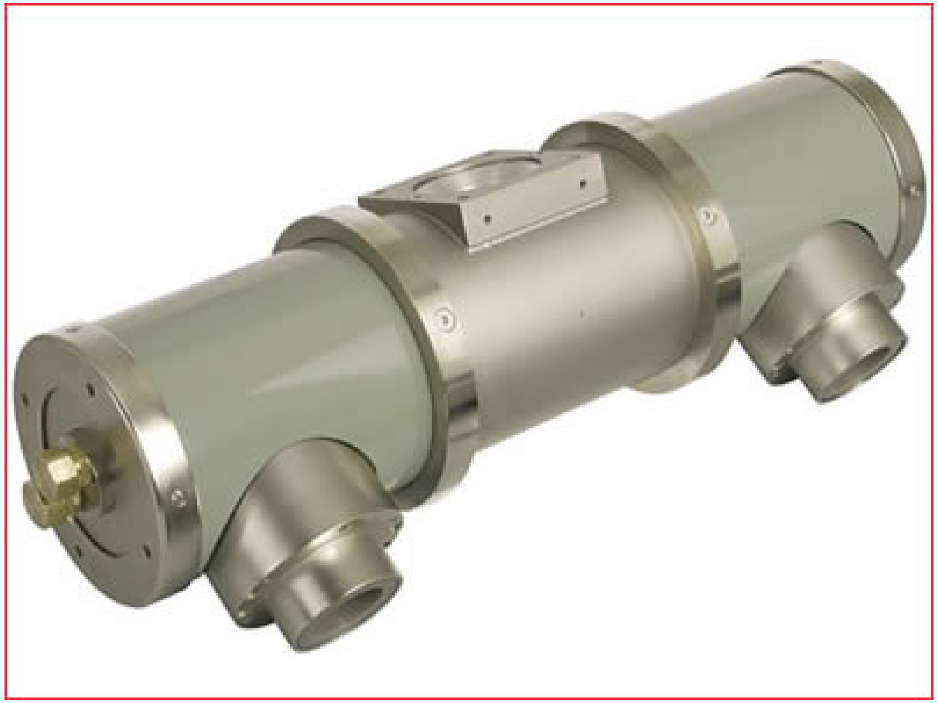

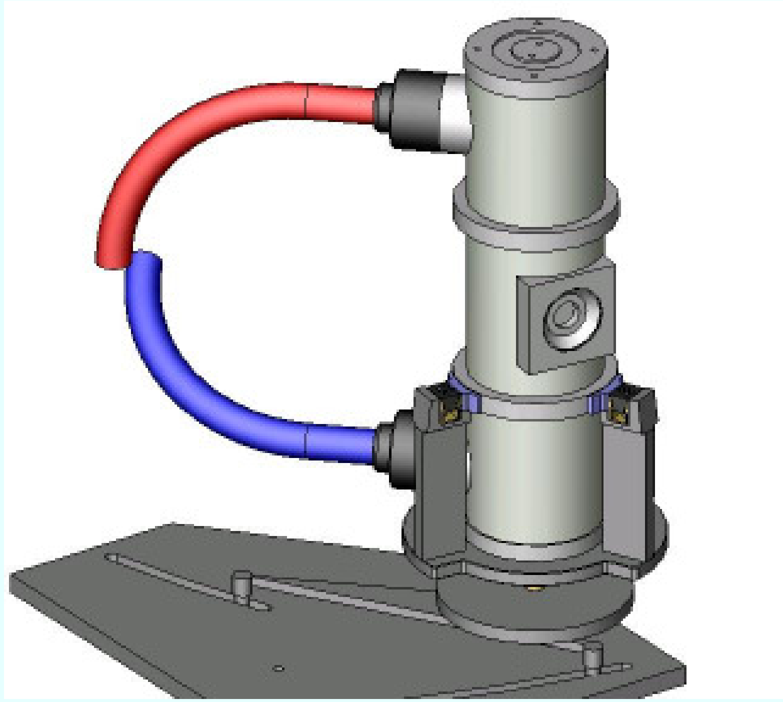

A removable 320 kV X-ray tube has been mounted before the flight tube.
This allows for alternate X-ray tomography in the identical beam geometry!

Comparison and combination of X-ray and neutron images

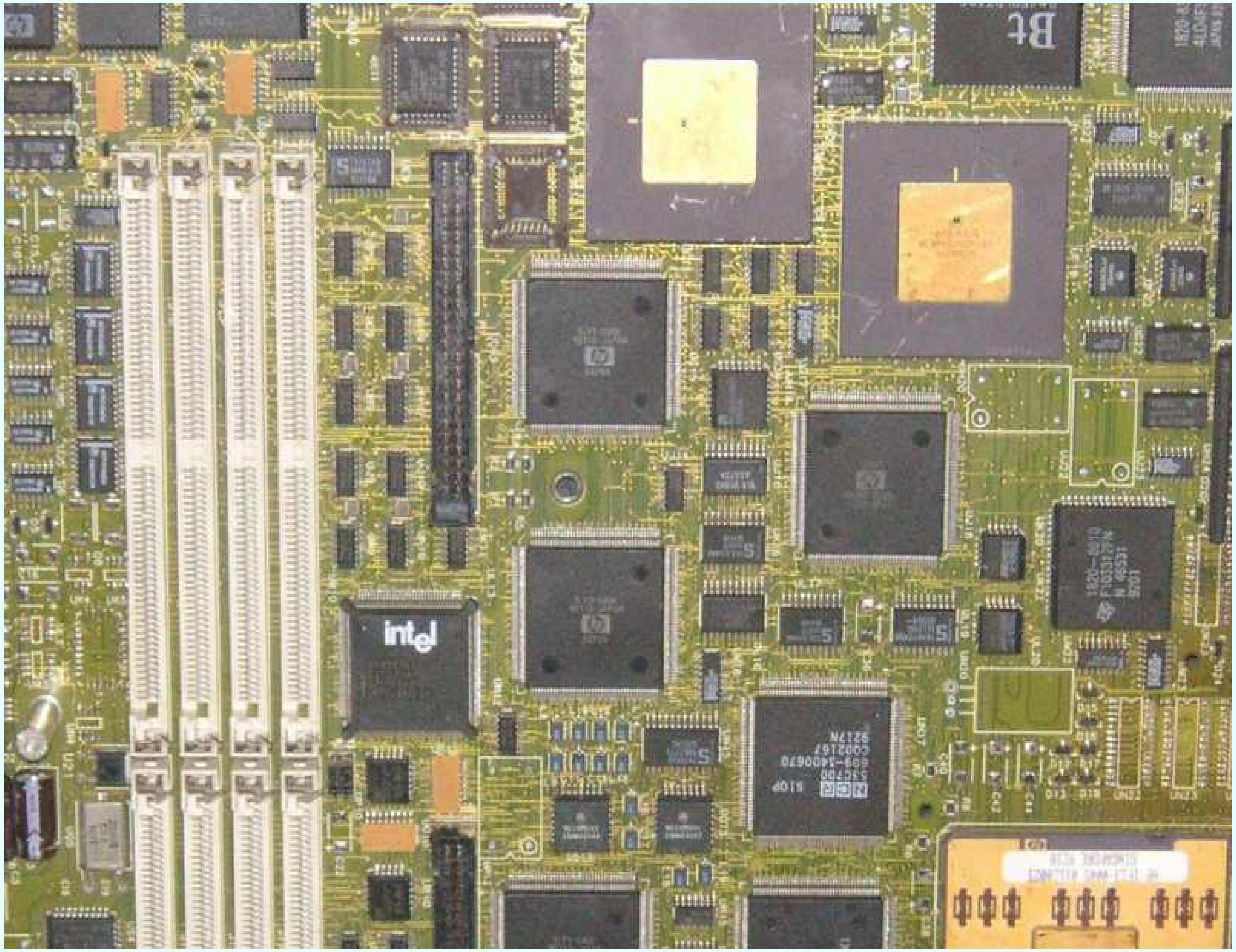

Images
M. Schulz,
TUM

Photo of a printed circuit board.
Note many parts with plastic or ceramic cases and lots of pins.

Comparison and combination of X-ray and neutron images

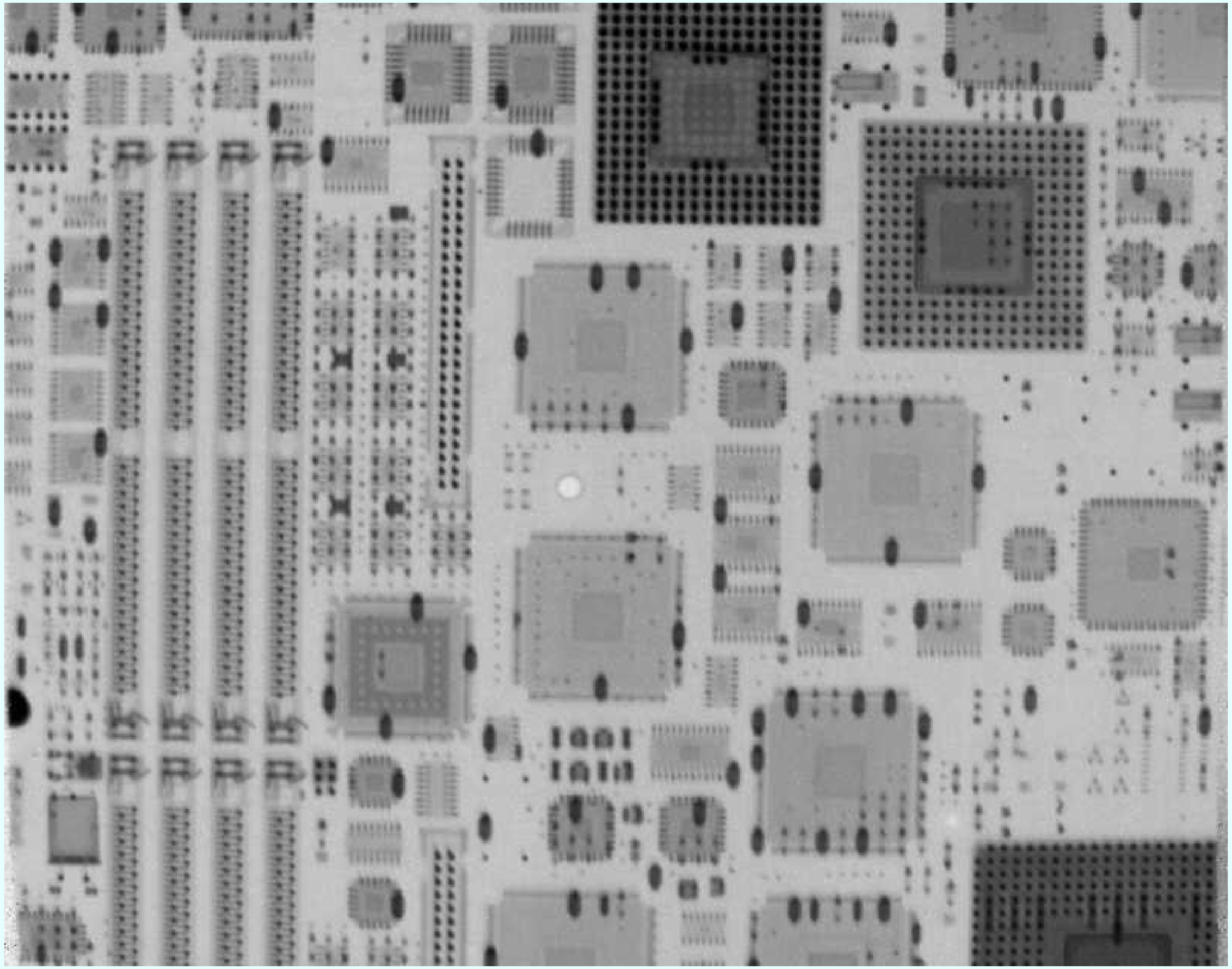

X-ray image.
Most contrast is given by the metal pins.

Comparison and combination of X-ray and neutron images

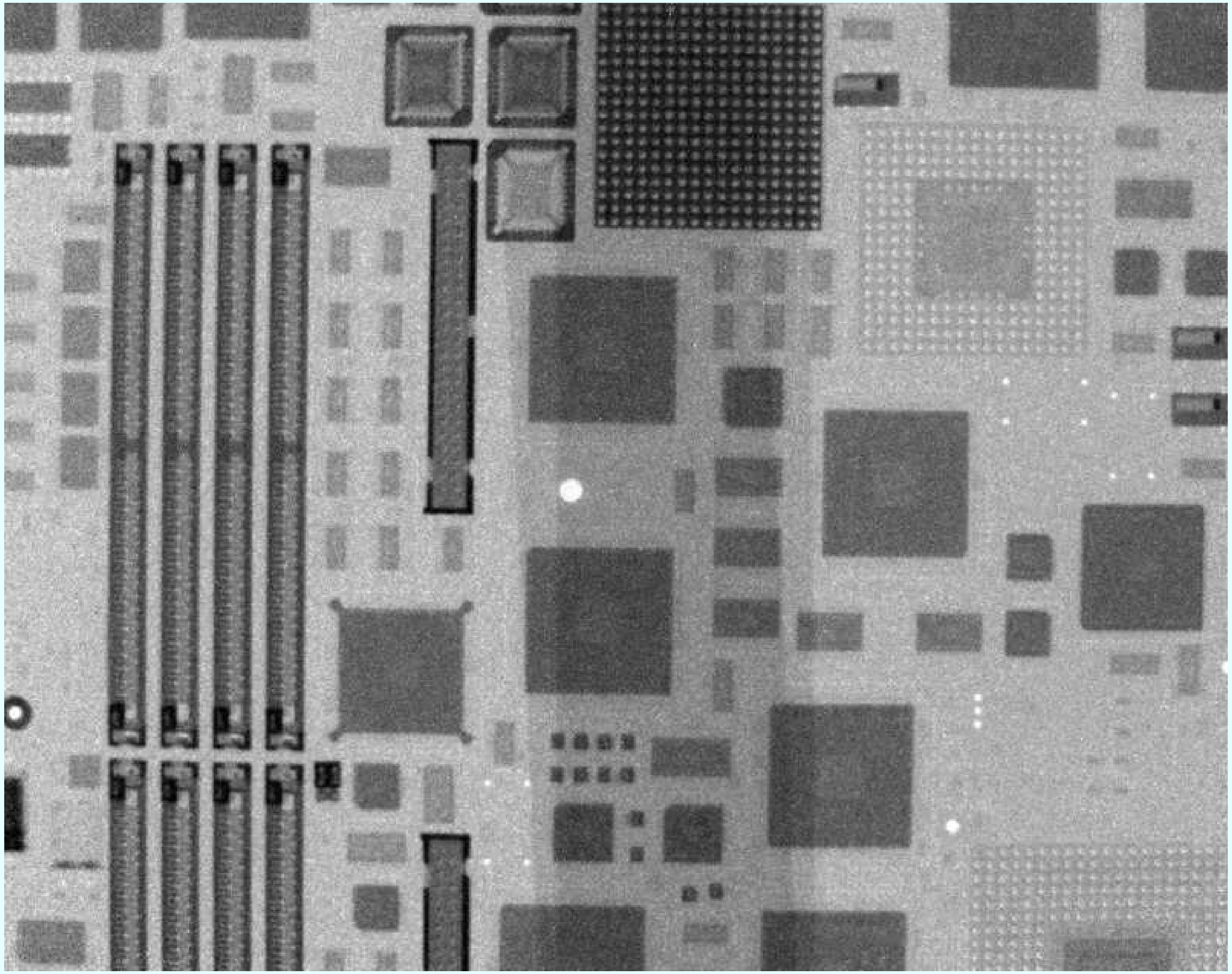

Neutron image.

Most contrast is given by plastic parts, the metal pins are nearly transparent.

Comparison and combination of X-ray and neutron images

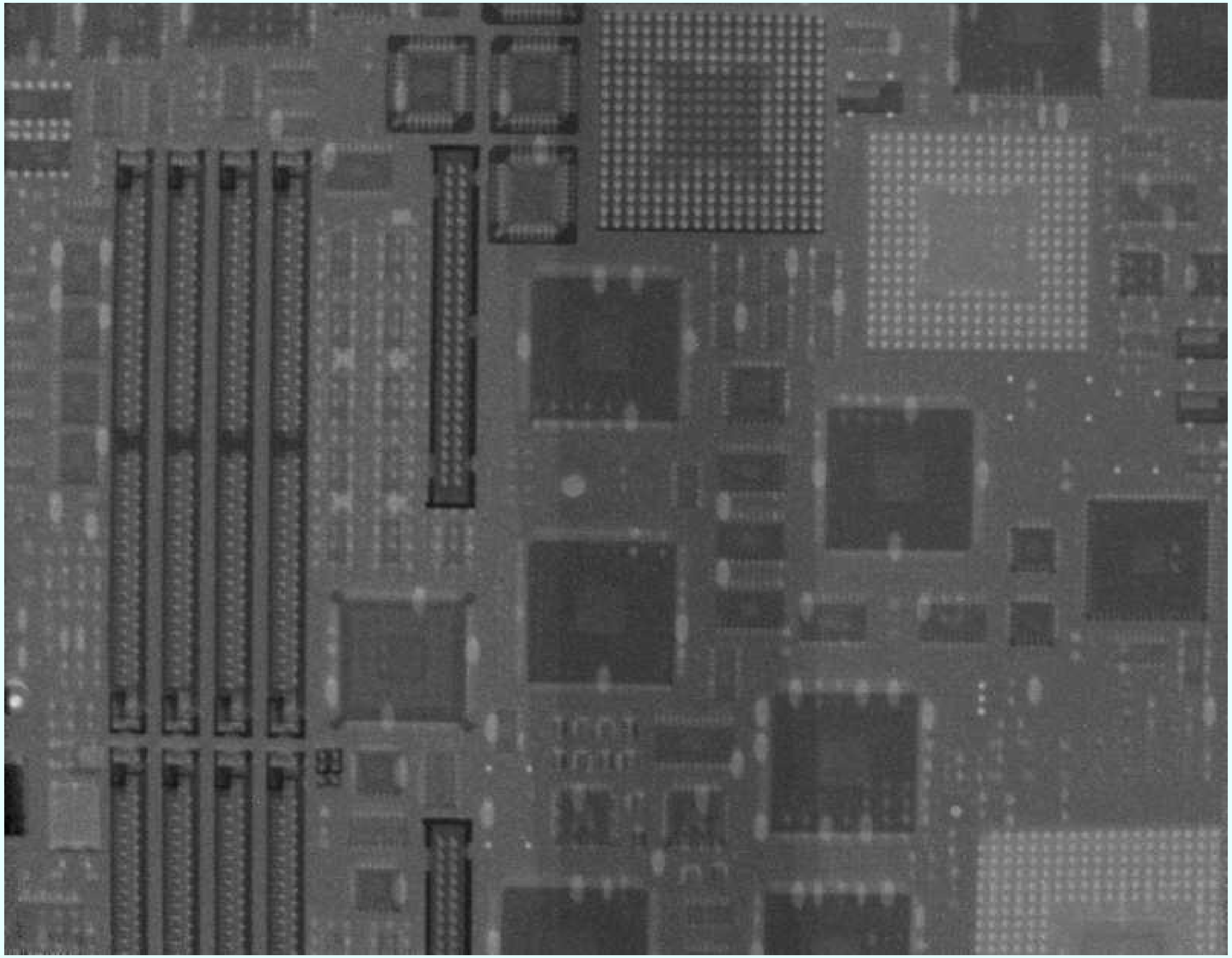

Combination of both images.
The X-ray image was subtracted from the neutron image.

Comparison and combination of X-ray and neutron images

Photo of an unfinished ice hockey knee protector containg a chainmail mesh.

Comparison and combination of X-ray and neutron images

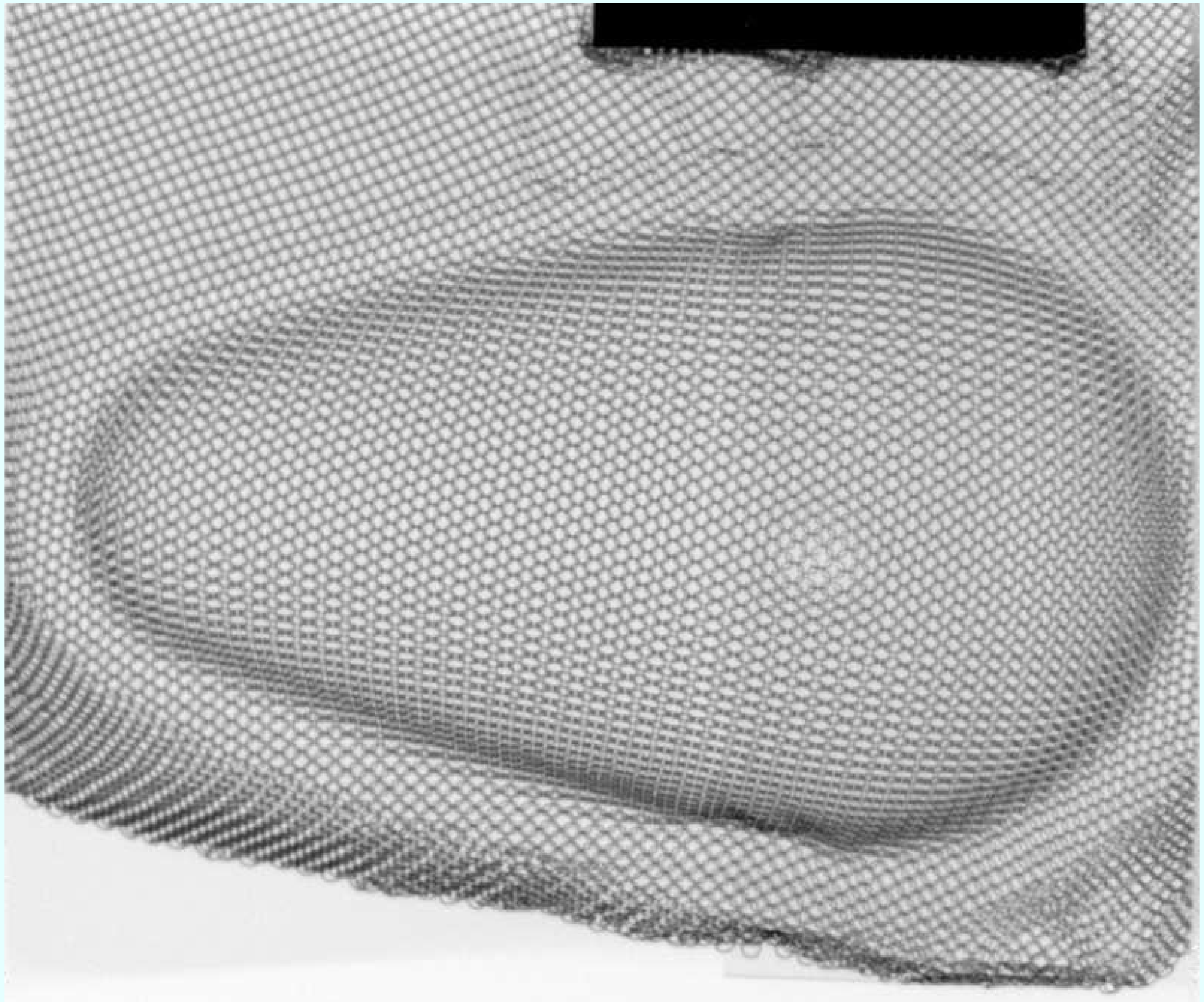

The X-ray image shows dents and even some faults without revealing the causes.

Comparison and combination of X-ray and neutron images

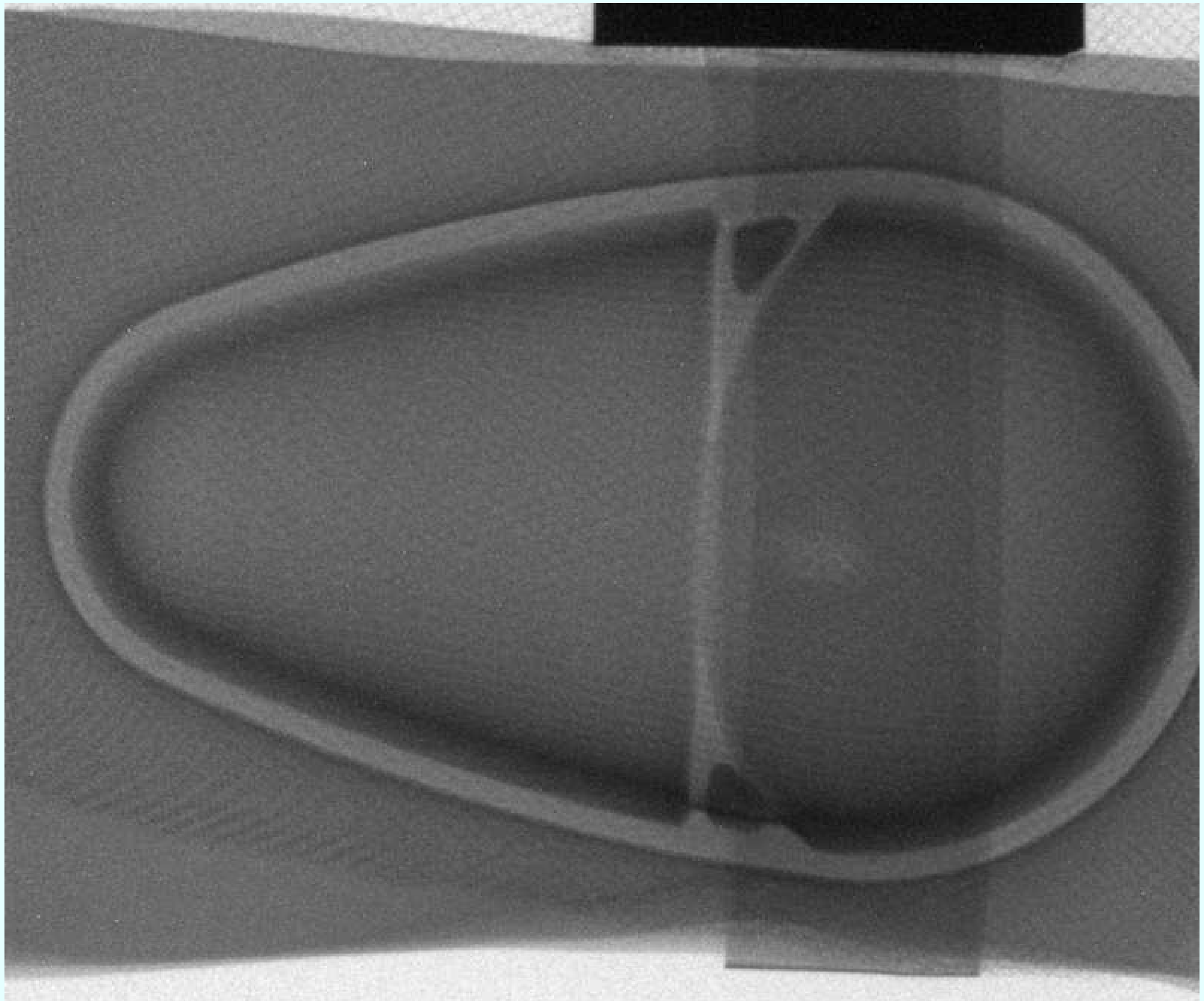

The Neutron image gives very gould contrast on the hydrogen of the foam material, but rather low contrast on the chain mail.

Comparison and combination of X-ray and neutron images

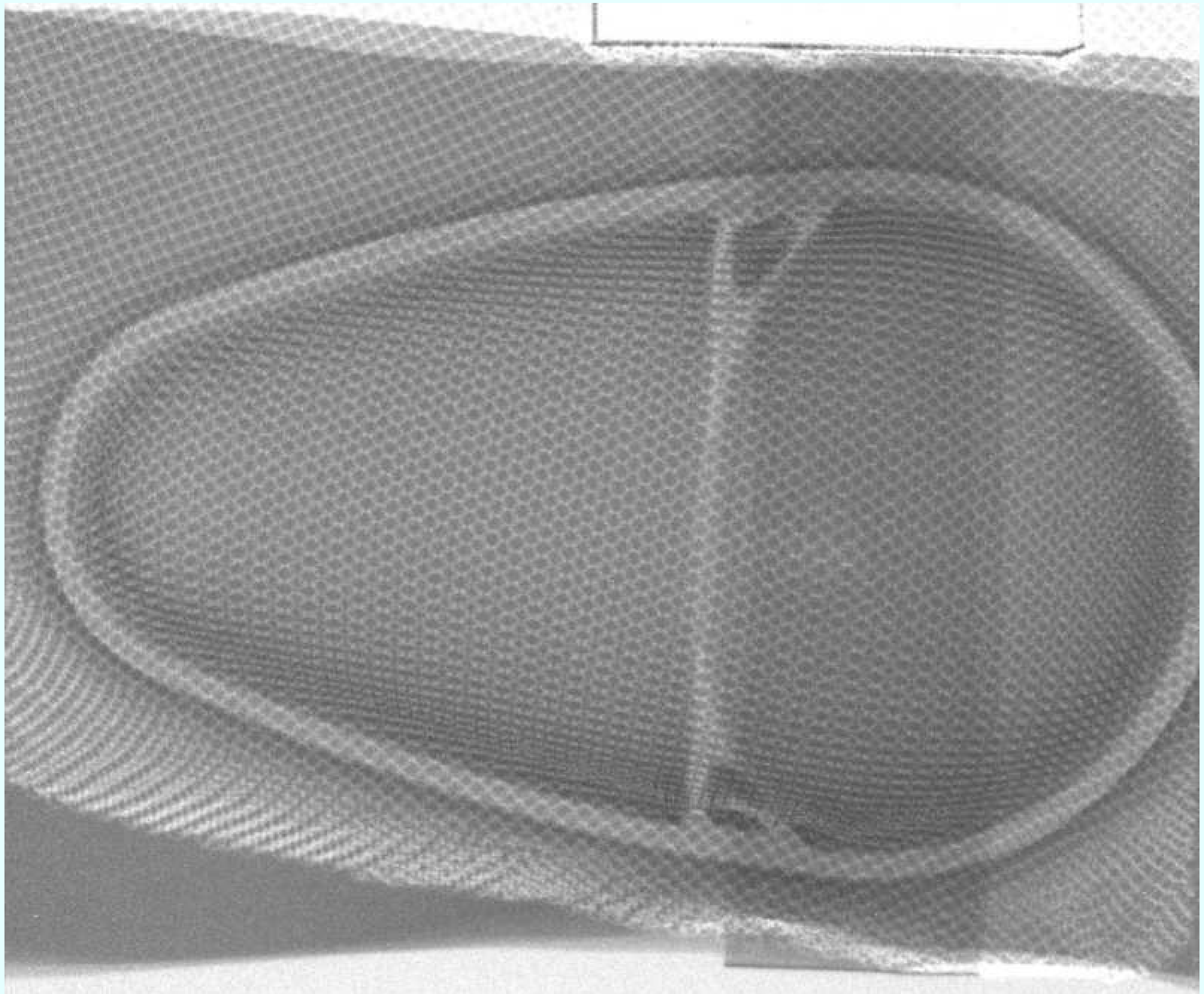

The combination of both images reveals the shape of the rubber foam as well as the embedded chain mail.

Comparison and combination of X-ray and neutron images

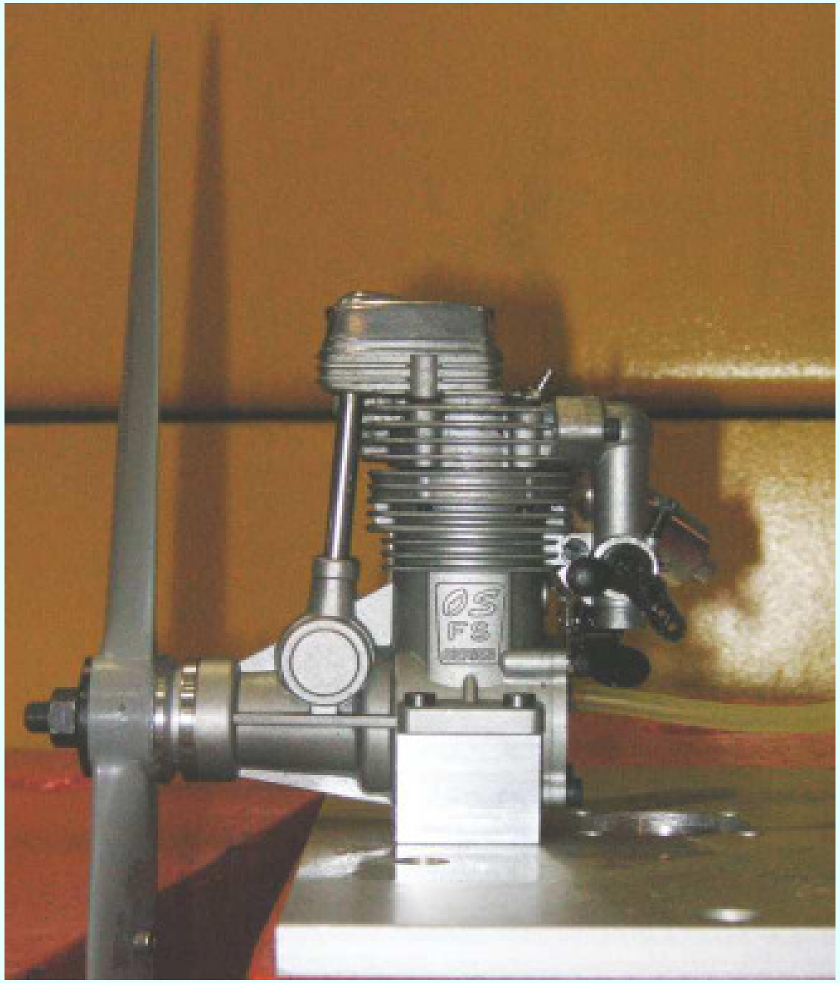

A toy plane combustion engine with a plastic propeller is another good example for the different properties of X-rays and neutrons.

Comparison and combination of X-ray and neutron images

The X-rays easily penetrate the plastic propeller, still penetrate the Aluminium well, but are heavily attenuated by steel parts.

Comparison and combination of X-ray and neutron images

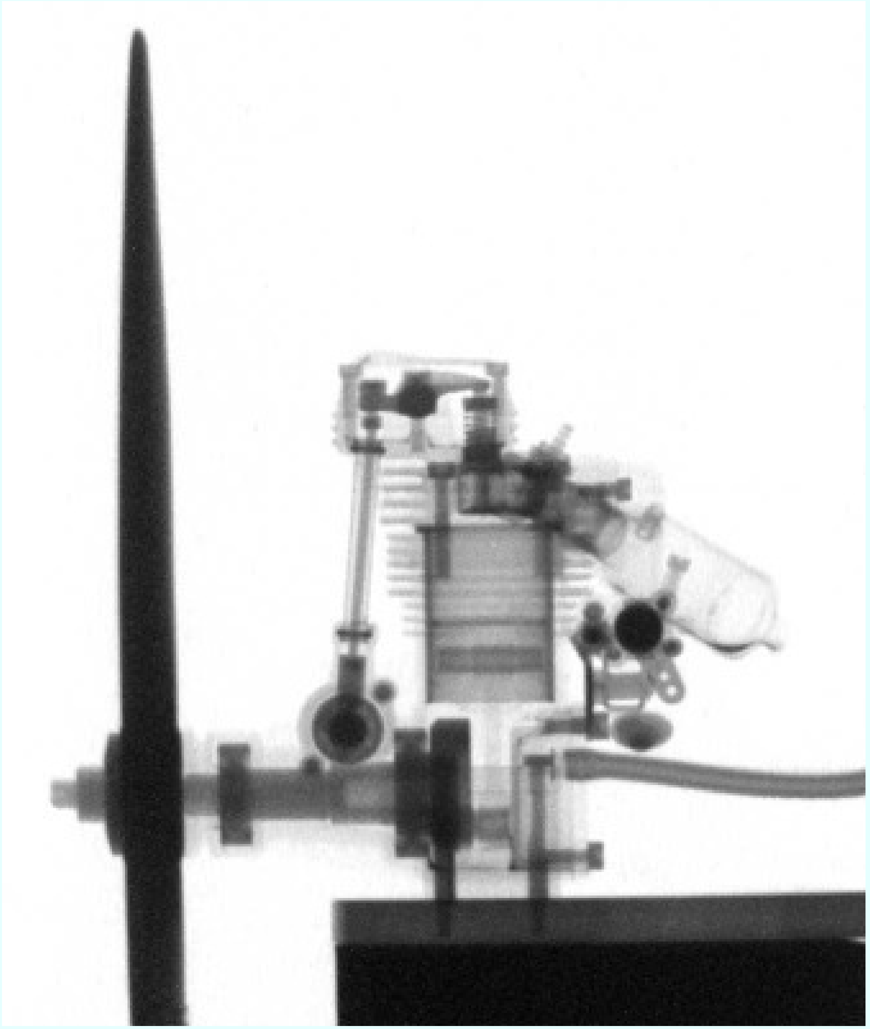

Aluminium is very transparent for neutrons, steel is better penetrated than by X-rays, but plastic is very opaque..

Neutron computed tomography

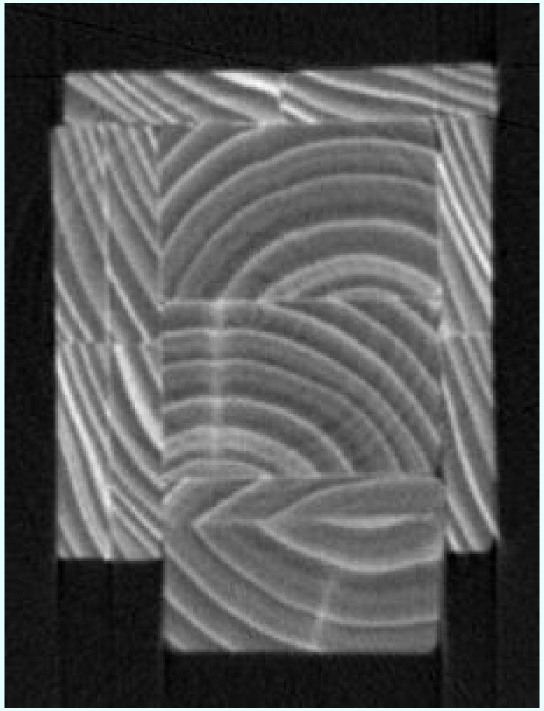

wood
block

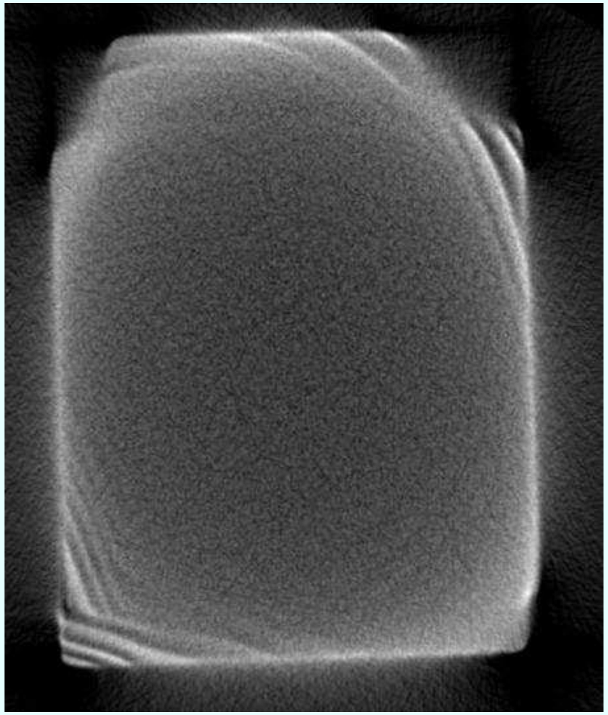

X-ray

neutrons

Neutrons are not always better...

...but in many cases, they are!

First Tomographies at FRM-II.



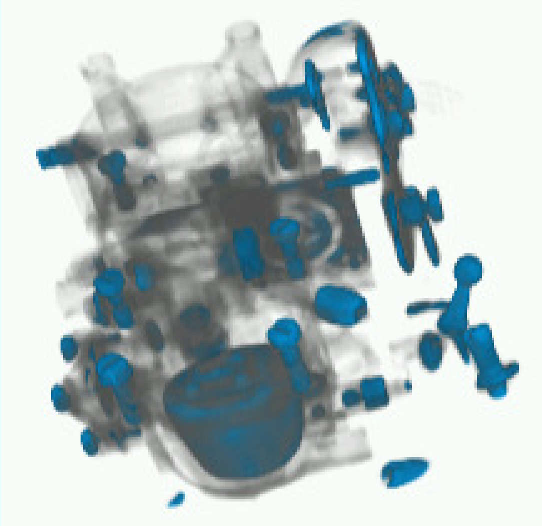
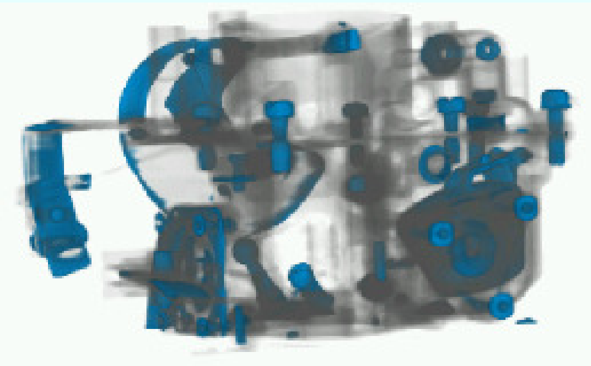
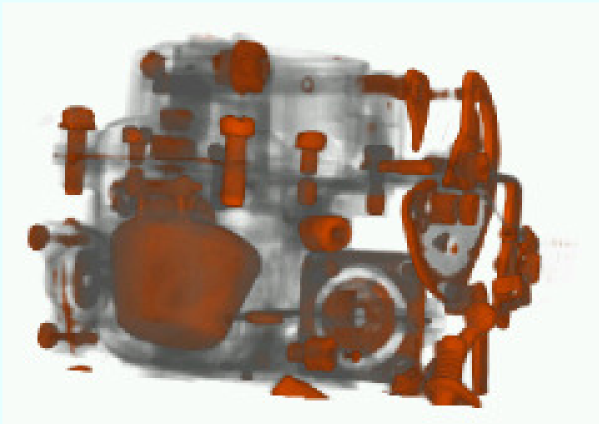


First results

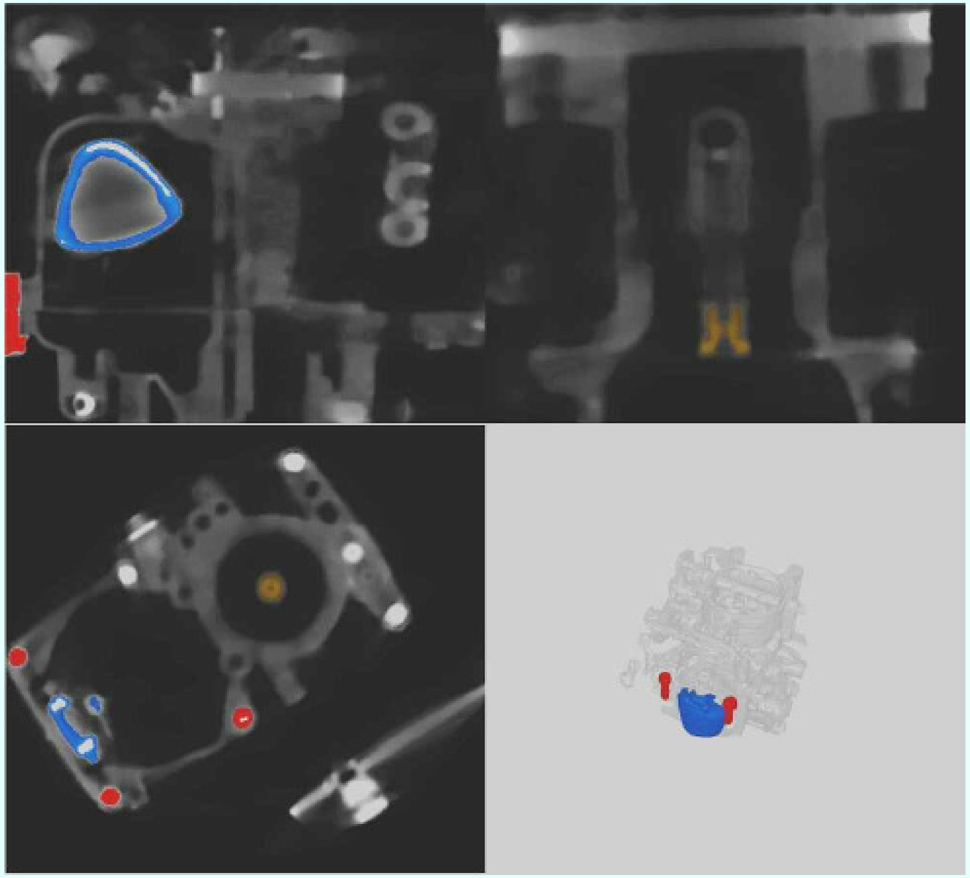

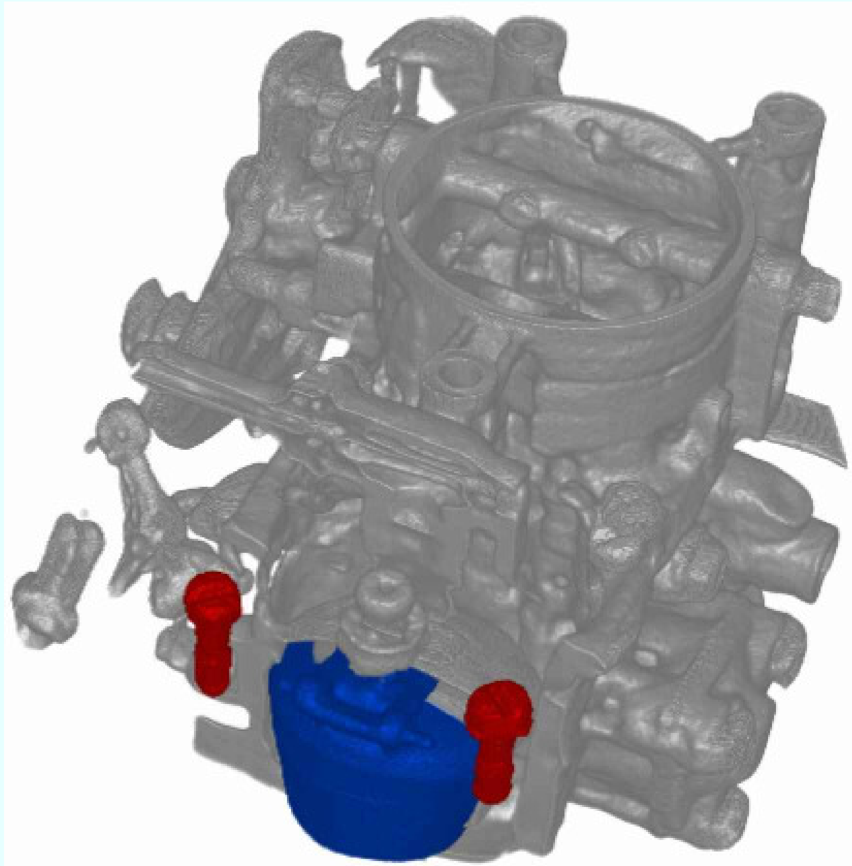

Segmentation of the data

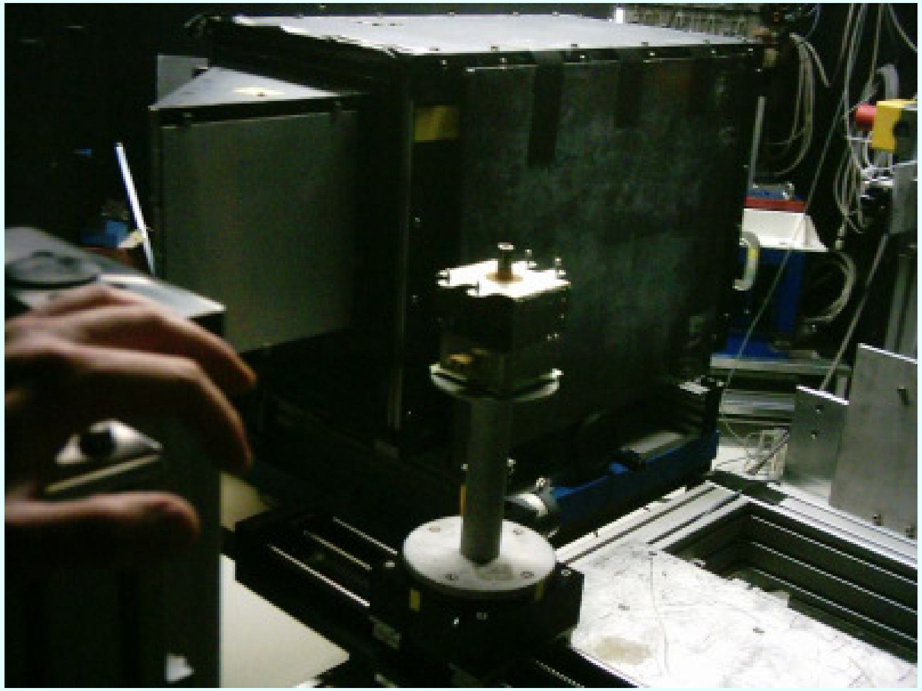

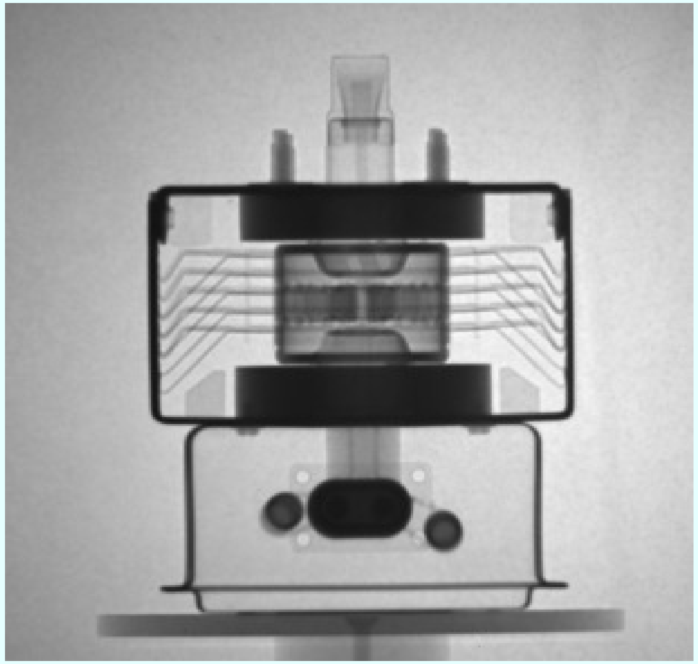

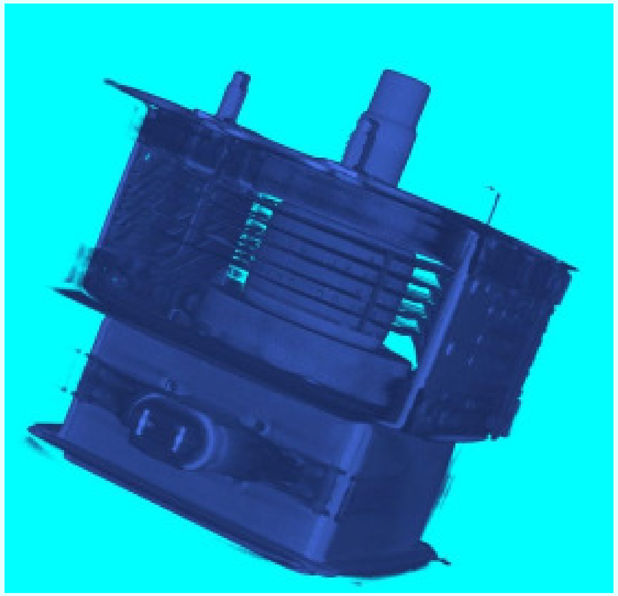

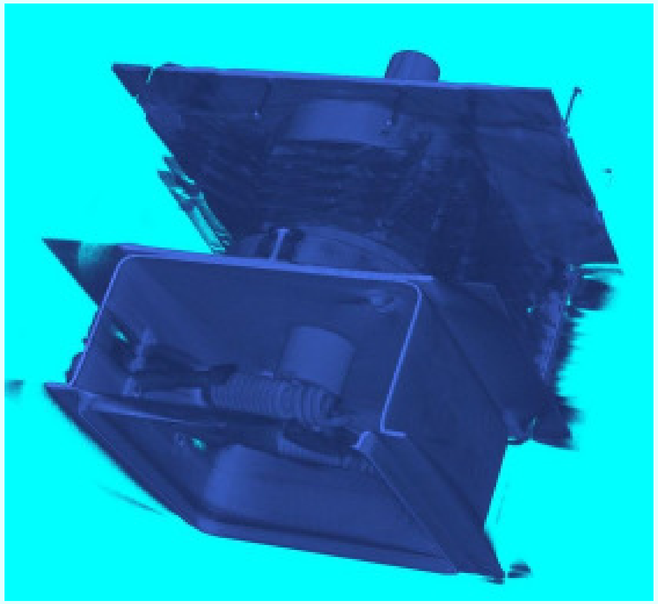

Radiography and tomography of a microwave klystron

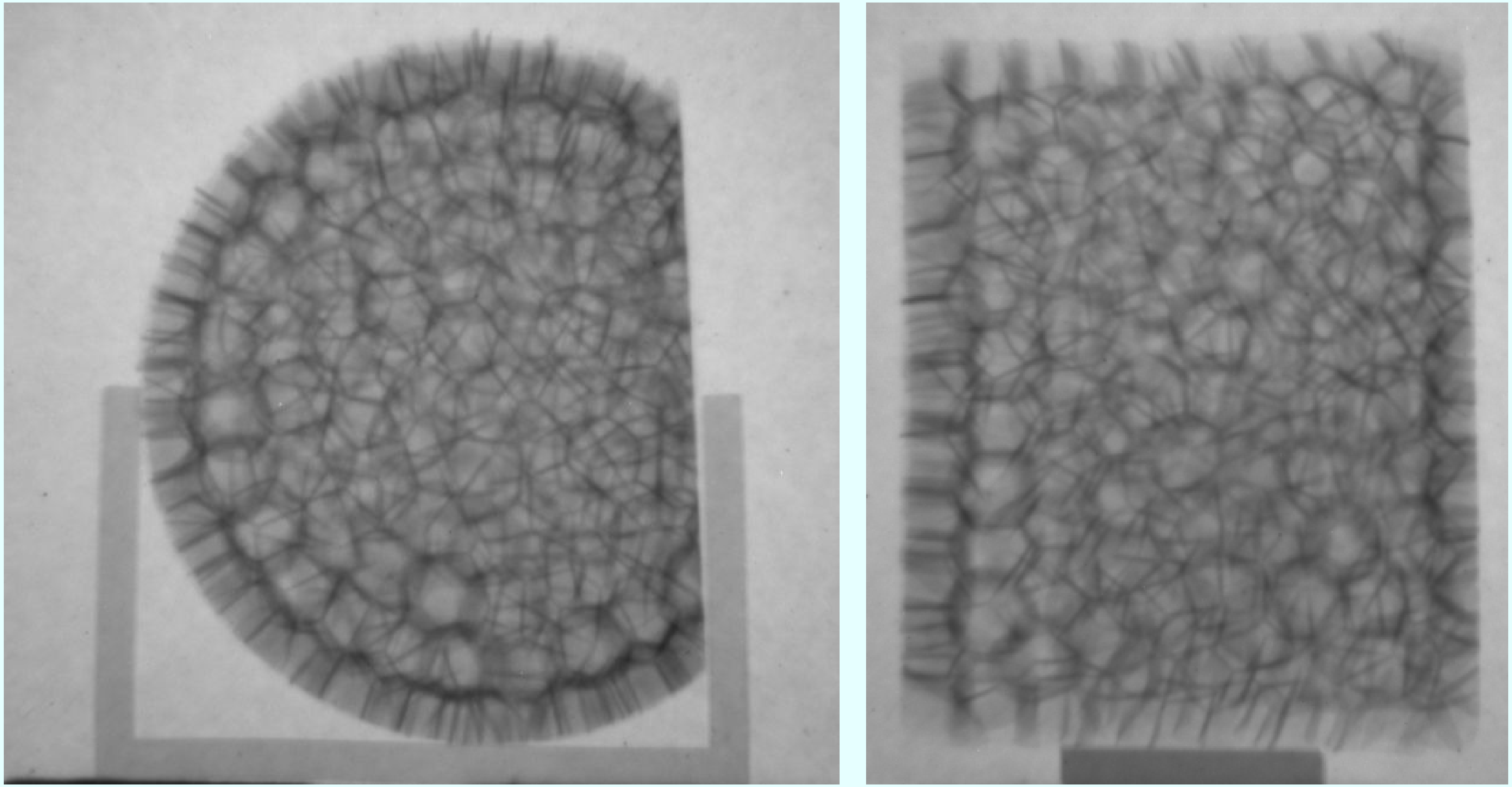

Radiography of a metal foam

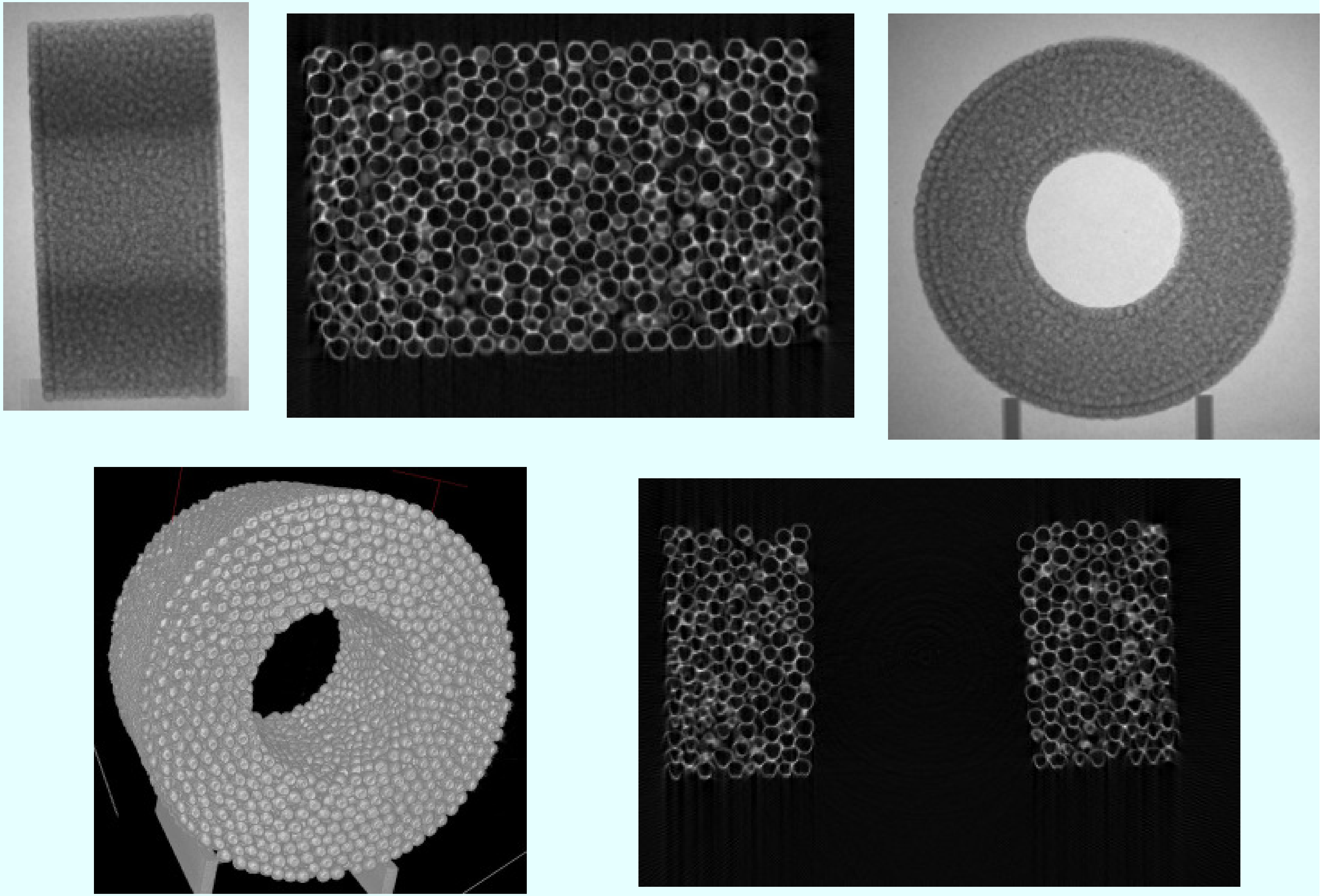

Radiography and tomography of a hollow spheres catalyst

B.Schillinger

Small Angle Scattering

in Neutron Computed Tomography:

Detection of texture alteration in Al parts

using Neutron Computed Tomography

B. Schillinger, M. Hofmann
TU München FRM-II / Physik E21
A. Steuwer, R. Gähler
Institut Laue-Langevin, Grenoble
L. Edwards
The Open University , Milton Keynes

Detection of imprinted car chassis numbers

in smooth-polished metal sheets

E. Calzada, H. Li
TU München FRM-II / Physik E21

The standard method:
Measurement of residual stress with neutron diffraction

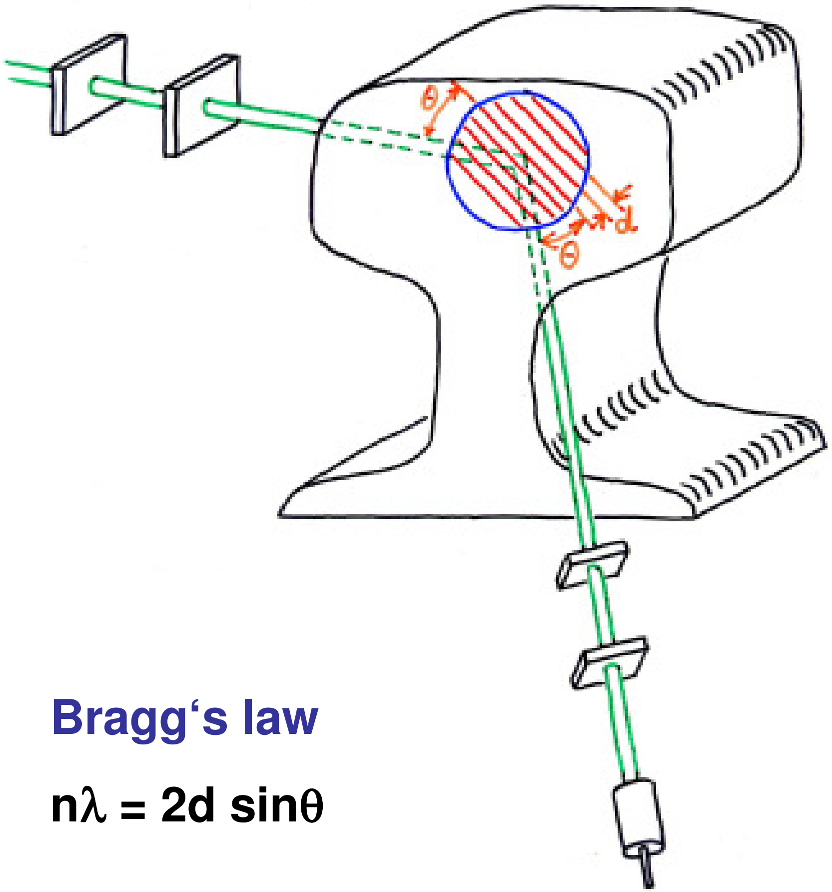

Bragg‘s law

$$n\lambda = 2d \sin\theta$$

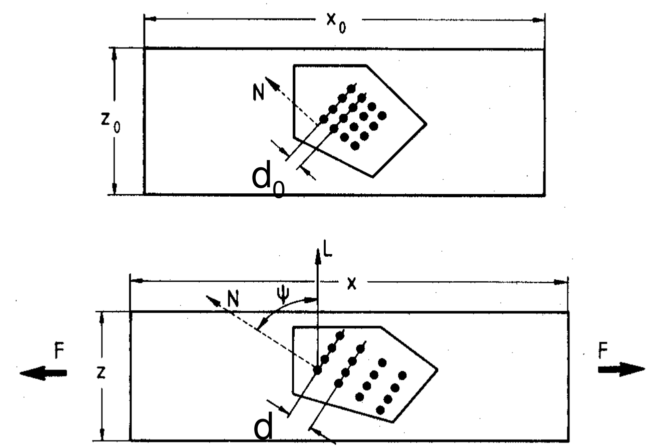

Residual stress

$$\sigma = E * \frac{\Delta d}{d}$$

STRESS-SPEC at FRM-II

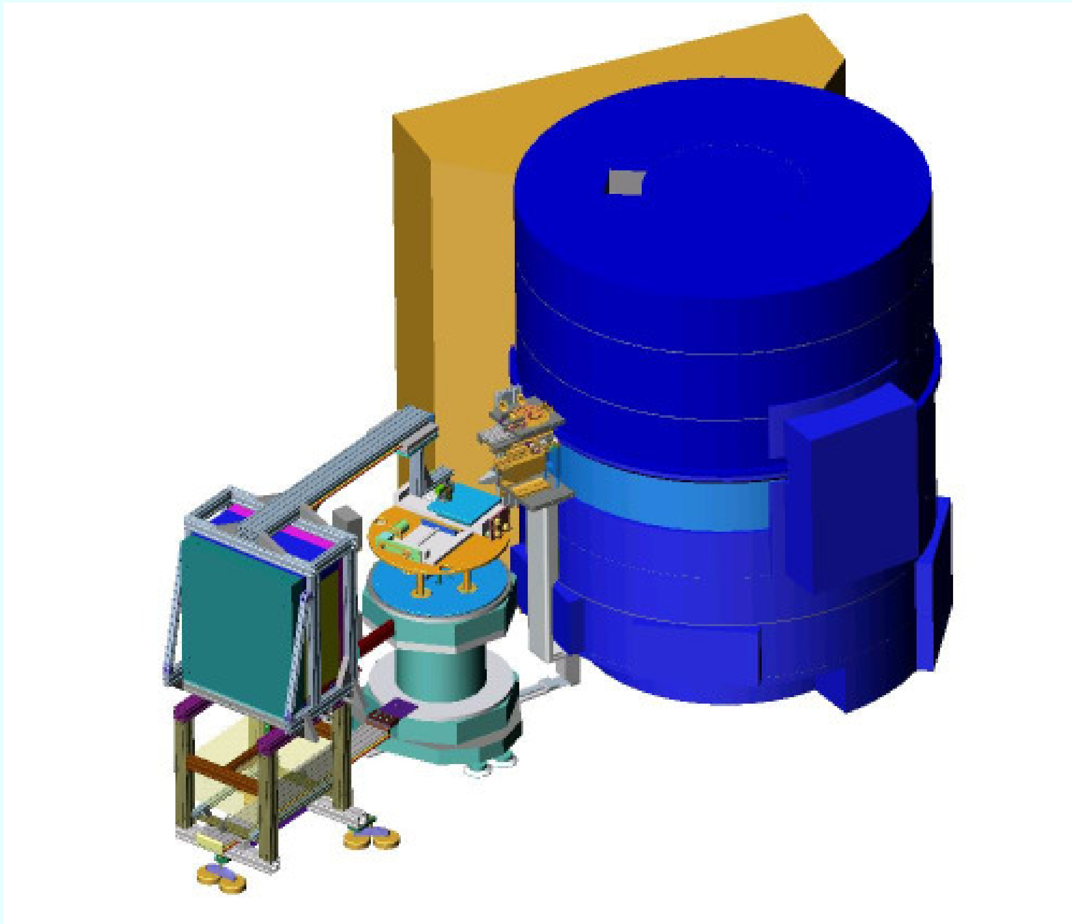

Optimised diffractometer

- neutron flux
- sample geometries
- gauge volume
- resolution

Peak analysis

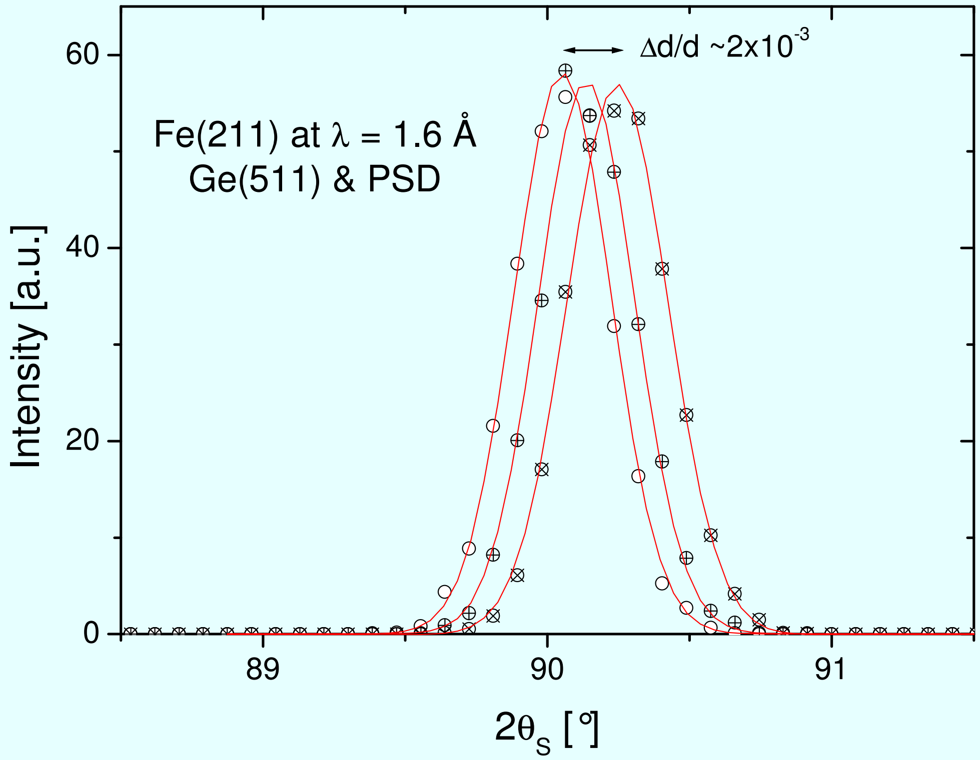

- Gaussian peak profile
- Peak shift simulated using Fe(*211*) reflection with Q-values: 5.3439 Å^{-1}, 5.3492 Å^{-1} , 5.3545 Å^{-1}

Cold expanded fastener holes

- The primary source of aircraft fatigue is at joints.
- Cold expansion increases joint durability.
- Quantification of the benefits of cold expansion requires accurate reliable residual stress estimation.

The cold expansion process

- The most common method is FTI split sleeve expansion.
- At present, air worthiness authorities do not allow the benefits of cold expansion to be included in design calculations.

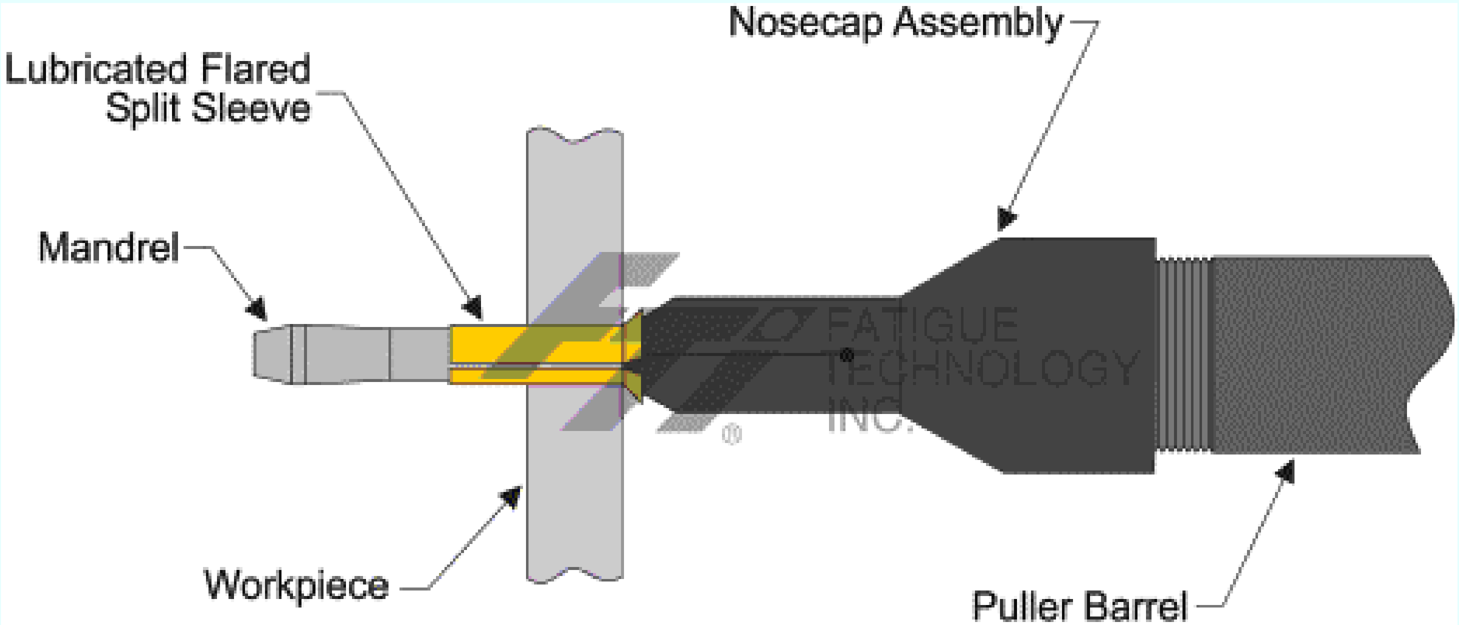

Picture:*http://www.fatiguetech.com/products/splitsleeve.html*

The Split Sleeve Cold Expansion Process

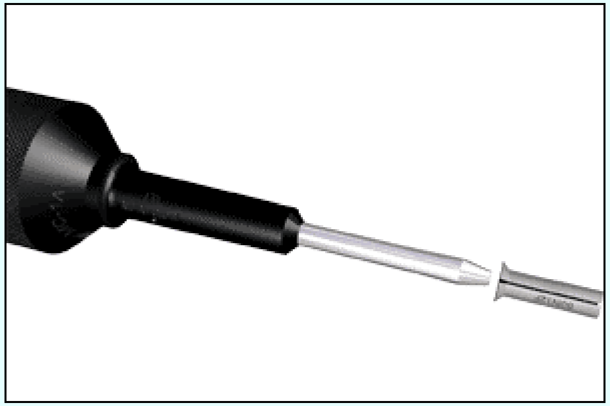

. **Step 1** After verifying the starting hole size, slip the pre-lubricated split sleeve onto the mandrel, which is attached to the hydraulic puller unit.

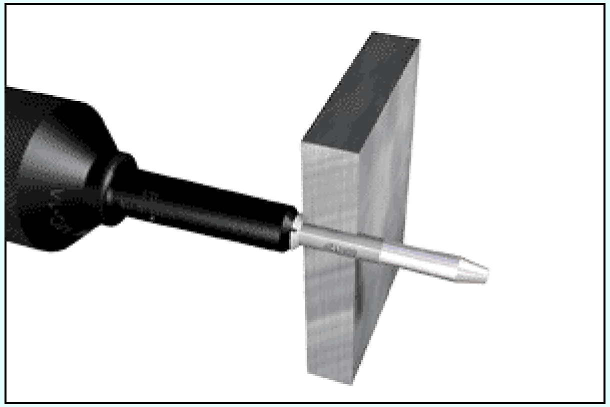

. **Step 2.**Insert the mandrel and sleeve through the hole with the nosecap held firmly against the work piece

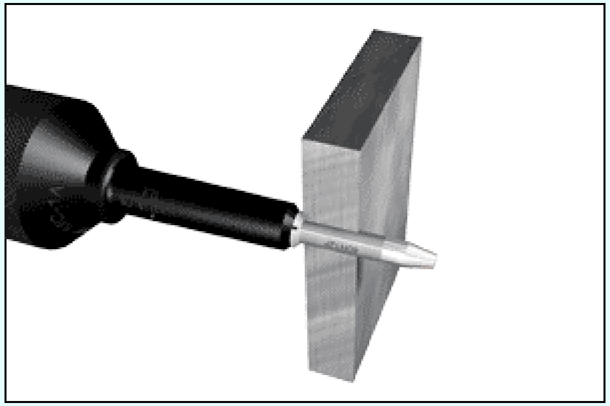

Step 3. Activate the puller unit. The mandrel is drawn through the sleeve and the hole. The combined thickness of the sleeve and the mandrel major diameter radially expand the hole. The lubricated sleeve reduces the pull force required, protects the hole, and allows the mandrel to exert radial forces through the entire thickness of the material.

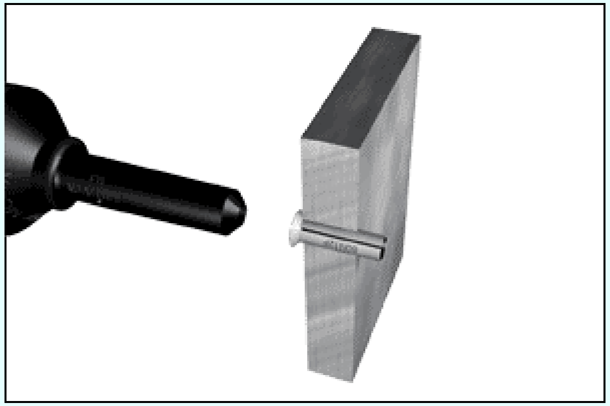

Step 4. Remove and discard sleeve

Measurement of Aluminium aircraft component by neutron computed tomography: (Idea by R. Gähler, ILL)

•Holes are drilled with less than the required diameter,

• then the holes are cold expanded with a thorn.

• At the edges, the Aluminium is compressed and deformed, the inner structure is altered.

•This is done to introduce compressive stress into the material to anticipate tensile stress from rivets in the hole.

• This leads to increased small angle scattering, showing more attenuation around the hole edge.

•The effect is NOT visible at ordinary holes.

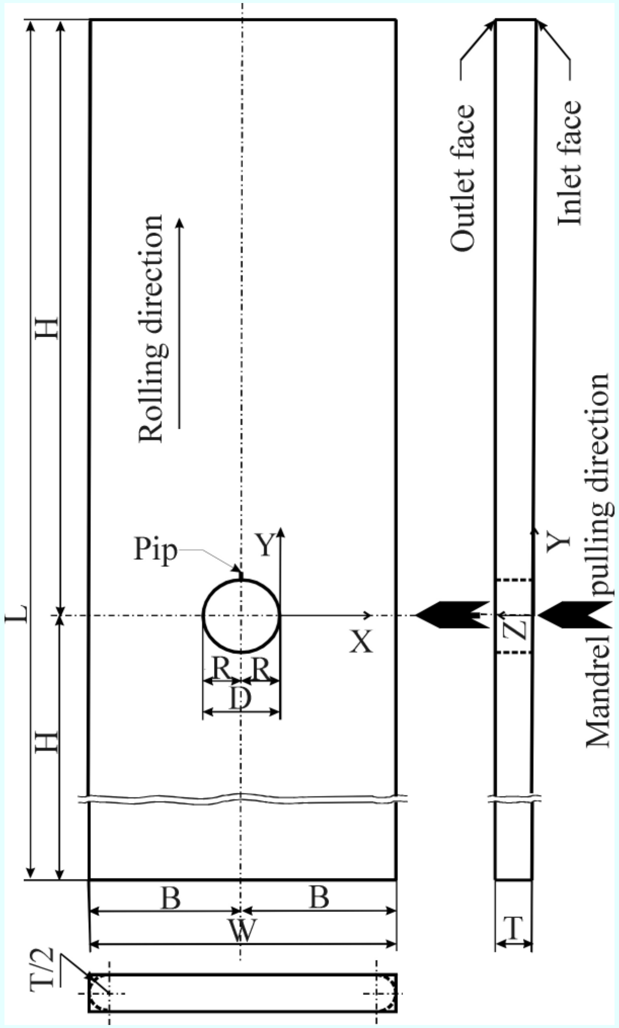

Test sample:

Aluminium sheet

Rolled out along the longitudinal direction

180 mm length, 40 mm width, 5 mm thickness

Initial hole drilled with diameter 9.52mm (3/8inch)

Cold expansion (4%) to 10 mm diameter

Strain measurements with synchrotron radiation, neutrons, and simulated data

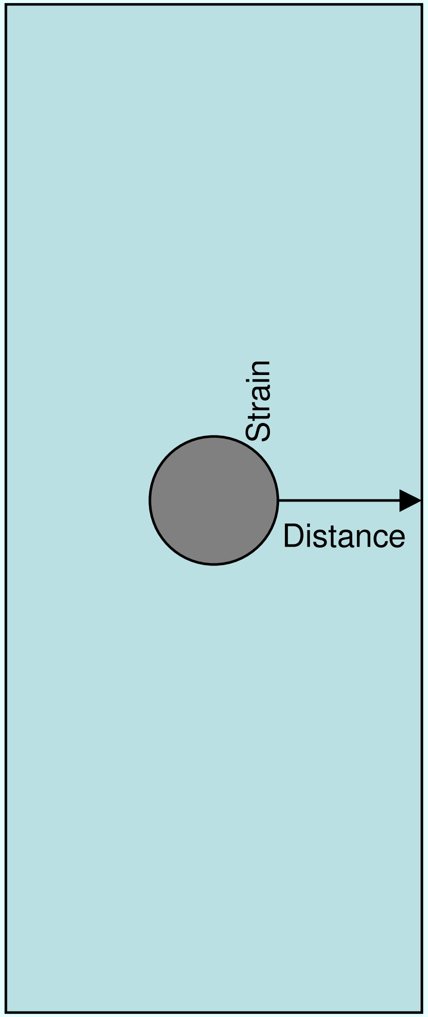

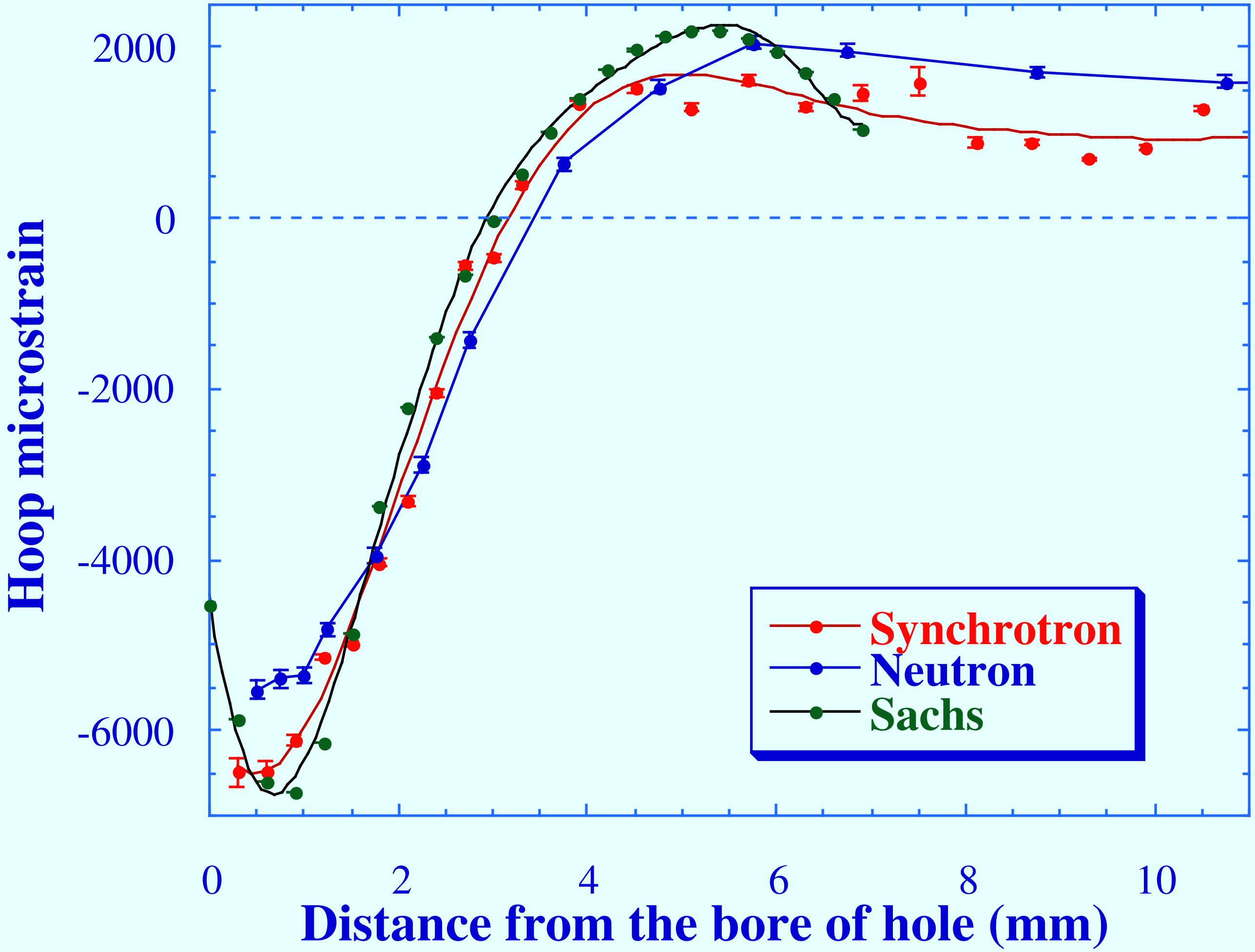

Measurement of a 3D computed tomography of the test sample

• Distance sample to detector was approx. 50 cms.

• 400 projections recorded for calculation of the tomography

• The tomography delivers a range interval of gray values for the attenuation of Aluminium

• For visualisation of the 3D tomography, nearly the whole attenuation range for Aluminium is set transparent, only the most attenuating part is set visible.

•The expanded area at the hole rim produces increased small angle scattering,
which in turn leads to increased attenuation of the transmitted beam.
The area clearly shows up in the computed tomography.

•Surprise: Even a wave structure resulting from the rolling of the Aluminium sheet is visible!

Piece of tape

Pieces of glue

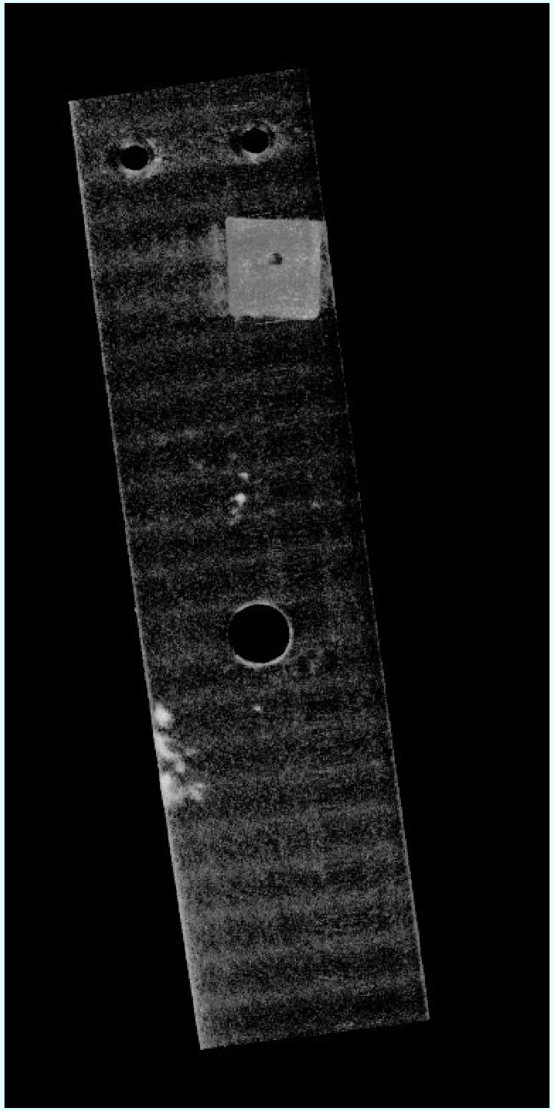

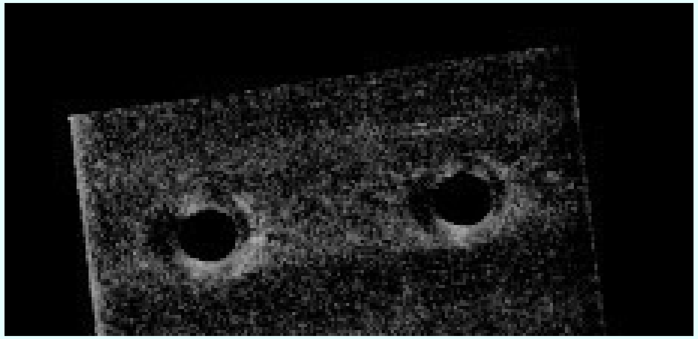

Ordinary holes with phased edges

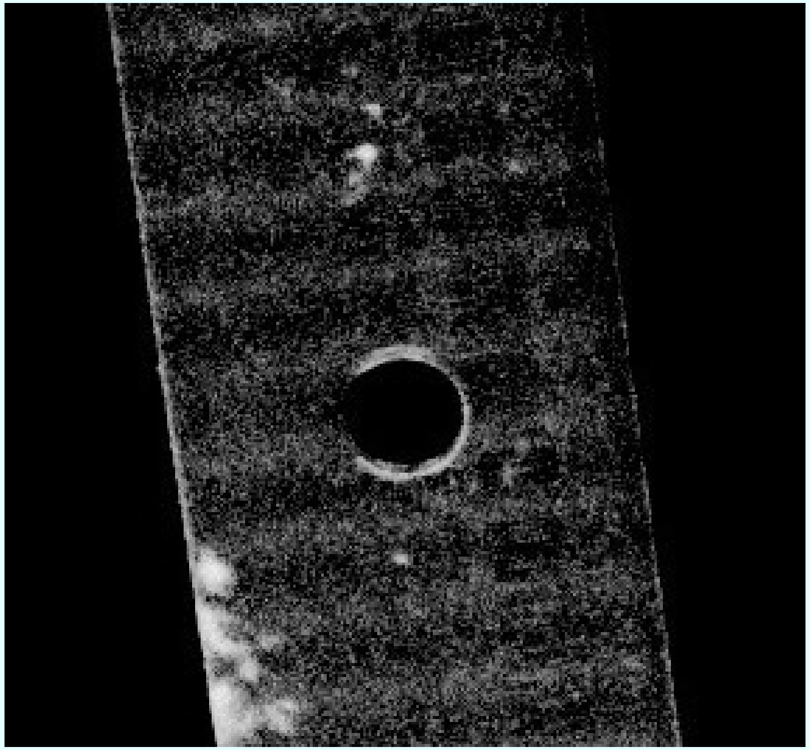

Widened hole compressed Edges.

The widening was asymmetric.

Surprise: Even a wave structure resulting from the rolling of the Aluminium sheet is visible!

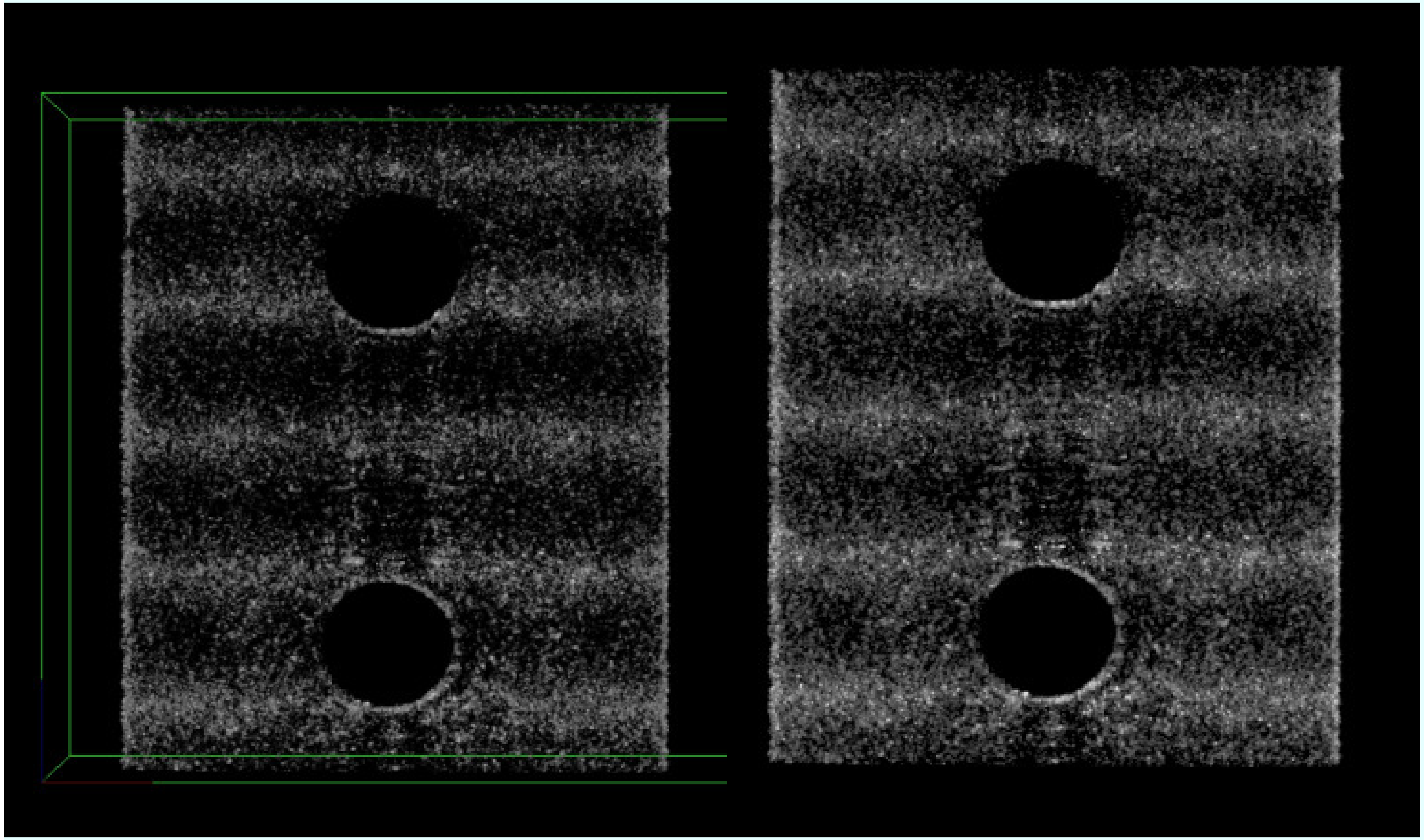

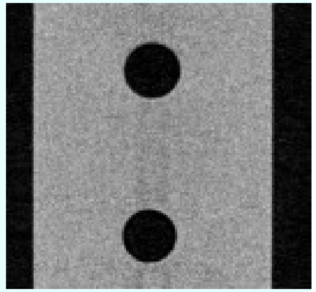

Above: Normal full view of the piece.

Second hole drilled for second tomography.

This was recorded with a smaller detector with less dynamics and sensitivity.
The distance to the detector was only 25 cms, but still, the difference is clearly visible!

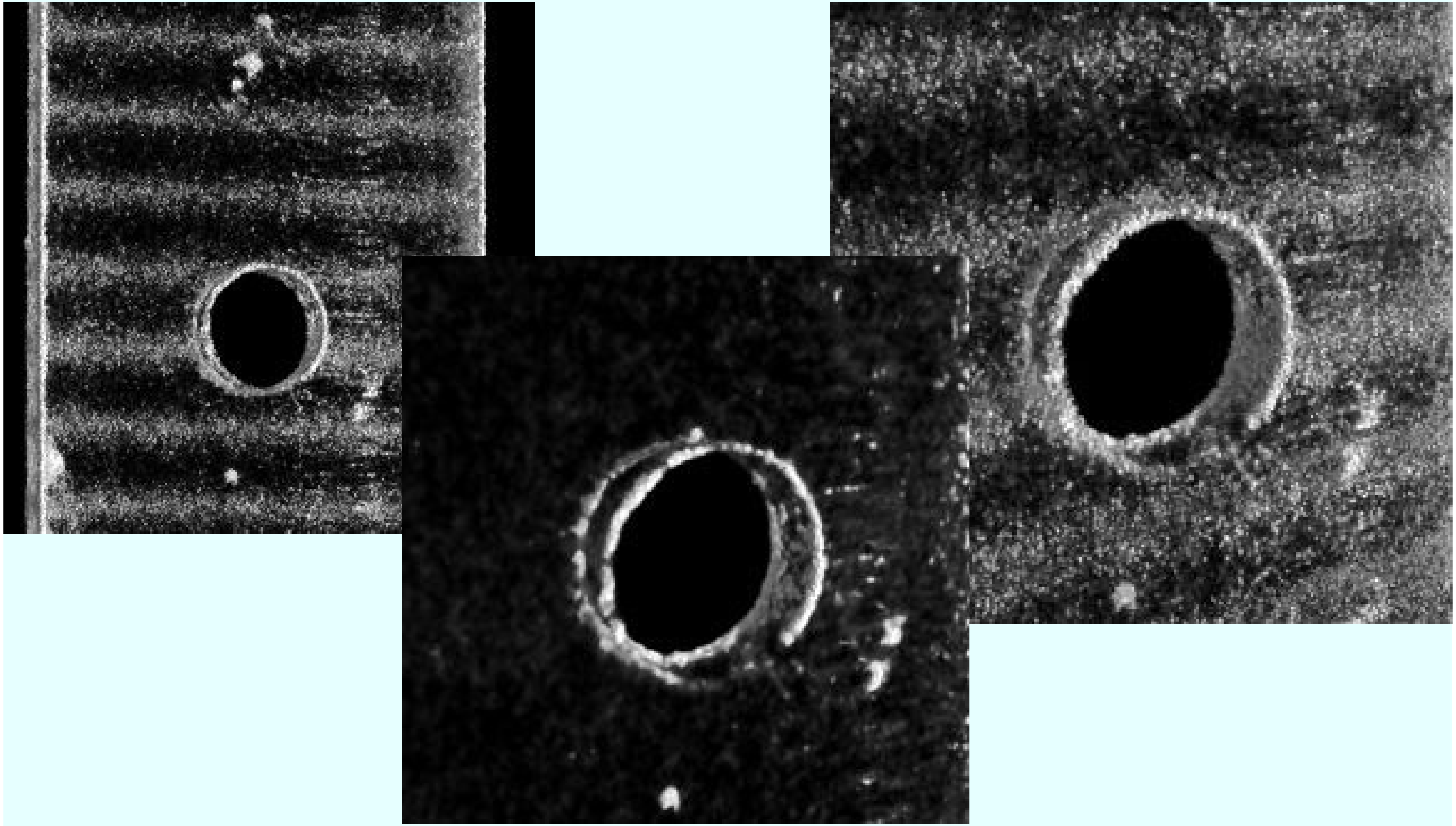

These pictures show more clearly that they represent a true 3D tomography.

Detection of imprinted car chassis numbers in smooth-polished metal sheets

E. Calzada, H. Li
TU München FRM-II / Physik E21

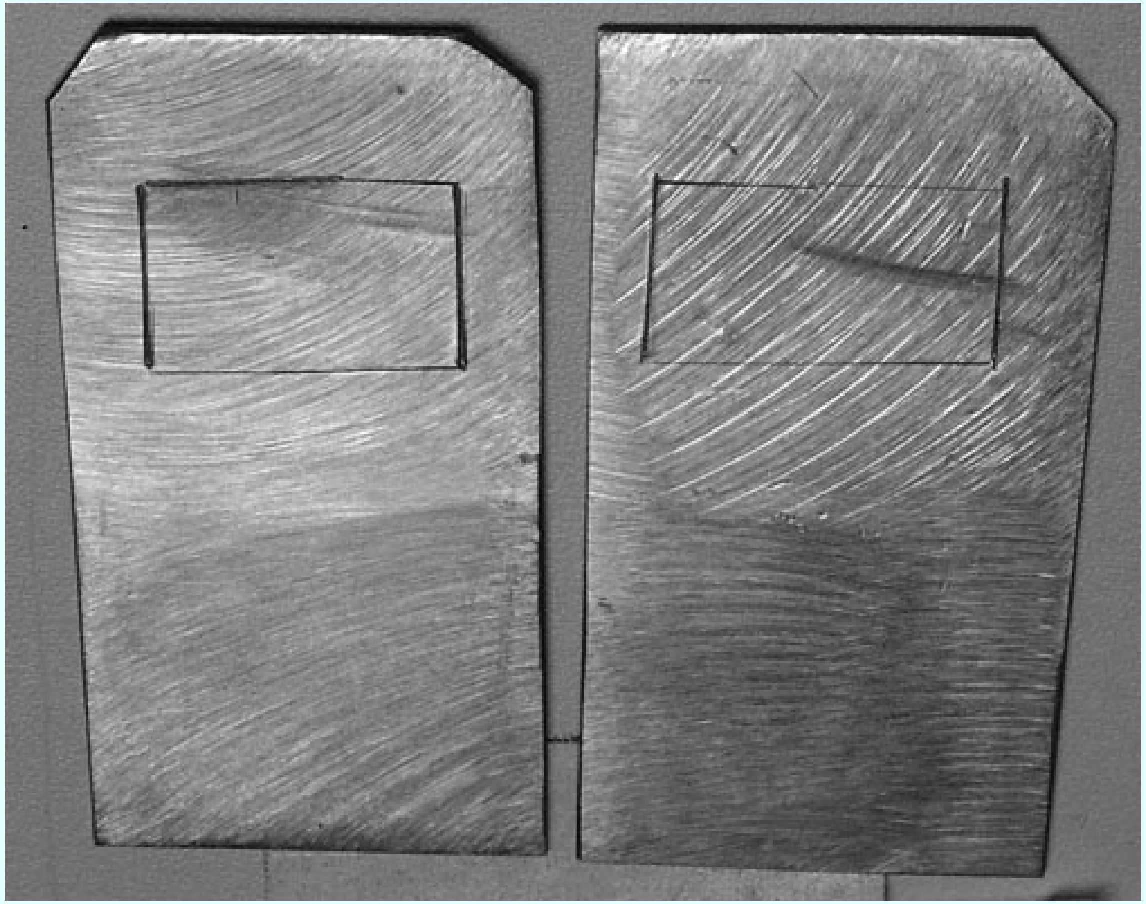

The police brought us two smooth-polished metal sheets, where originally the car chassis numbers had been imprinted.

Nothing is visible on the surface, but deep in the metal, the structure has been altered…

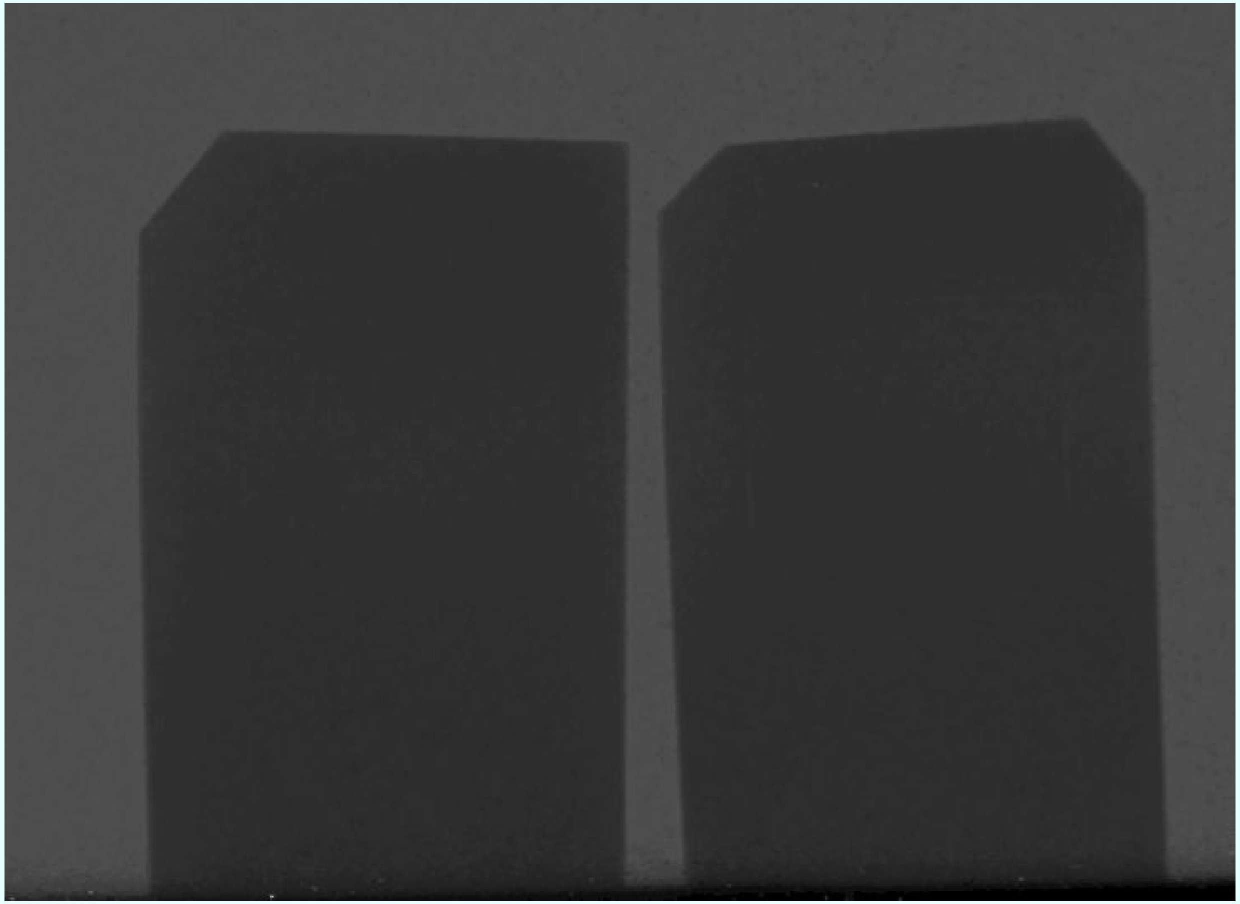

The normal radiography shows nothing at all.

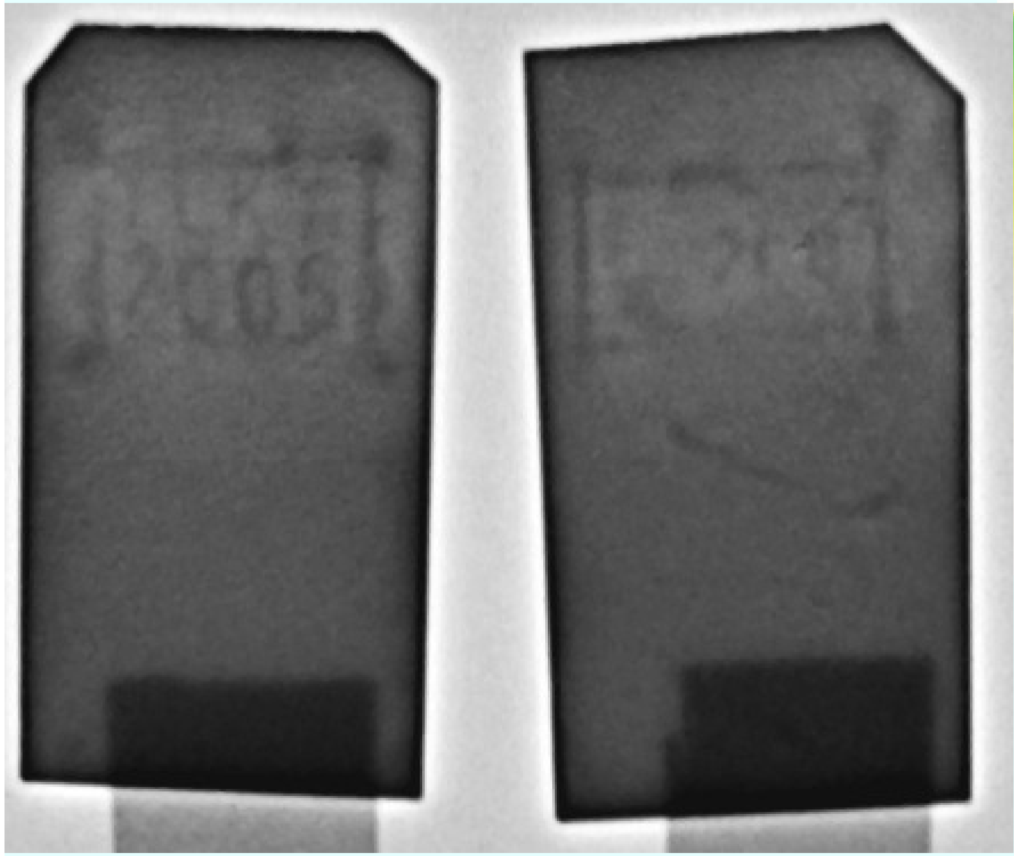

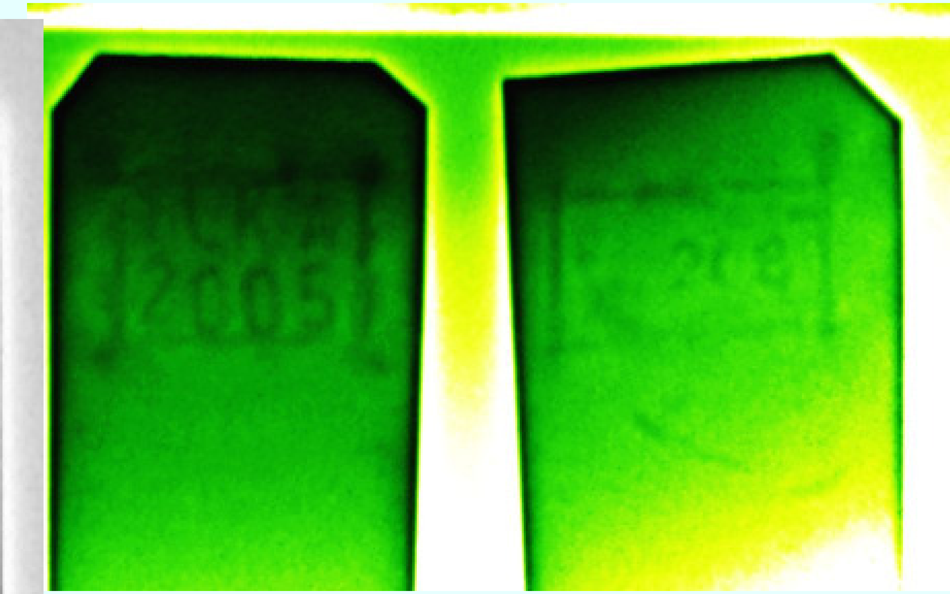

But with a 7 mm pinhole, and 2 meters distance to the detector…

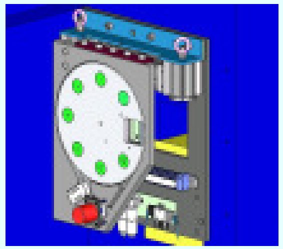

Non-destructive Testing with Phase Contrast Imaging

K. Lorenz, E. Lehmann, E. Steichele, P. Vontobel

1. **Introduction**
2. **Theory**
3. **Experimental Setups at PSI and FRM-II**
4. **Applications of the Phase Contrast Effect**
5. **Phase Retrieval**

Phase Contrast Radiography with X-Rays and Synchrotron Light

X-ray image of a genetically engineered mouse (source: www.xrt.com.au):

Conventional radiography

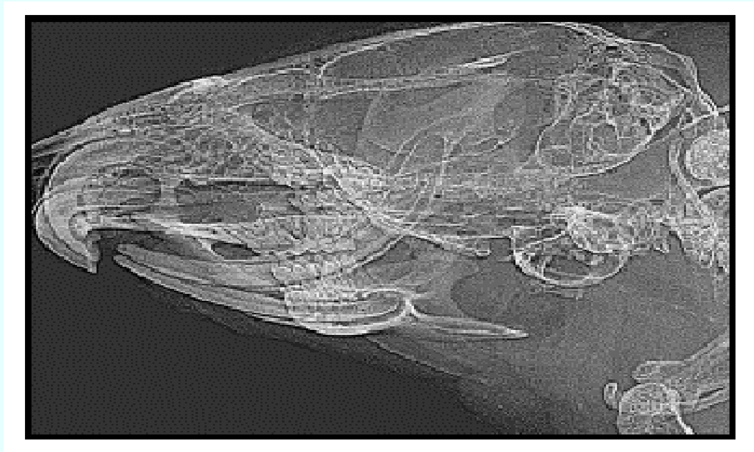

Phase contrast radiography

Refraction of a wave by a medium

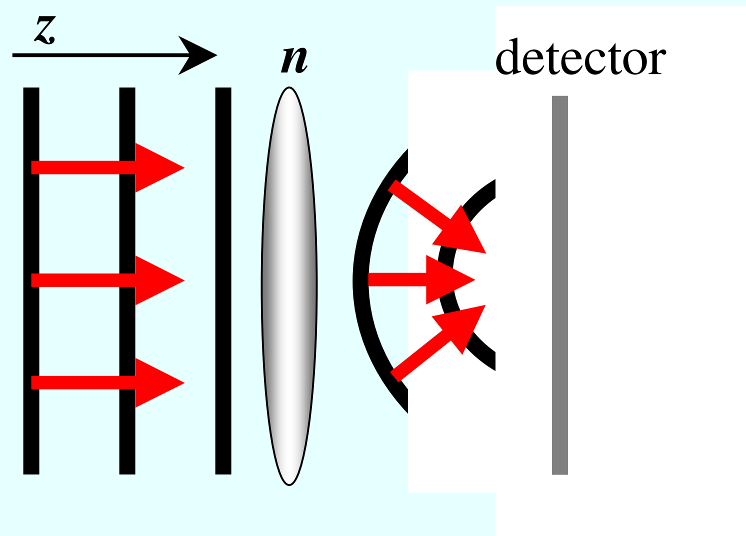

Refractive index:

phase shift absorption

$n = 1 - \delta - i\beta$

Angular deviation of the normal: $\Delta\alpha \propto \lambda \left| \nabla_{\perp} \varphi \right|$

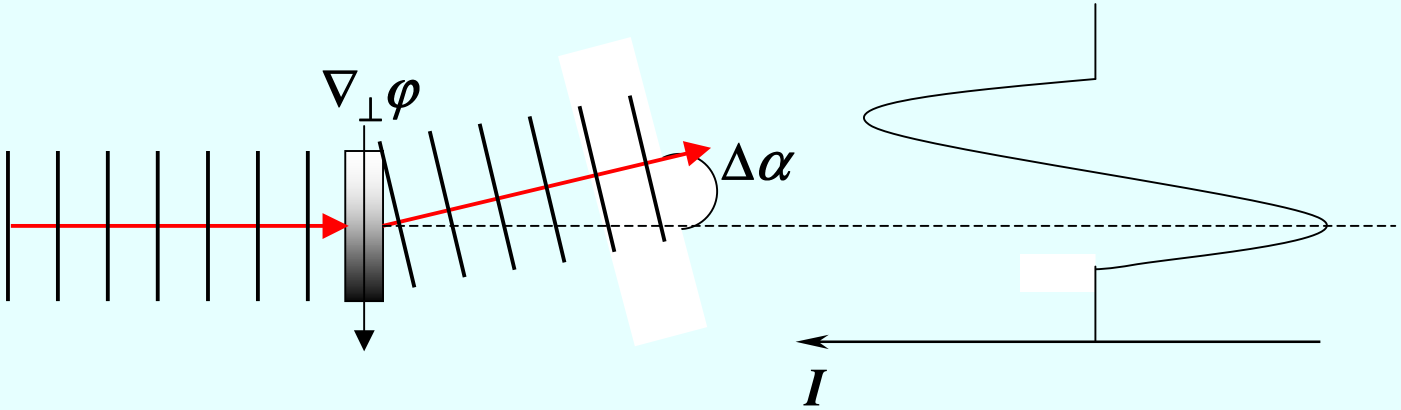

Fresnel diffraction

Phase shift of a wave on its way s through a spherical object Ω, with a refractive index $n = 1 - \delta_\Omega$:

$$\varphi(x, y; z, \lambda) = -\frac{2\pi}{\lambda} \int_s \delta_\Omega(x, y, z, \lambda) ds$$

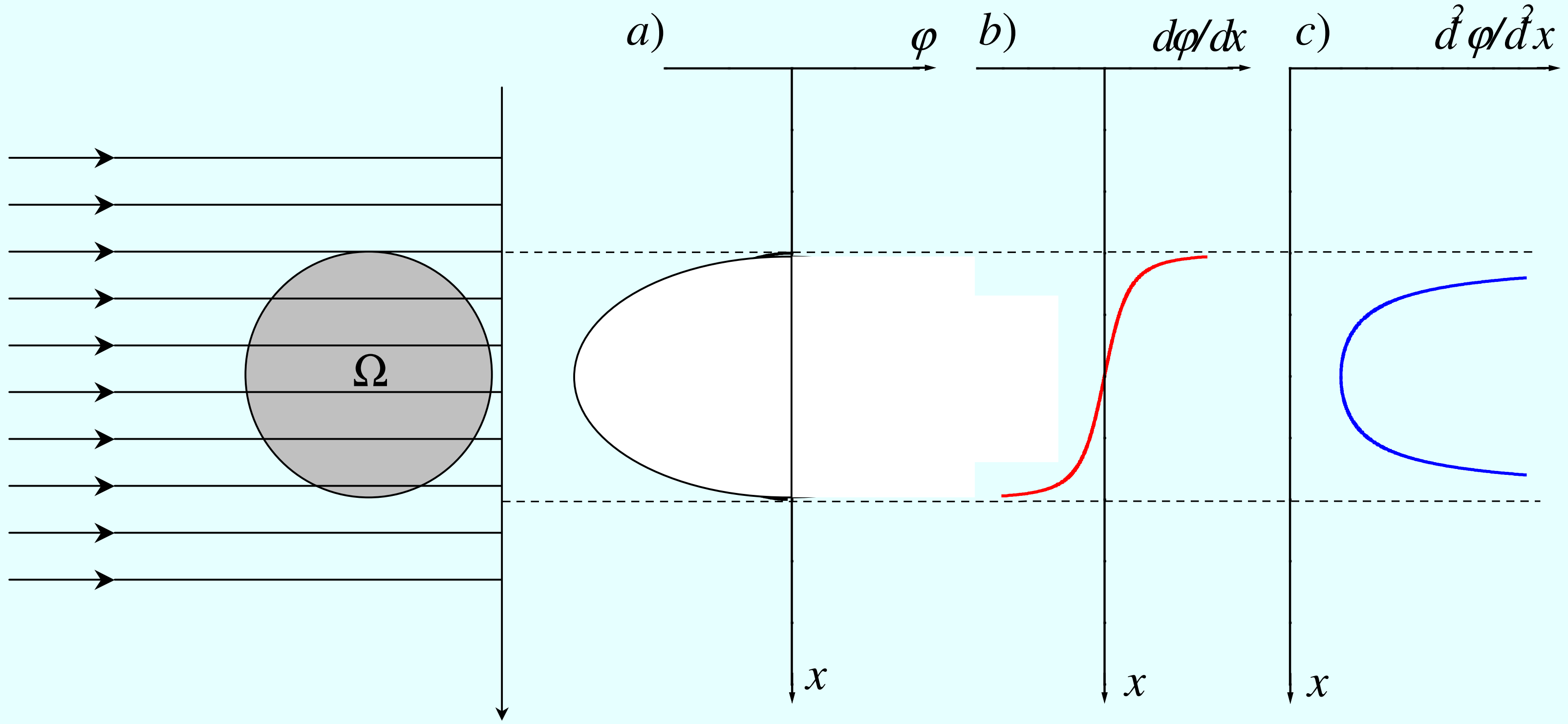

Requirements for Phase Contrast

1. Neutron beam with a high lateral spatial coherence length
2. The detector plane must be in the near field region

Schematic of a phase contrast radiography setup:

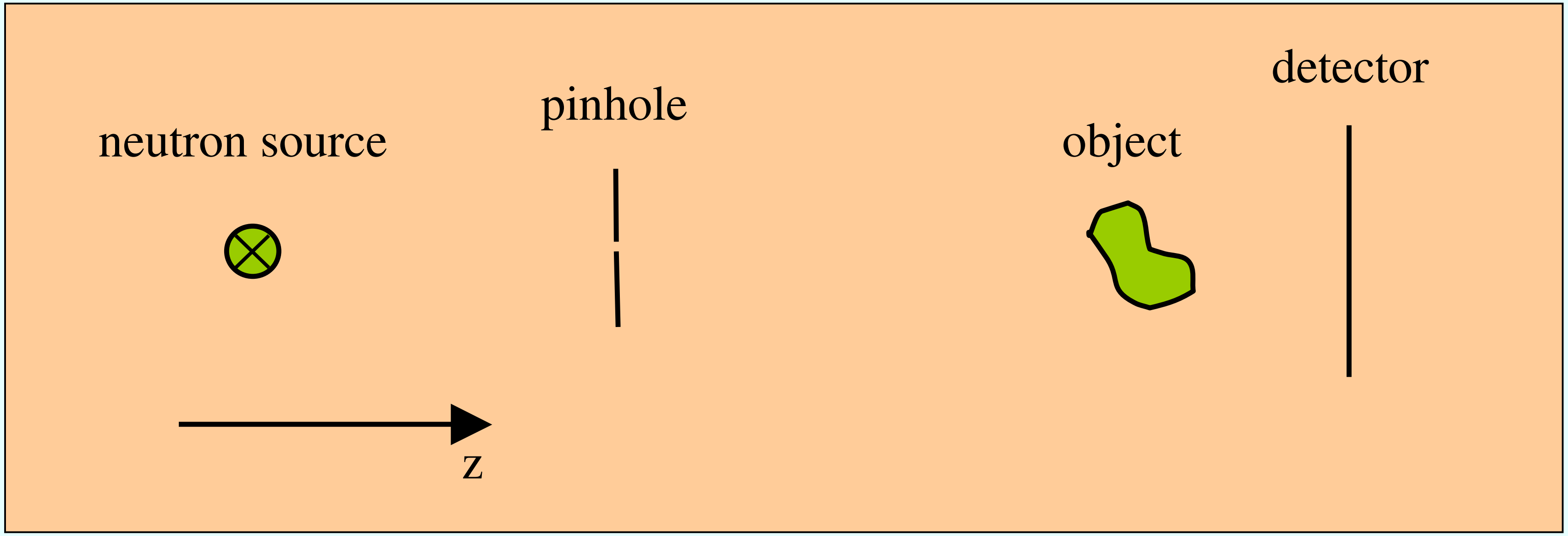

Non-destructive testing of casted components

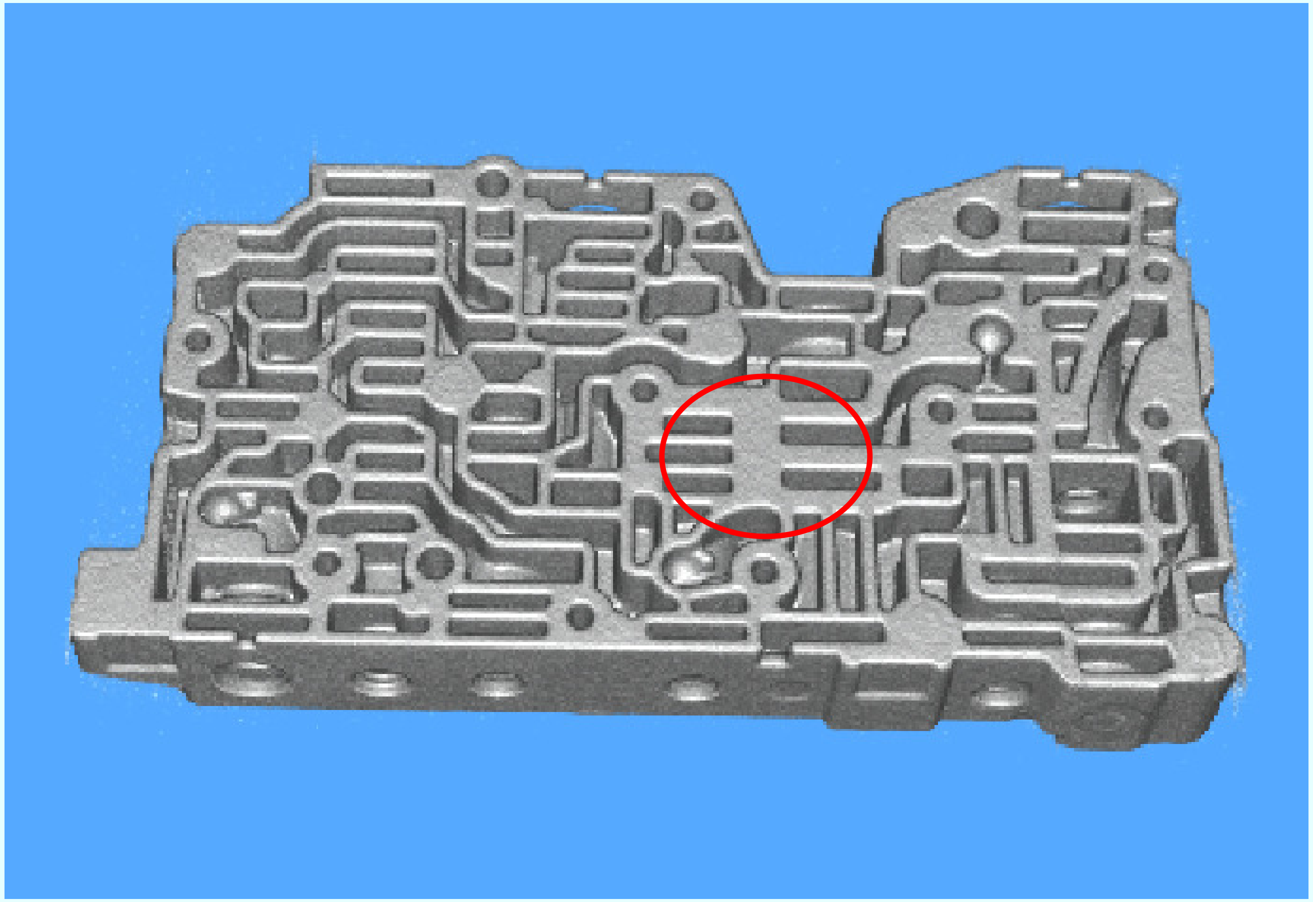

Non-destructive testing of casted components

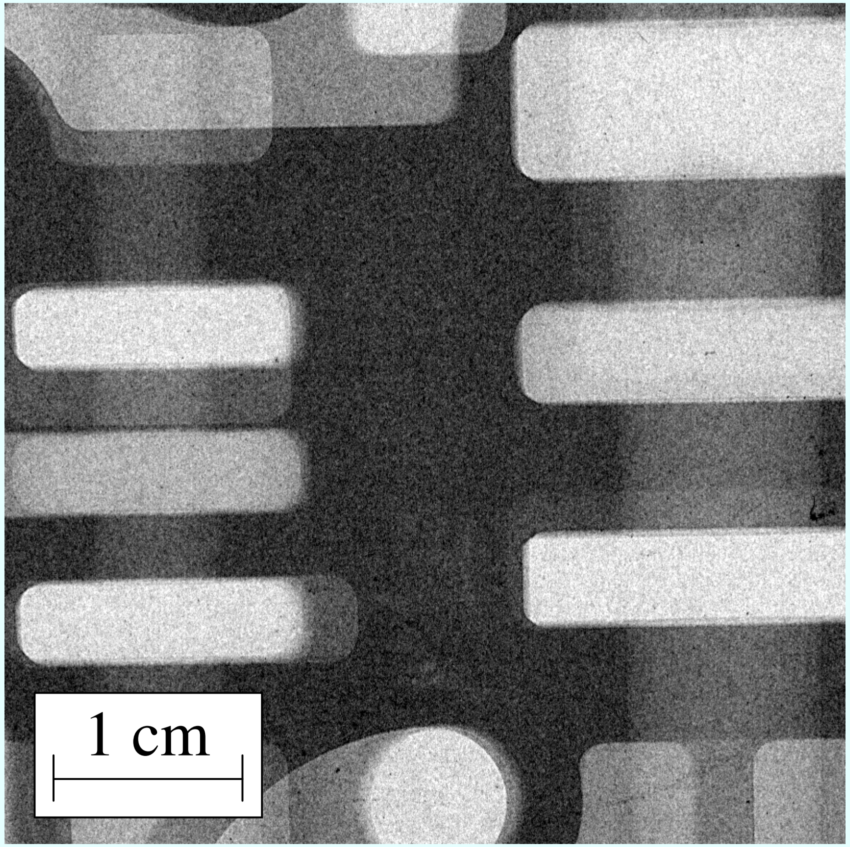

conventional radiography

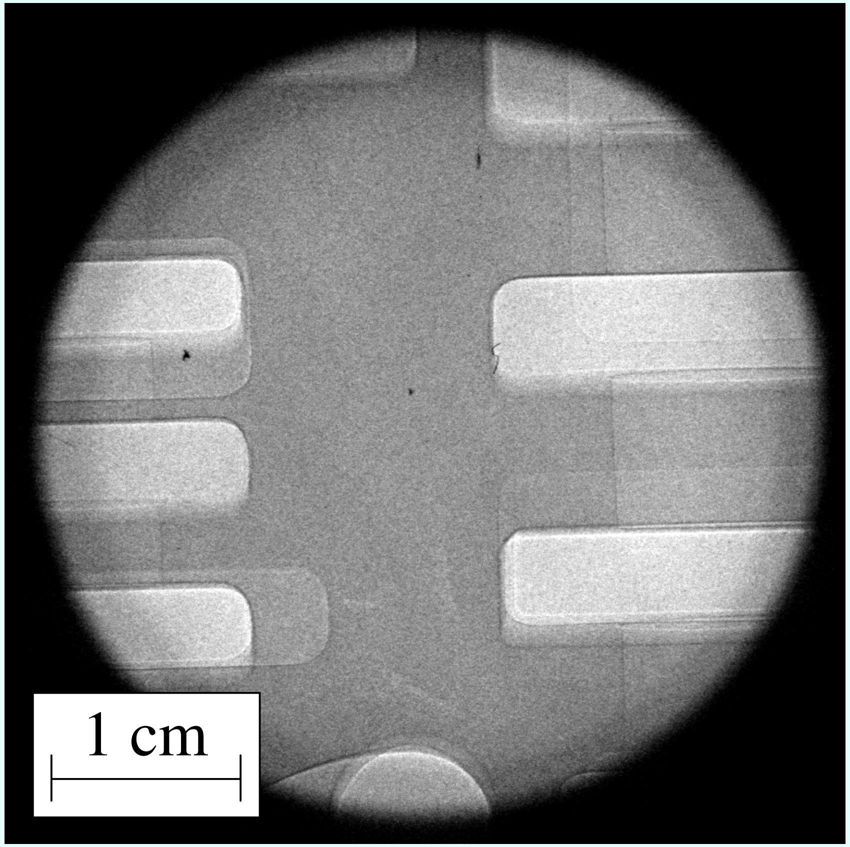

phase contrast radiography

Investigations on metal foams

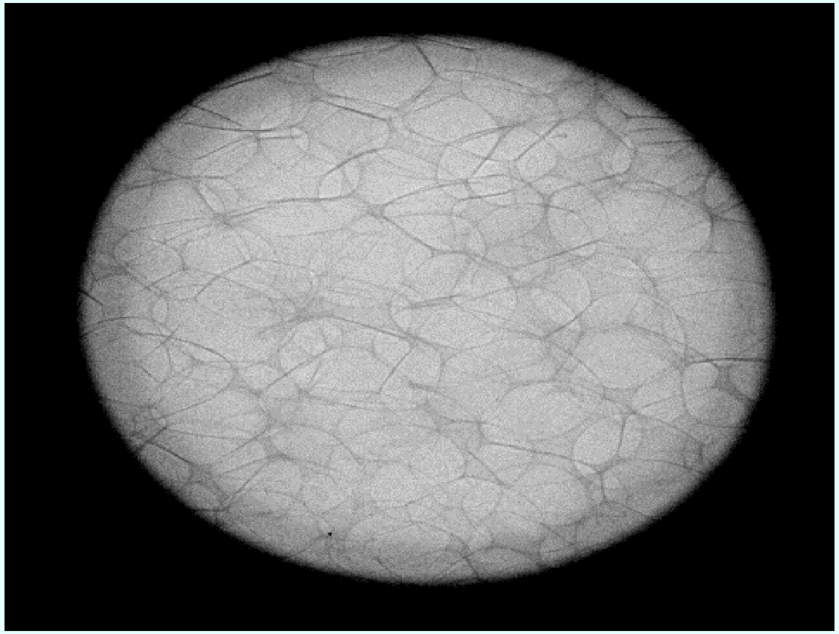

1cm

Phase contrast radiography of an aluminum foam, made at NEUTRA

Diameter of the pinhole: 0.5 mm
Distance pinhole-sample: 6.7 m
Distance sample-detector: 80 cm
Exposure time: 180 min
Detector: Imaging plates

Investigations on metal foams

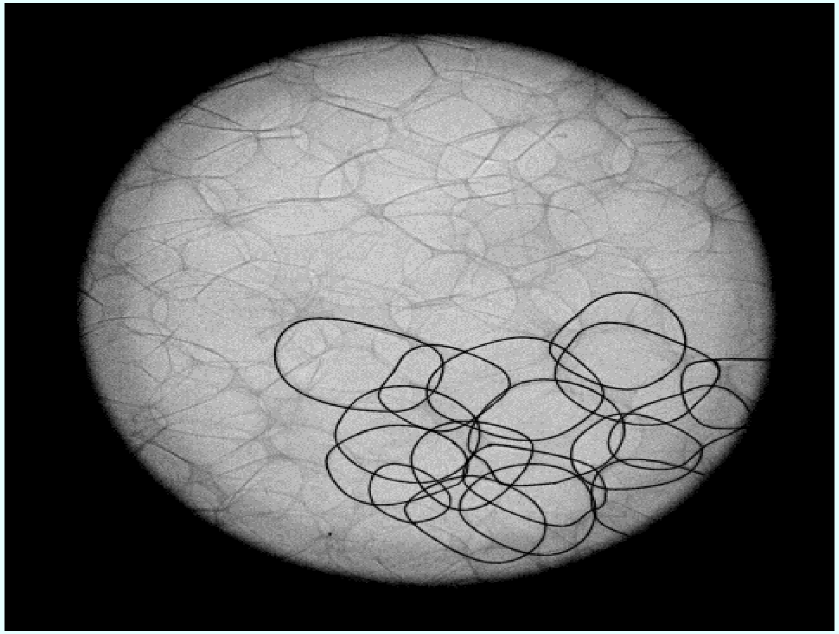

1cm

Each bubble in the foam creates a closed line in the phase contrast radiography.

An edge detection program can determine the 2D-distribution of the bubbles very quickly.

This non-destructive testing technique delivers quick information about the
- average bubble size
- standard deviation from it
- homogeneity of the distribution of the bubbles

Investigations on metal foams

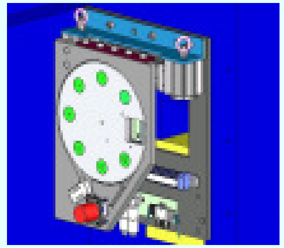

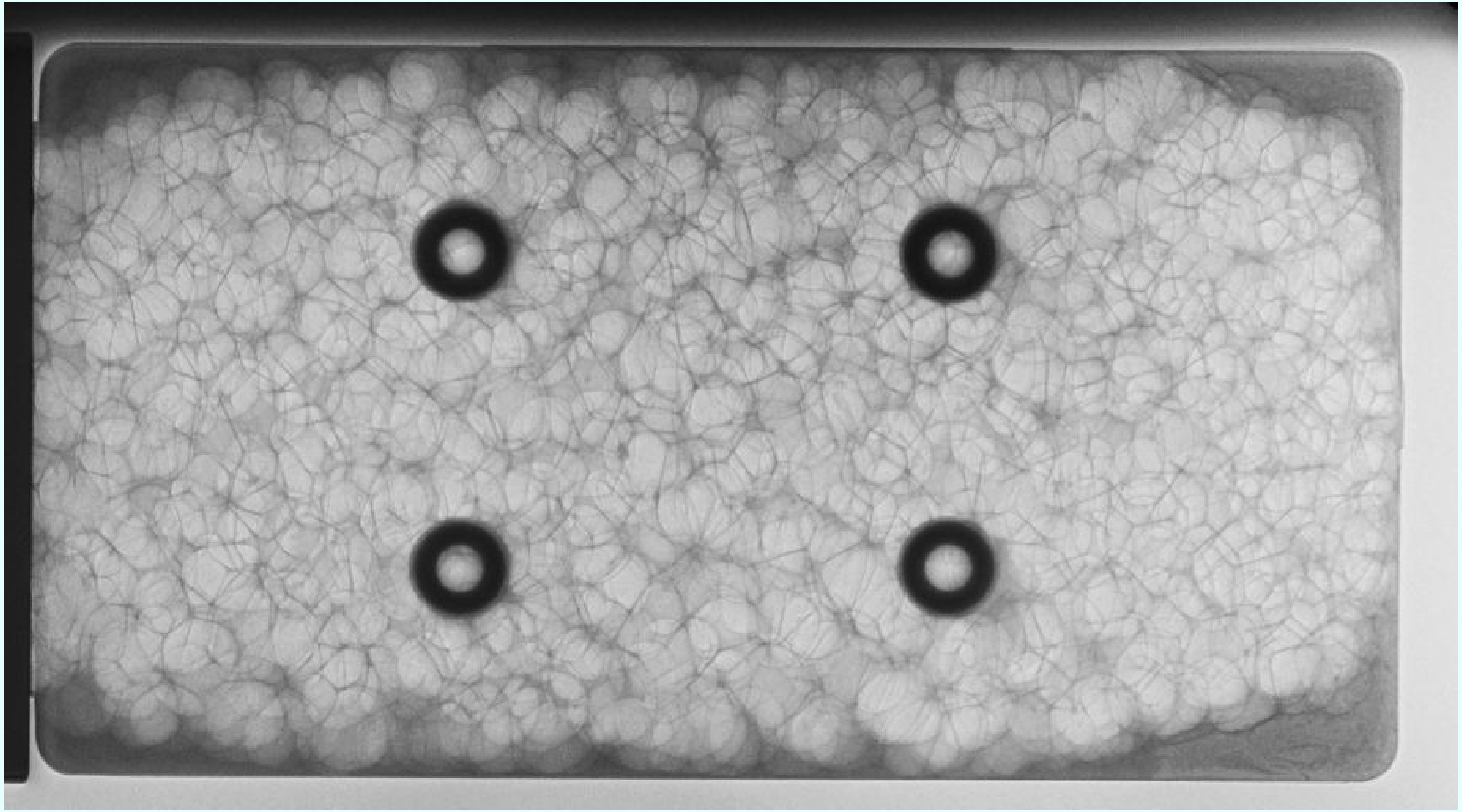

The ANTARES facility offers an even bigger field ov view…

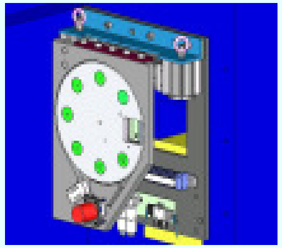

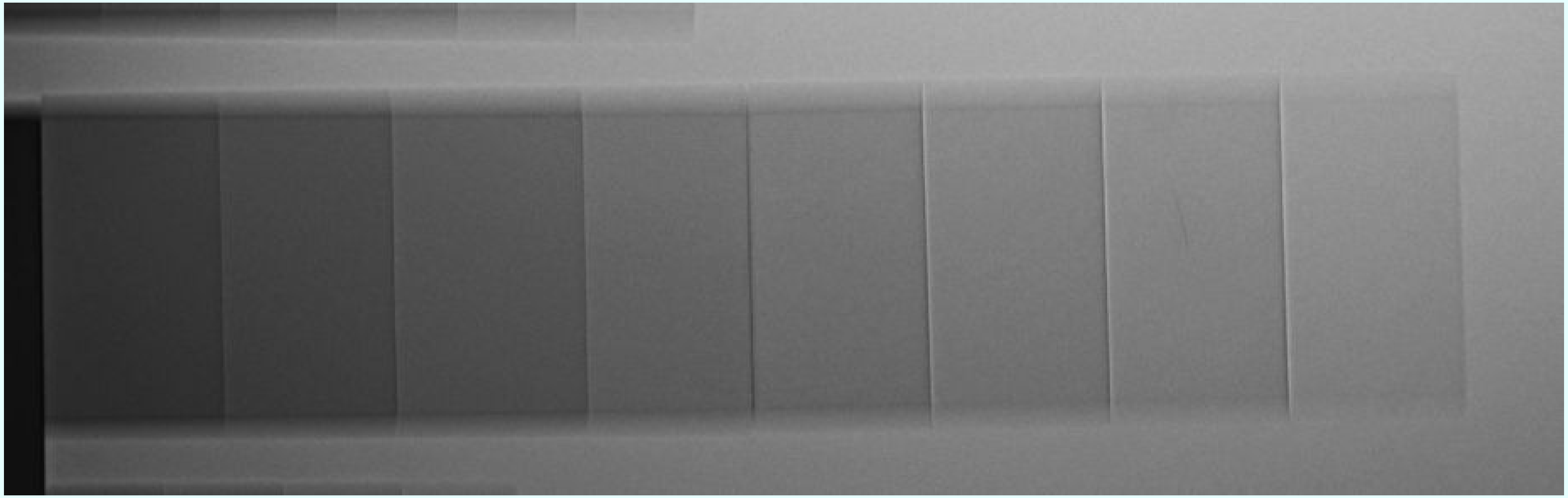

On a massive step wedge, we can even see
the bright and dark part of the edge enhancement!

Quantitative phase contrast

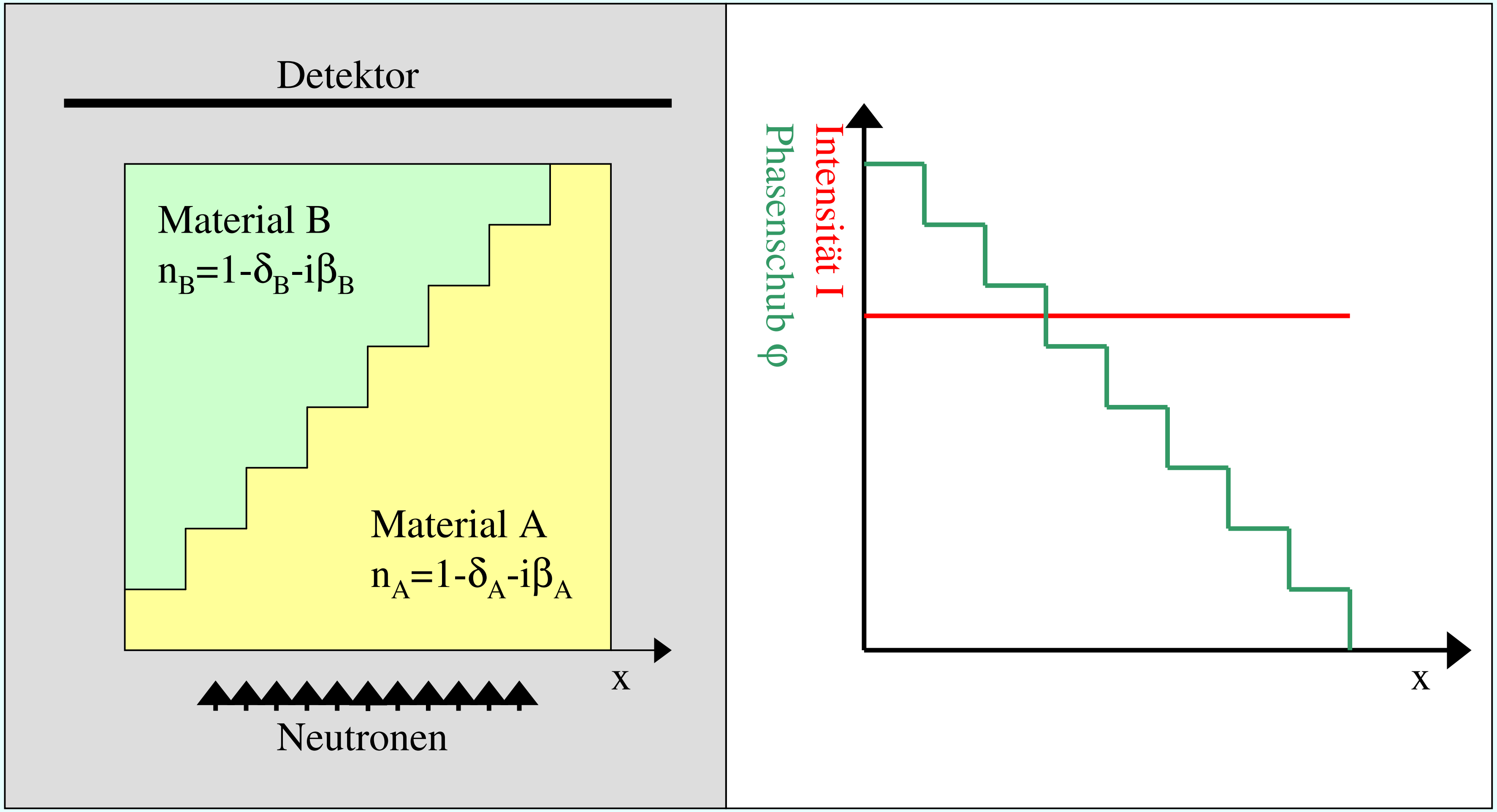

Stroboscopic imaging with neutrons

What do we mean by “continuous fast imaging with neutrons“?

1) **High-speed imaging of very fast, singular processes requiring several thousand frames per second**

Problems:

- the number of neutrons/photons in one time window becomes very low and may be below the detector noise

- in classic detectors, the number of detector pixels that can be read out in one time window becomes very small, drastically decreasing resolution

Example: Gun shot...

....hardly feasible for neutrons!

But: New detectors are becoming fast enough (see below), the neutron flux is the main limiting factor!

What do we mean by “stroboscopic fast imaging with neutrons“?

2) Stroboscopic imaging of very fast but periodical processes

Advantage:

- the number of neutrons/photons in one time window is still very low, but many exposures of the same time window of the periodic process may be accumulated on the detector before read-out, thus increasing the available intensity

Disadvantage:

- Only one time window of the periodic process can be recorded in one sequence, the periodic process has to be recorded in a sequence of many consecutive time window accumulations, sacrificing most neutrons.

Example: Fuel injection / oil flux in a combustion engine

Physical limitations

- Available neutron/photon flux in a time window
- Decay time of scintillation light
- readout speed of the detector
- gating time of the detector (if applicable)

Decay time of typical $ZnS+^{6}LiF$-Scintillator from datasheet:

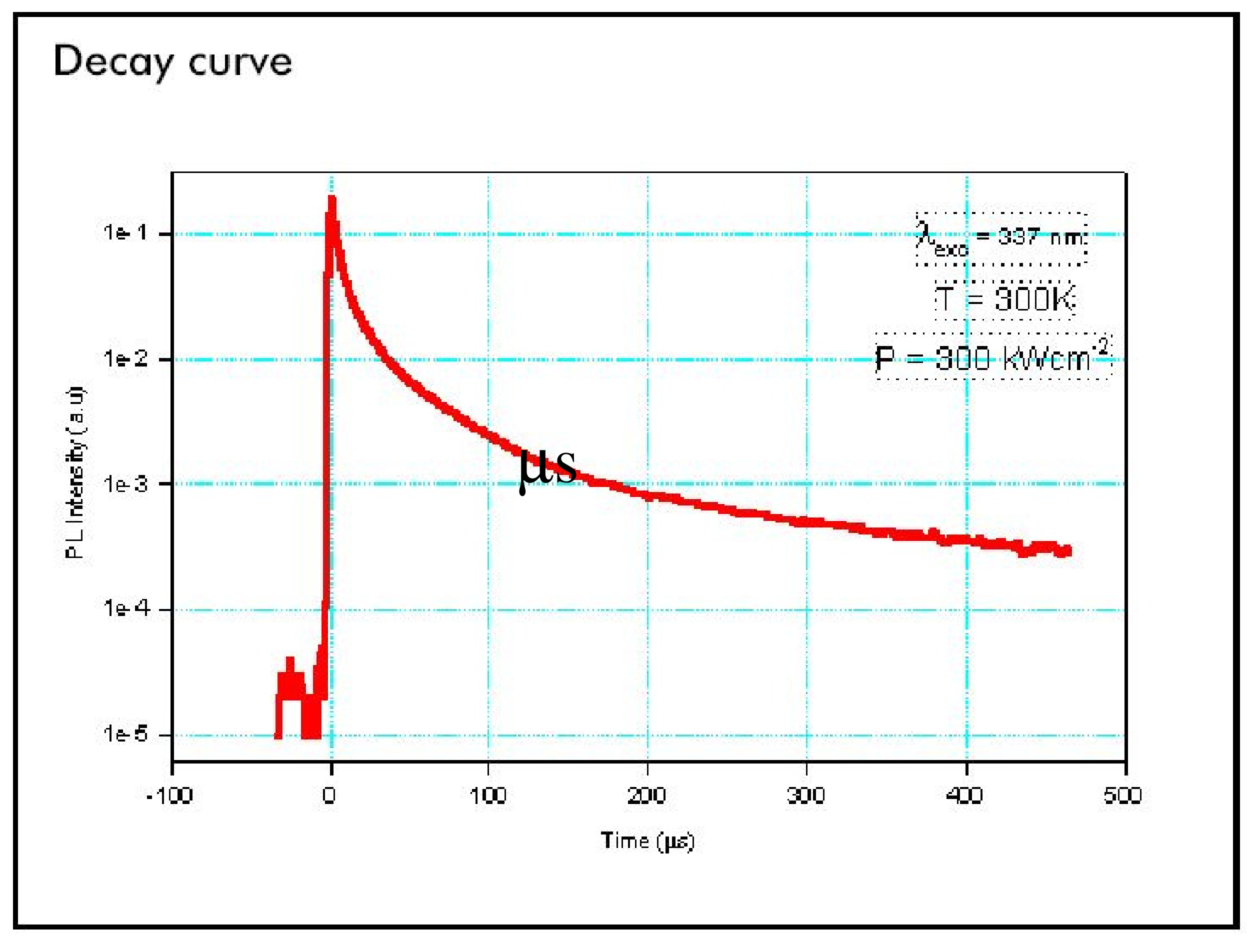

Decay to 10% in 80 µs

→ exposure times well below 100 µs seem to make no sense!

BUT: There is experimental evidence of better data... (see below)

Working principle of a MCP image intensifier

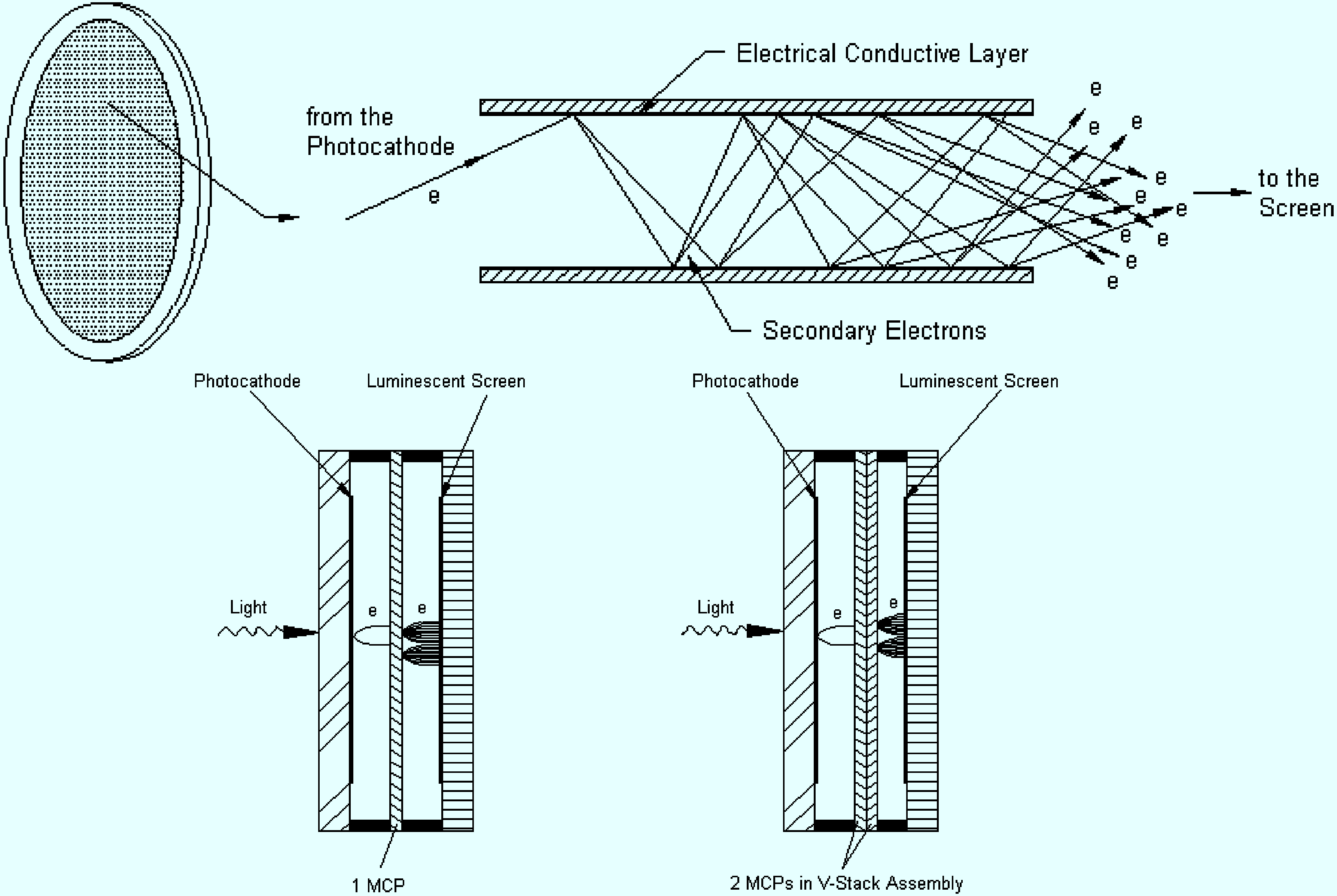

Measurements on a BMW engine

The beam NEUTROGRAPH at ILL Grenoble is the most intense neutron radiography beam in the world,

with a flux of $3*10^9$ n/cm^{2}s and a collimation of L/D=140.

ILL, Universität Heidelberg, Paul-Scherrer-Institut and TU München collaborated on the measurement of an electrically driven four-piston BMW engine.

The engine was driven by a 2kW electro motor, mounted on a vertical translation stage.

Since water cooling was not possible, the spark plugs were removed to reduce drag and heat production.

The full cycle of this four-stroke engine running at 1000 rpm was split into

120 individual frames over 2 rotations,

Measurements on a BMW engine

150 individual images were recorded as an on-chip accumulation of a 200 microseconds exposure each.

The total exposure time for the full run was in the order of 18 minutes only.

The field of view was 24 cm * 24 cm.

The observation area could be varied by displacement of the full set-up.

First-time visualisation of the oil cooling of the pistons!

Valves
(two behind each other)

Oil spreads on the piston bottom

Oil jet ejected from below onto the piston bottom

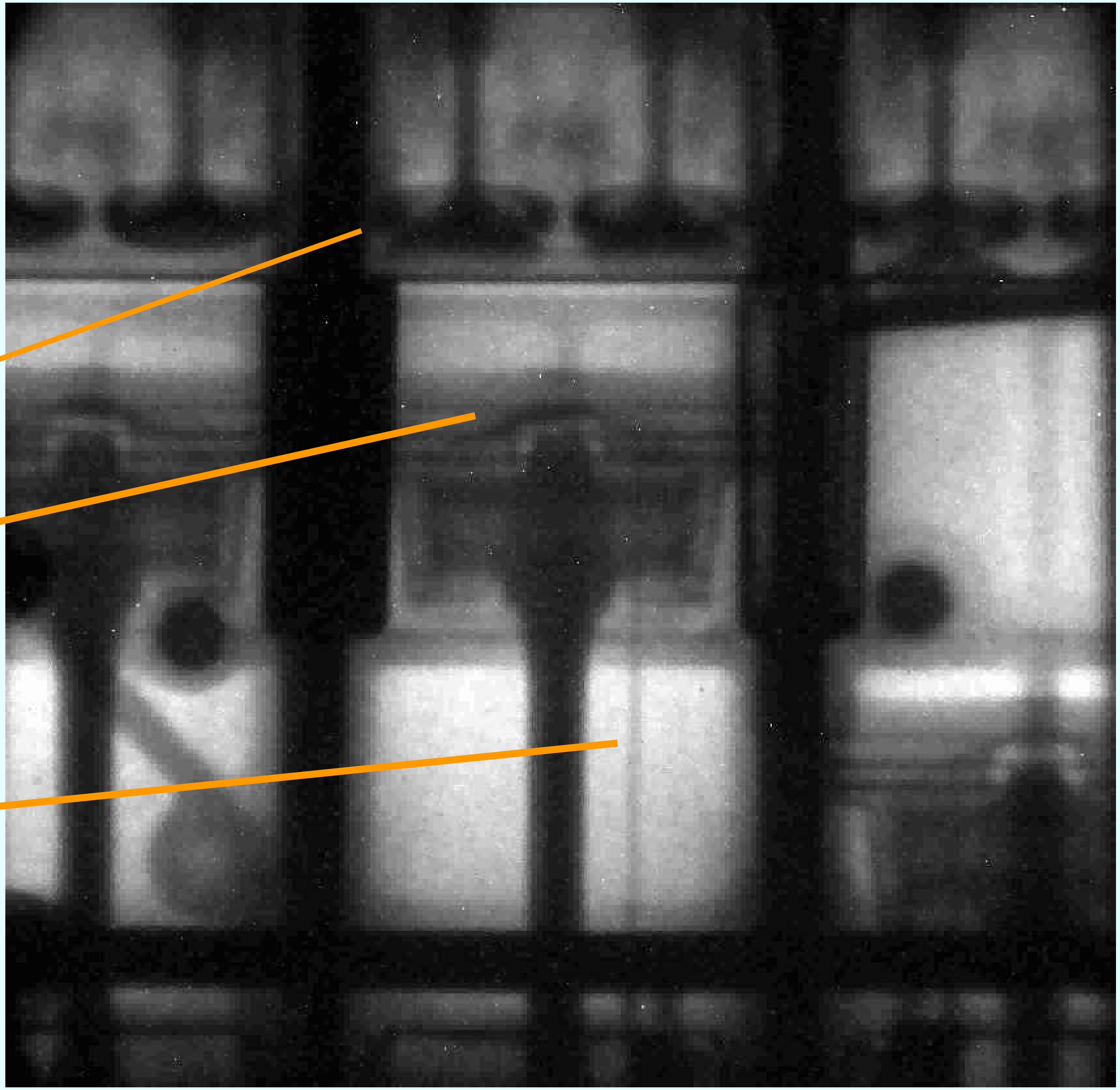

Measurements at ANTARES, FRM-II

The ANTARES facility at FRM-II offers a lower flux (10^8 n/cm^{2}s), but higher collimation (L/D=400).

The time window was extended to 1 ms,
the rotation speed was reduced to 600 rpm,
which is well below the nominal idle speed of the engine.

The images show more motion unsharpness,
but better definition on the stationary parts.

At this rotation speed, the oil pump did not produce its nominal pressure,
the oil pressure was pulsed and produced blobs in the cooling oil jet.

Measurements at ANTARES, FRM-II

Static radiography
of the engine,

with horizontal
pressure tubes and
vertical backflow tubes
empty

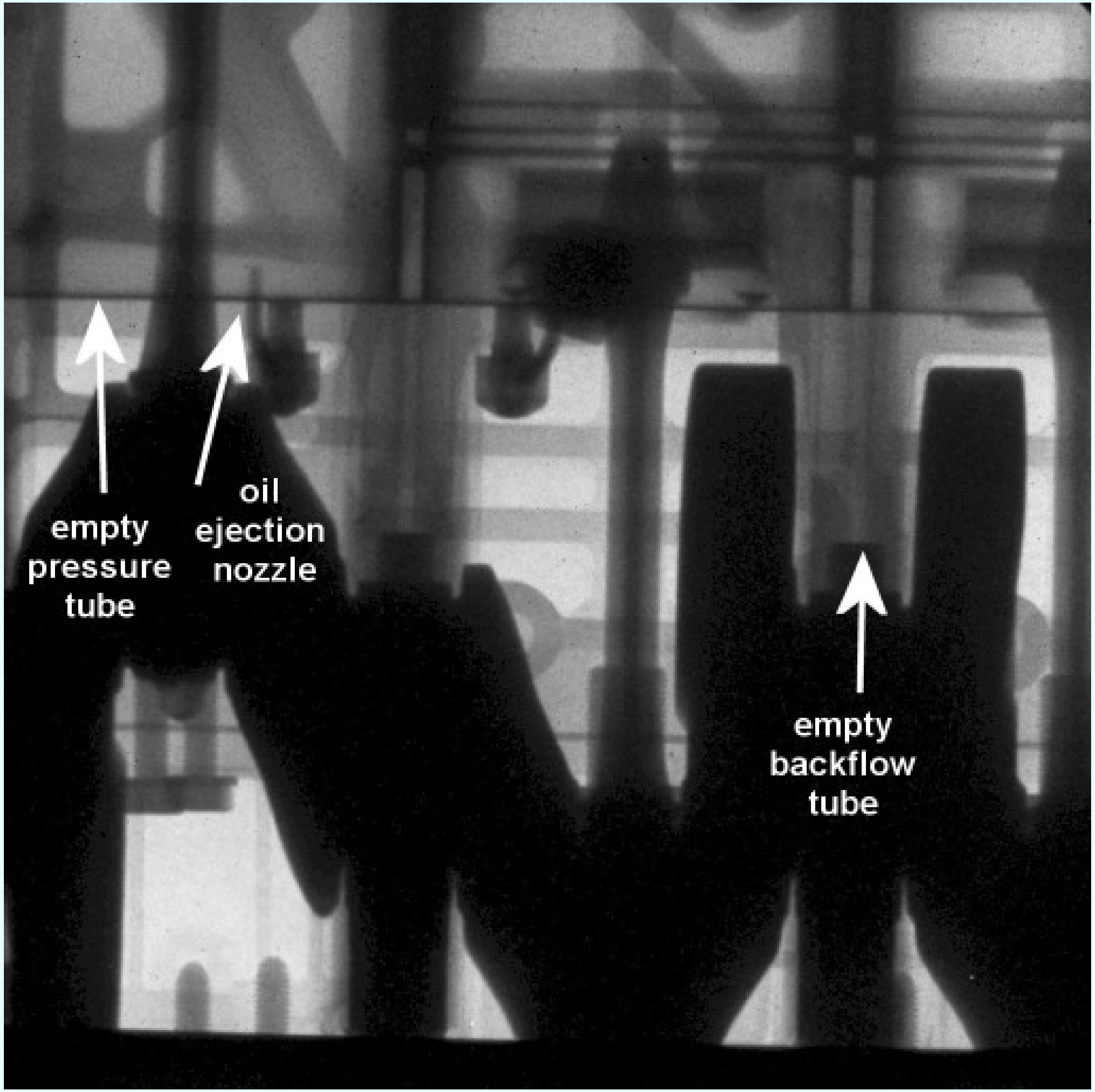

Measurements at ANTARES, FRM-II

Dynamic radiography of the engine,

with oil filled horizontal pressure tubes and vertical backflow tubes,

and an oil blob within the oil jet to the piston bottom

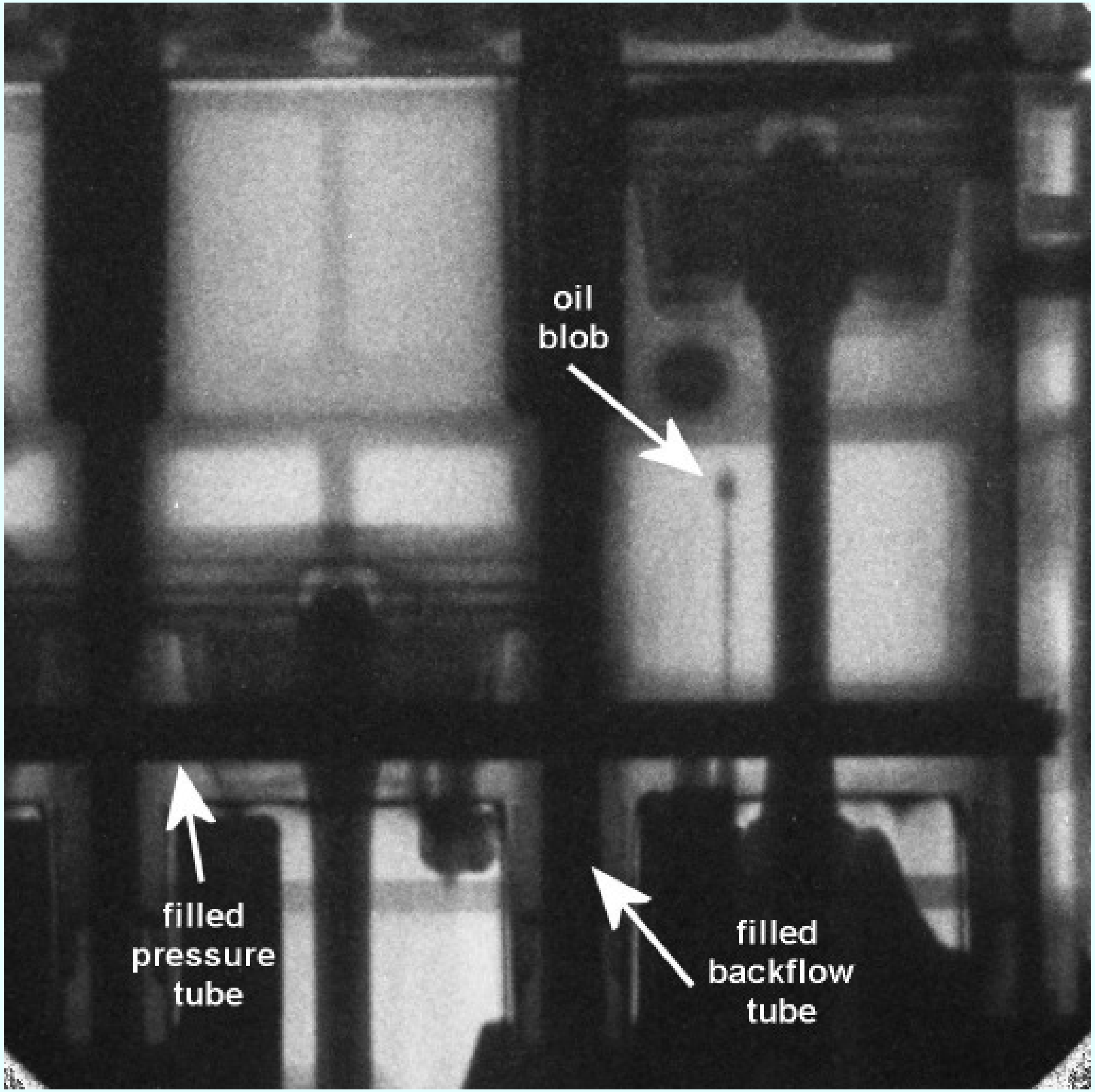

Measurements at ANTARES, FRM-II

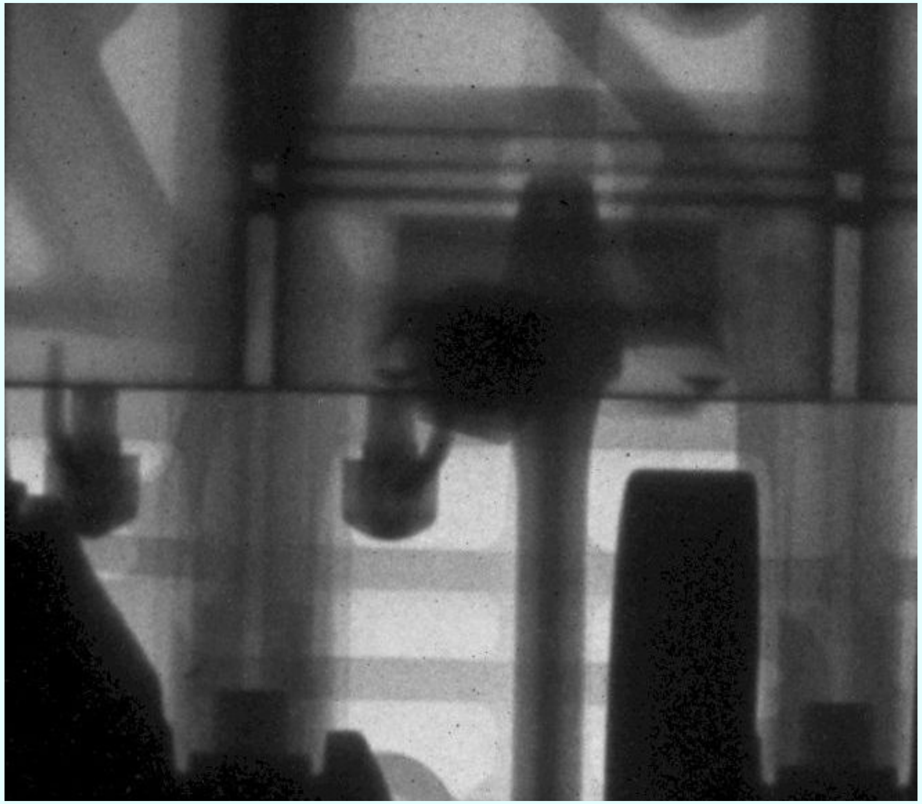

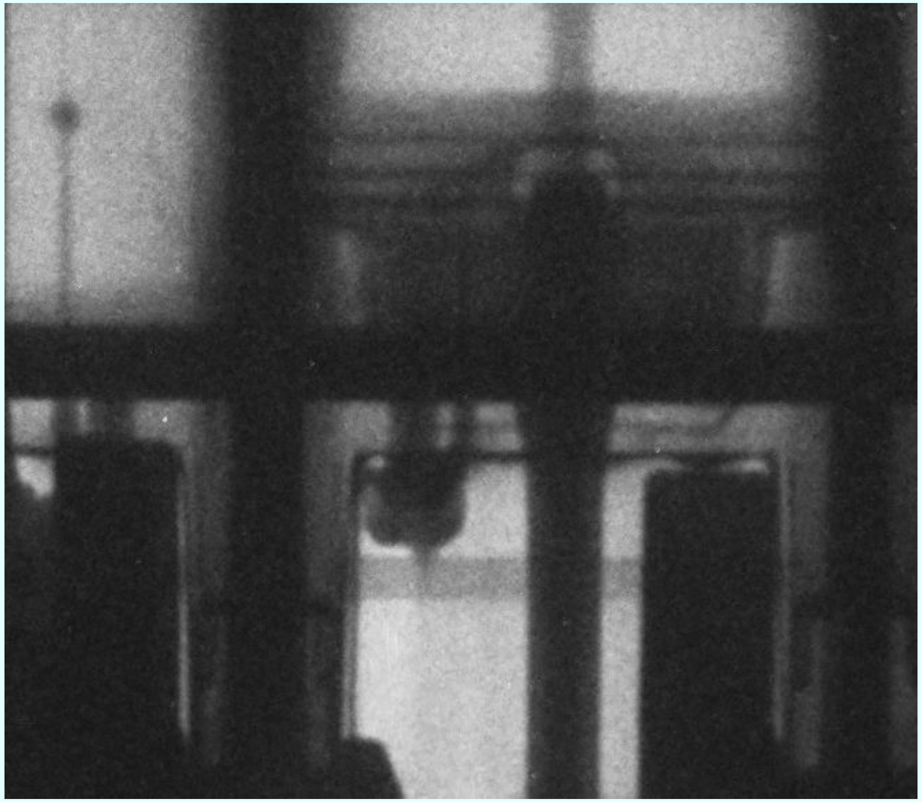

A static and a dynamic cutout beside each other.

The cylinders are not identical.

Backflow tubes are filled in the dynamic image,

the piston shows motion unsharpness.

Blobs in jet

Oil curtains detaching

Oil curtains detaching

Haben Sie nun eine Idee,
wo Neutronen helfen können,
Ihr Problem zu lösen?

Bitte gehen Sie auf

www.frm2.tum.de

oder schreiben Sie

Burkhard.Schillinger@frm2.tum.de

Für ein neues Problem ist eine Probeaufnahme kostenlos.